ELECTRICAL COMMUNICATION

1959
VOLUME 36
NUMBER 1

THE TECHNICAL JOURNAL OF ITT

INTERNATIONAL TELEPHONE AND TELEGRAPH CORPORATION

ELECTRICAL COMMUNICATION

Technical Journal Published Quarterly by

INTERNATIONAL TELEPHONE and TELEGRAPH CORPORATION

67 Broad Street, New York 4, New York

President: H. S. Geneen

Secretary: C. D. Webb

Subscription: $2.00 per year; 50¢ single copy

ELECTRICAL COMMUNICATION

The Technical Journal of
INTERNATIONAL TELEPHONE AND TELEGRAPH CORPORATION
AND ASSOCIATE COMPANIES

CONTENTS

VOLUME 36 **1959** **NUMBER 1**

Gaussian-Response Filter Design *by Milton Dishal*.....3

Transformers for 70-Megacycle Intermediate-Frequency Amplifiers
by W. F. Glover and E. D. Peakall.....27

On the Design of Some Rhombic Antenna Arrays
by A. A. de Carvalho Fernandes.....30

Thermal Noise in Multisection Radio Links *by B. B. Jacobsen*.....42

Refractive Index of the Atmosphere as a Factor in Tropospheric
Propagation Far Beyond the Horizon *by R. E. Gray*.....60

United States Patents Issued to International Telephone
and Telegraph System; August—October 1958.....70

Recent Telecommunication Developments—

Award for Automatic Radio Direction Finders in Aircraft.....26

Metal Rectifier Engineering (Book).....59

Transistor Circuits (Book).....69

Contributors to This Issue.....75

Modern-Network-Theory Filter Design

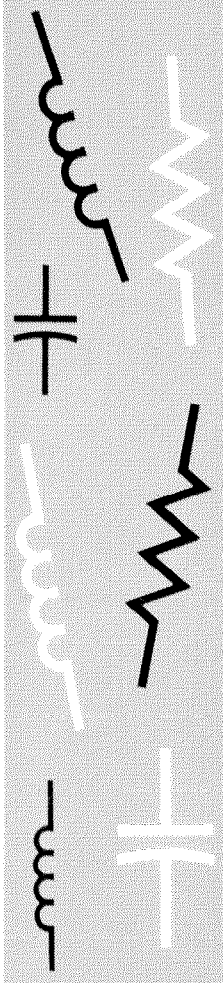

For more than three decades, filters have been designed according to the image-parameter theory. Their commercial acceptance is due in no small part to the highly approximate requirements for most filters. Where more-exact characteristics are required, shifting of element values in the actual filter has usually resulted in an acceptable design. For precise amplitude and phase response in the pass band, the simple and approximate solutions obtained through image-parameter theory must give way to equations based on modern network theory.

Modern network theory is an elegant extension of Kirchhoff's laws to the calculation of filter parameters. From prescribed specifications for the amplitude, phase, or time response of a desired filter, the equations produce exact values of each element that must be incorporated in the filter without the inherent limitations of the image-parameter method with its physically impracticable terminating impedances and lossless reactances.

Over a decade ago, the first of a series of practical papers on the modern network theory of filter design appeared in Electrical Communication. Another in the series will be found in this issue.

Gaussian-Response Filter Design

By MILTON DISHAL

ITT Laboratories, a division of International Telephone and Telegraph Corporation; Nutley, New Jersey

FILTERS having a gaussian response shape are useful in pulse systems because of the small under- and overshoots or ringing they produce following rapid signal changes. This paper first gives a resumé of the magnitude, phase, impulse response, step response, and effective thermal noise bandwidth of perfect gaussian filters. A physically realizable approximation to the magnitude characteristic is then given. The complex frequency roots of this approximation (up to the 9th order) are supplied. Then considered, in order of synthesis complexity, is the use of these roots to design stagger-tuned systems, lossless and uniformly lossy filters resistively loaded on one end only, and the same filters resistively loaded on both ends; all designs supplying nth-order gaussian magnitude approximations. Numerical design data is supplied in 7 tables; a low-pass and a band-pass design example are given.

• • •

In many communication systems, particularly those involving pulses, it is desirable that the system response-magnitude-versus-bandwidth characteristic be gaussian in shape.

This paper does not consider the system aspects of this problem, but it may be mentioned that some of the desirable qualitative results of using gaussian response shapes are very-small over- and undershoots and/or ringing following rapid signal changes, and the symmetrical pulse outputs that can be obtained when impulses are applied.

This paper is written to supply exact data that will enable successful design and construction of both low- and band-pass filters having magnitude-versus-frequency characteristics that are nth-order approximations to the perfect gaussian amplitude response, where n is the number of elements in the over-all filter. (With low-pass filters, the word elements stands for reactances; with band-pass filters, for resonators.) As will be shown in a later section, an infinite number of elements is required to produce a perfect gaussian response and thus it is always necessary to approximate this response when a finite number of elements are used.

1. Perfectly Gaussian Response Characteristics

For reference purposes this section gives resumés of five of the often-used characteristics of the perfect gaussian response.

1.1 Relative Attenuation Magnitude versus Bandwidth

Equation (1) gives the magnitude of the perfectly gaussian relative attenuation shape.

$$\left.\begin{aligned} |V_p/V| &= \exp\,(X/X_\beta)^2 \\ &= \exp\,[0.3466(X/X_{3db})^2], \end{aligned}\right\} \quad (1)$$

where V_p is the peak output voltage of the filter occuring, in this case, at zero bandwidth, V is the output at any bandwidth X, and X is the bandwidth variable (the actual radian frequency ω in the low-pass case and the fractional total bandwidth $BW/f_0 \equiv 2\,(f - f_0)/f_0$ in the symmetrical carrier-centered band-pass case). X_β is the normalizing bandwidth and, as usual, its meaning can be obtained from the equation in which it appears. For instance, a plot of (1) shows that when $X = X_\beta$, the relative attenuation is 1 neper or 8.68 decibels. From this same relative-attenuation plot, it will be seen that $X_{3db} = 0.588\,X_\beta$ and after renormalization to the 3-decibel bandwidth, the second right-hand side of (1) results. Taking 20 log of both sides of (1) to obtain relative attenuation in decibels gives the very-simple and useful (1A).

$$\text{Decibels} = 3\,(X/X_{3db})^2. \quad (1A)$$

At twice the 3-decibel bandwidth, the magnitude of the perfectly gaussian relative attenuation is 12 decibels; at 3 times the 3-decibel bandwidth it is 27 decibels; et cetera.

1.2 Relative Attenuation Phase (Phase Lag) versus Bandwidth

Based on the fact that a series with an infinite number of terms is required to represent the magnitude (1), it can be shown that perfectly

gaussian phase characteristic has infinite slope and is perfectly linear as given by

$$\theta_0 - \theta = \infty\ (X/X_{3db}), \qquad (2)$$

where θ_0 is the actual phase shift at the middle of the band-pass; or at zero frequency for the low-pass response. Infinite linear slope of the phase characteristic gives infinite time delay for signals passing through a perfectly gaussian filter. Approximation of the gaussian response by a finite number of network elements results in a finite time delay.

1.3 Impluse Response versus Time

The impulse response of the perfectly gaussian filter is

$$(v/v_p)_{\text{impulse}} = \exp\left[-0.721(\omega_{3db}\Delta t)^2\right], \qquad (3)$$

where Δt is the time difference (plus and minus) figured from the infinite delay existing at the center of the pulse response, v is the output at any time Δt, and v_p is the peak output (occurring at $\Delta t = 0$). A plot of (3) shows that the total time width between the half-amplitude points is $0.312/f_{3db}$, the 10-percent-amplitude total time width is $0.570/f_{3db}$, the 1-percent-amplitude total time width is $0.808/f_{3db}$, and the 0.1-percent-amplitude time width is $0.988/f_{3db}$, where f_{3db} is the actual 3-decibel-down frequency for the low-pass case and is half the total 3-decibel bandwidth for the symmetrical carrier-centered band-pass case.

1.4 Step Response versus Time

The step response of the perfectly gaussian filter is

$$v/v_\infty = \tfrac{1}{2} + \operatorname{erf}(1.20\omega_{3db}\Delta t), \qquad (4)$$

where Δt is the time difference (plus and minus) figured from the infinite delay time existing halfway up the step response. A plot of (4) shows that the 10-to-90-percent rise time equals $0.344/f_{3db}$ and the 5-to-95-percent rise time equals $0.437/f_{3db}$, where f_{3db} is the actual 3-decibel-down frequency for the low-pass case, and is half the total 3-decibel bandwidth for the symmetrical carrier-centered band-pass case.

1.5 Effective Noise Bandwidth

To calculate the expected thermal-noise-limited sensitivity of a radio receiver, it is necessary to know the effective noise bandwidth of the receiver selectivity characteristic. For the gaussian relative response shape,

thermal noise bandwidth
= 3.4-decibel-down bandwidth
= 1.07 × (3-decibel-down bandwidth).

The effective thermal noise bandwidth is the width of that rectangular voltage-*squared* relative response shape that has the same peak response and same total area as the actual voltage-*squared* response shape.

2. *Approximation to the Gaussian Magnitude Characteristic Using n Network Elements*

As has been mentioned, a desired network function that required an infinite number of terms when expressed in polynomial form would require a synthesized lumped linear network containing an infinite number of elements. It is thus necessary in practice to *approximate* the perfect gaussian responses detailed in section 1. The design engineer must decide whether to approximate the magnitude characteristic, the phase characteristic, the phase-slope characteristic, the impulse response characteristic, the step response characteristic, et cetera. This paper deals with the problem of approximating the gaussian magnitude characteristic.

2.1 Equation for Relative Attenuation Magnitude

As has been pointed out many times (see, for example, Darlington's paper[1]), a lumped linear network of a finite number of elements producing a continuously increasing attenuation outside the pass band will always produce a relative-attenuation magnitude equation of the form

$$\left|\frac{V_p}{V}\right|^2 = \frac{1}{|\Delta|^2_{\min}} M^2. \qquad (5)$$

M^2 is a polynomial in the normalized bandwidth variable $(X/X_\beta)^2$, of highest power n, where n is the number of network elements, and $|\Delta|^2_{\min}$ is the numerical value of this polynomial at that bandwidth at which the polynomial has minimum value. By subtracting and adding $|\Delta|^2_{\min}$ to the constant term of the M^2 polynomial, (5) may obviously be written in the form

$$\left|\frac{V_p}{V}\right|^2 = 1 + \frac{1}{|\Delta|^2_{\min}}\left[\text{polynomial in } \left(\frac{X}{X_\beta}\right)^2\right]. \qquad (5A)$$

[1] S. Darlington, "Synthesis of Reactance 4-Poles," *Journal of Mathematics and Physics*, volume 18, pages 257–353; September, 1939.

Thus, to relate the desired gaussian relative-attenuation magnitude equation (1) to physically realizable networks, it is necessary to write the series for the square of (1) and not for (1) directly because (5) shows that the square of the relative attenuation magnitude must be used if the number of terms in the polynomial is to be related to the number of elements in the network.

2.2 Resulting Magnitude Approximation

When the above-mentioned squaring is done and then the well-known convergent infinite series for $\exp y$ is used[2] we obtain

$$\left|\frac{V_p}{V}\right|^2 = \exp^2\left(\frac{X}{X_\beta}\right)^2$$

$$= 1 + 2\left(\frac{X}{X_\beta}\right)^2 + \frac{2^2}{2!}\left(\frac{X}{X_\beta}\right)^4 + \frac{2^3}{3!}\left(\frac{X}{X_\beta}\right)^6 + \frac{2^4}{4!}\left(\frac{X}{X_\beta}\right)^8 + \frac{2^5}{5!}\left(\frac{X}{X_\beta}\right)^{10} + \frac{2^6}{6!}\left(\frac{X}{X_\beta}\right)^{12} + \cdots \quad (6)$$

[2] B. O. Peirce, "A Short Table of Integrals," 3rd edition, Ginn and Company, Boston, Massachusetts; 1929: see page 89.

In keeping with the powerful generalization of (5) concerning the highest power of its polynomial, it can be seen that a two-element (reactances for low-pass circuits; resonators for band-pass circuits) filter can satisfy the first three terms of (6), a three-element filter the first four terms, et cetera. In general, an n-element filter can satisfy the first $n + 1$ terms of (6).

There are a number of mathematically different ways of specifying a best approximation to a desired curve; in this paper the approximation used is the straightforward one of satisfying as many as possible of the actual numerical coefficients in (6).

The gaussian magnitude approximation shapes obtainable with n-element networks can now be plotted. Figure 1, for that part of the curve inside the 3-decibel-down point, and Figure 2, for the part outside the 3-decibel point, are the resulting curves for networks containing up to 10 elements. After plotting against X/X_β, the relation X_{3db}/X_β was noted and all curves were then renormalized to their own 3-decibel-down point. From these curves it is a simple matter for the

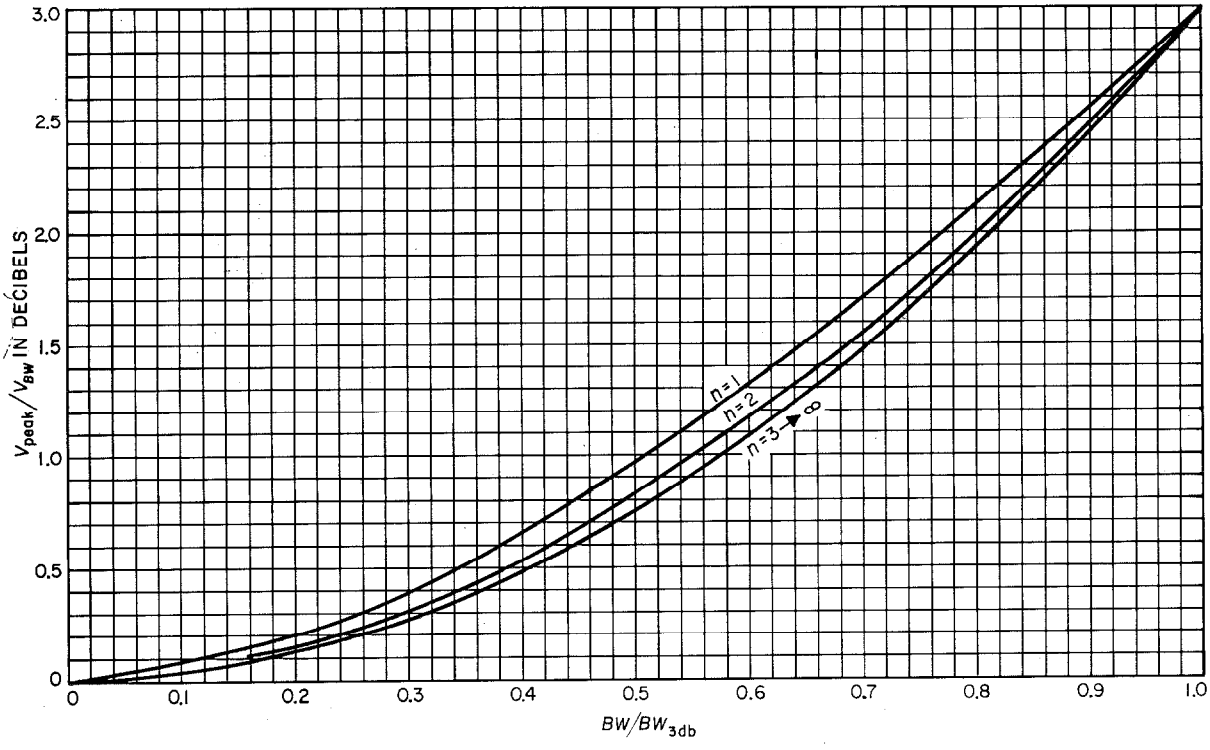

Figure 1—Relative attenuation shape *inside* the 3-decibel-down point of nth-order gaussian magnitude approximation filters. n = number of elements in the filter.

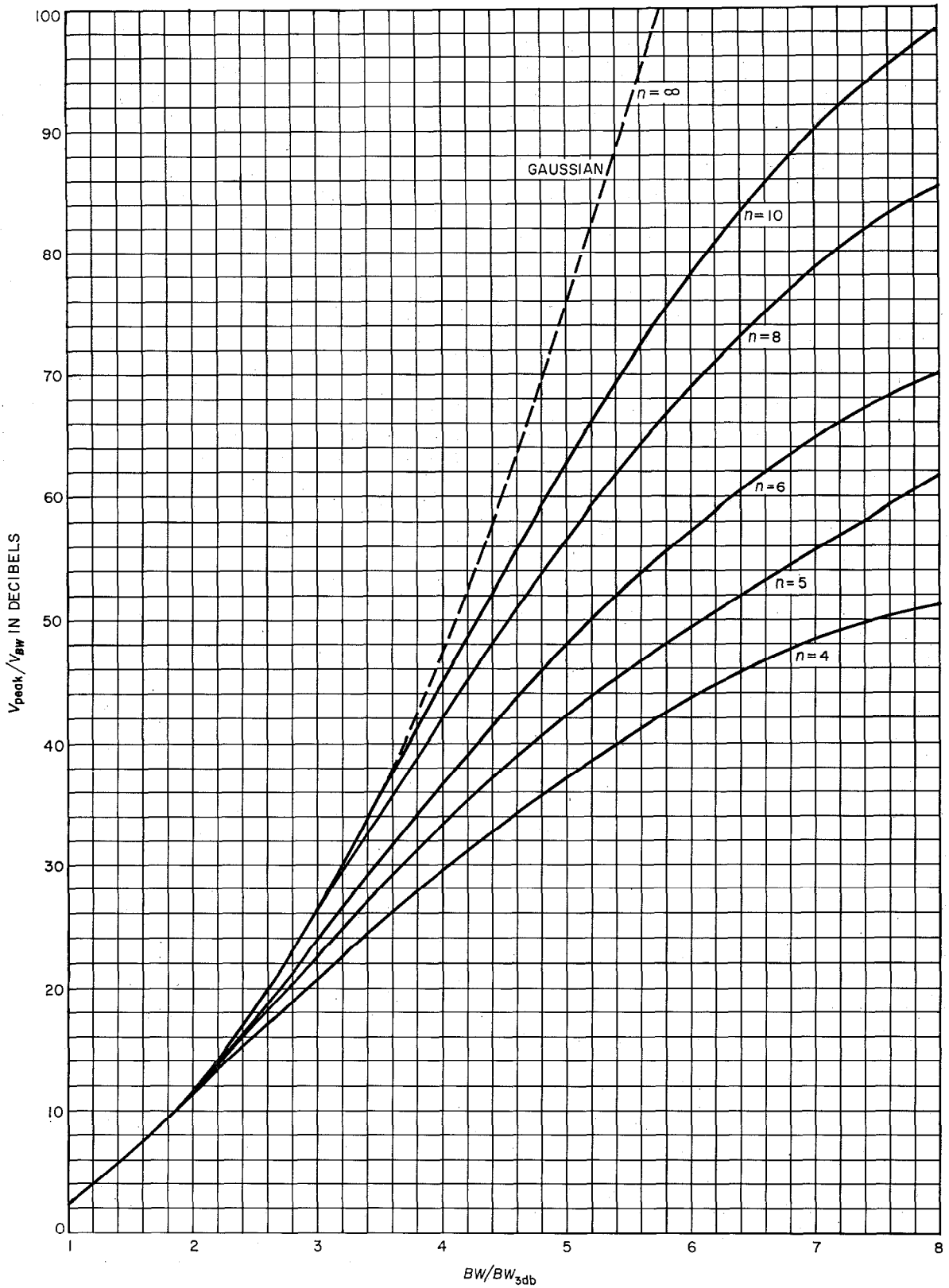

Figure 2—Relative attenuation shape *outside* the 3-decibel-down point of *n*th-order gaussian magnitude approximation filters.

engineer to determine the number of network elements required to satisfy a specified approximation. From Figure 2, the important fact should be noted that the number of elements used in the filter determines how far up on the relative attenuation curve (that is, how far down on the relative response curve) the approximation satisfies the perfect gaussian response; for example, a four-element filter can approximate the gaussian response within 1 decibel down to about the 11-decibel point; 6 elements down to about 18 decibels; 8 elements to about the 26-decibel point; 10 elements to about the 34-decibel point; et cetera.

How far down must the perfect gaussian response be satified? This is an important question that depends on the requirements of specific systems and cannot be dealt with in this paper.

3. *Complex Frequency Roots of the Gaussian Magnitude Approximation and Application to Stagger-Tuned Amplifier Design*

When synthesizing a network to produce an exactly prescribed continuously increasing attenuation magnitude, it is always necessary to solve for the $2n$ complex roots of the prescribed attenuation equation, where n is the highest power of the prescribed polynomial and is also the number of elements that must be used in the filter. For the gaussian approximation now being considered, these important root values or pole locations are obviously obtained by picking the proper number of terms for (6)—the first $n + 1$ terms—setting them equal to zero, and then solving for the $2n$ resulting X/X_β roots. Network functions are rational functions of $j(X/X_\beta)$, not of X/X_β; therefore, for use in the network synthesis procedure, it is necessary to multiply the above-obtained X/X_β roots by j. The result of the above steps is detailed in Table 1 for gaussian approximations up to the 9th order. In each case the obtained pole locations have been renormalized to the 3-decibel-down point of the response and since only the n left-half-plane poles are used for network synthesis, minus signs only are shown with the real parts of the roots.

3.1 Stagger-Tuned Amplifier Design Using Single-Tuned Interstages

If it is practical to satisfy a specification by designing a stagger-tuned intermediate-frequency amplifier using single-tuned interstages, then the figures of Table 1 constitute the complete design data for the amplifier interstages.

For example, if a five-interstage stagger-tuned amplifier were to produce a 5th-order gaussian approximation, there would be needed: Two single-tuned circuits with individual 3-decibel bandwidths of 1.448 . . . times the desired over-all 3-decibel bandwidth; these two circuits would be detuned (one above and one below) the desired midfrequency by frequency intervals equal to half of 1.563 . . . times the desired over-all 3-decibel bandwidth. Then there would be two single-tuned interstages with individual 3-decibel bandwidths equal to 1.704 . . . times the desired over-all 3-decibel bandwidth; these two circuits would be detuned (one above and one below) the desired midfrequency by frequency intervals equal to half of 0.719 . . . times the desired over-all 3-decibel bandwidth. Finally, there would be one single-tuned interstage with a 3-decibel bandwidth of 1.776 . . . times the desired over-all 3-decibel bandwidth; this circuit would not be detuned from the midfrequency.

The total gain required of the amplifier can be proportioned among the five stages in any desired distribution.

3.2 Double-Tuned Interstages Producing the Gaussian Magnitude Approximation

If the system selectivity requirement is satisfied by using low-order interstages separated by tubes, then, of course, for a given number of stages a higher-order approximation than that of section 3.1 can be accomplished by using double-tuned interstages. The pole location data of Table 1 can also be used directly to design such double-tuned interstages. For the synchronously tuned $Q_1 = Q_2$ case, which the author strongly recommends (because slight mistunings have much less effect than in the $Q_1 \neq Q_2$ case), the required value of $Q_1 = Q_2$ is directly obtained from the fact that the quantity $(f_0/BW_{3db})/Q$ must equal the real part of the pole pair being

supplied by that double-tuned circuit. The required coefficient of coupling K is directly obtained from the fact that the quantity $K/(BW_{3db}/f_0)$ must equal the imaginary part of this pole pair. BW_{3db} in the above expressions is the desired over-all 3-decibel bandwidth of the whole amplifier.

physical networks to which the resulting design information can be directly applied.

4.1 Low-Pass Ladder Networks

Figure 3 shows the well-known basic low-pass ladder that can be designed to produce gaussian response approximations. Writing (by applica-

TABLE 1

The n Left-Half-Plane Roots of the Gaussian Magnitude Approximation

Order n	Root	Numerical Value
1	$\left(j\frac{X}{X_{3db}}\right)_1$	$-1.00000000 + j0$
2	$\left(j\frac{X}{X_{3db}}\right)_{1,2}$	$-1.28963240 \pm j0.534183236$
3	$\left(j\frac{X}{X_{3db}}\right)_{1,2}$	$-1.3825708 \pm j0.94620542$
	$\left(j\frac{X}{X_{3db}}\right)_3$	$-1.5200495 + j0$
4	$\left(j\frac{X}{X_{3db}}\right)_{1,2}$	$-1.42105525 \pm j1.27582461$
	$\left(j\frac{X}{X_{3db}}\right)_{3,4}$	$-1.63074266 \pm j0.394581663$
5	$\left(j\frac{X}{X_{3db}}\right)_{1,2}$	$-1.44825063 \pm j1.56351694$
	$\left(j\frac{X}{X_{3db}}\right)_{3,4}$	$-1.70450631 \pm j0.719334299$
	$\left(j\frac{X}{X_{3db}}\right)_5$	$-1.77672511 + j0$
6	$\left(j\frac{X}{X_{3db}}\right)_{1,2}$	$-1.46877155 + j1.82226145$
	$\left(j\frac{X}{X_{3db}}\right)_{3,4}$	$-1.75830108 \pm j1.00219826$
	$\left(j\frac{X}{X_{3db}}\right)_{5,6}$	$-1.87711870 \pm j0.323271071$
7	$\left(j\frac{X}{X_{3db}}\right)_{1,2}$	$-1.48495991 \pm j2.05945318$
	$\left(j\frac{X}{X_{3db}}\right)_{3,4}$	$-1.79979710 \pm j1.25639445$
	$\left(j\frac{X}{X_{3db}}\right)_{5,6}$	$-1.95195537 \pm j0.604065299$
	$\left(j\frac{X}{X_{3db}}\right)_7$	$-1.99851591 + j0$
8	$\left(j\frac{X}{X_{3db}}\right)_{1,2}$	$-1.4981483 \pm j2.2797794$
	$\left(j\frac{X}{X_{3db}}\right)_{3,4}$	$-1.8330679 \pm j1.4893763$
	$\left(j\frac{X}{X_{3db}}\right)_{5,6}$	$-2.0106305 \pm j0.85597285$
	$\left(j\frac{X}{X_{3db}}\right)_{7,8}$	$-2.0904874 \pm j0.28007143$
9	$\left(j\frac{X}{X_{3db}}\right)_{1,2}$	$-1.5091585 \pm j2.4864331$
	$\left(j\frac{X}{X_{3db}}\right)_{3,4}$	$-1.8605114 \pm j1.7058275$
	$\left(j\frac{X}{X_{3db}}\right)_{5,6}$	$-2.0582730 \pm j1.0866159$
	$\left(j\frac{X}{X_{3db}}\right)_{7,8}$	$-2.1634996 \pm j0.53088289$
	$\left(j\frac{X}{X_{3db}}\right)_9$	$-2.1967728 + j0$

4. Multielement Gaussian Filter Networks

When simple (one-pole and two-pole) *isolated* networks *cannot* be used to build up a desired relative-attenuation shape and a single lumped filter unit is thus required, the necessary synthesis procedure still must make use of the pole locations given in section 3, but knowledge of these pole locations is only the first step in the procedure. Before proceeding with the additional steps, it will be helpful to show some of the tion of Kirchhoff's laws) the phasor transfer function for n elements of such a network, the reader will see that this network is adequately described by: (A) the coefficient-of-coupling values K—giving the relations between *immediately adjacent reactances* and (B) the Q values that describe the resistive loss associated with each *individual* reactance. It is important to note that the Q values of the *end* reactances include not only their own internal losses but,

even more important, the effect of the resistances of the generator or load that are connected to these end elements. These K and Q relations are detailed in Figure 3. It will be noted that the required *actual* coefficients of coupling [for example, $1/(L_1C_2)^{1/2}$] and decrements (G/C or R/L) are obtained by multiplying the *normalized* values (small k's and inverse q's) by the normalizing bandwidth variable ω_{3db}.

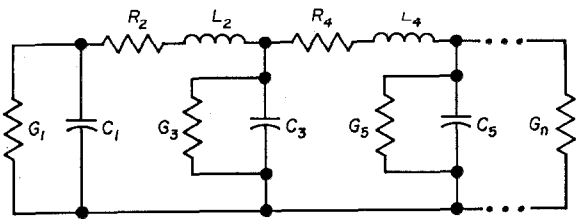

Figure 3A—For ladders starting with a shunt capacitor, the relations between the 3-decibel-bandwidth normalized k's and q's and the L's, C's, and R's are: $q_1 = \omega_{3db}C_1/G_1$, $q_2 = \omega_{3db}L_2/R_2$, $q_3 = \omega_{3db}C_3/G_3$, et cetera. $k_{12} = 1/\omega_{3db}(C_1C_2)^{1/2}$, $k_{23} = 1/\omega_{3db}(L_2C_3)^{1/2}$, $k_{34} = 1/\omega_{3db}(C_3L_4)^{1/2}$; et cetera.

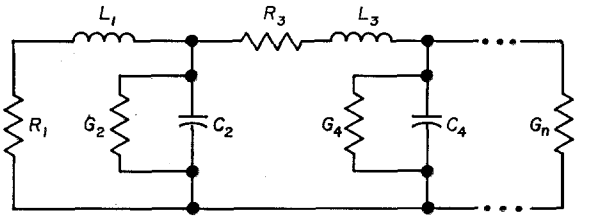

Figure 3B—For ladders starting with a series inductor, the relations between the 3-decibel-down normalized k's and q's and the L's, C's, and R's are: $q_1 = \omega_{3db}L_1/R_1$, $q_2 = \omega_{3db}C_2/G_2$, $q_3 = \omega_{3db}L_3/R_3$, et cetera. $k_{12} = 1/\omega_{3db}(L_1C_2)^{1/2}$, $k_{23} = 1/\omega_{3db}(C_2L_3)^{1/2}$, $k_{34} = 1/\omega_{3db}(L_3C_4)^{1/2}$, et cetera.

Figure 3—The low-pass ladders to which the design data of this paper can be applied directly. To design large-percentage-band-pass networks, first design the above low-pass structure using the *total* required 3-decibel radian bandwidth for ω_{3db}, then a resonating inductor is placed across each shunt capacitor and a resonating capacitor is put in series with each series inductor such that each resulting resonant circuit is tuned to the geometric mean frequency of the pass band $f_0 = (f_1f_2)^{1/2}$.

4.2 Band-Pass Ladder Networks

Figure 4 shows the well-known coupled-resonator band-pass circuits that are practical for the important case where a small-percentage band-pass is desired. Here also, application of Kirchoff's laws to the network and solving for the resulting transfer function will show that the network is exactly described by: (A) the coefficients of coupling K between immediately adjacent resonators and (B) the Q of each individual resonator; it is important to realize that the Q values of the end resonators are determined by the generator or load resistance connected to them as well as the internal losses of these resonators. These K and Q relations are detailed in Figure 4. The required *actual* coefficients of coupling [as $C_{12}/(C_1C_2)^{1/2}$] and decrements ($= 1/Q$) are obtained by multiplying the *normalized* values (small k's and d's) by the normalizing bandwidth variable BW_{3db}/f_0.

5. *Phasor Relative-Attenuation Equation and its Application to Networks Resistively Loaded on One End Only*

5.1 Phasor Relative-Attenuation Equation for Lossless or Uniformly Lossy Elements

Given a relative-attenuation magnitude equation in the necessary form of (5), the corresponding phasor equation can always be written in the form

$$\frac{V_p}{V} = \frac{1}{|\Delta|_{\min}}\left[\left(j\frac{X}{X_\beta}\right)^n + U_{n-1}\left(j\frac{X}{X_\beta}\right)^{n-1} + U_{n-2}\left(j\frac{X}{X_\beta}\right)^{n-2} + \ldots + U_0\right]. \quad (7)$$

For lossless elements, the coefficients U of the polynomial in square brackets are formed by simply multiplying out the n factors associated with the n left-half-plane roots of Table 1 and $|\Delta|_{\min}$ is simply the value of the magnitude of the bracketed polynomial at that bandwidth producing minimum magnitude. For the gaussian relative shape, the minimum magnitude of the polynomial occurs at zero frequency for the

low-pass case and at zero fractional bandwidth for the band-pass case; therefore $|\Delta|_{\min} = U_0$ for this response shape.

When each of the filter elements (reactances in the low-pass ladder and resonators in the band-pass case) has the same *finite* Q, then formation of (7) is still required but the n left-half-plane $j\omega/\omega_\beta$ roots of the desired relative attenuation must first be modified by reducing the magnitude of the real part of each root by an amount equal to the normalized unloaded decrement (inverse normalized unloaded Q) of each element.[1] The resulting modified or "predistorted" root values are then used in the n factors that are multiplied out to form (7). For this case, wherein modified root values are used, it should be realized that the resulting equation is not the phasor of our desired relative attenuation magnitude shape; it is instead the phasor corresponding to a "predistorted" magnitude shape.[1]

5.2 Continued-Fraction Expansion Procedure

The resulting coefficients of (7) can now be used directly to obtain the required R, L, C, and M values for the ladder networks of Figures 3 and 4 when either infinite-Q or uniformly finite-Q elements are used in the networks.

One procedure, of which the mathematical basis will be given in section 6, is as follows: the fraction given in (8) below is formed by simply writing the first, third, fifth, et cetera, terms of (7) as its numerator and writing the second, fourth, sixth, et cetera, terms of (7) as the denominator:

$$\frac{\left(j\frac{X}{X_\beta}\right)^n + U_{n-2}\left(j\frac{X}{X_\beta}\right)^{n-2} + U_{n-4}\left(j\frac{X}{X_\beta}\right)^{n-4} + \dots}{U_{n-1}\left(j\frac{X}{X_\beta}\right)^{n-1} + U_{n-3}\left(j\frac{X}{X_\beta}\right)^{n-3} + U_{n-5}\left(j\frac{X}{X_\beta}\right)^{n-5} + \dots}. \tag{8}$$

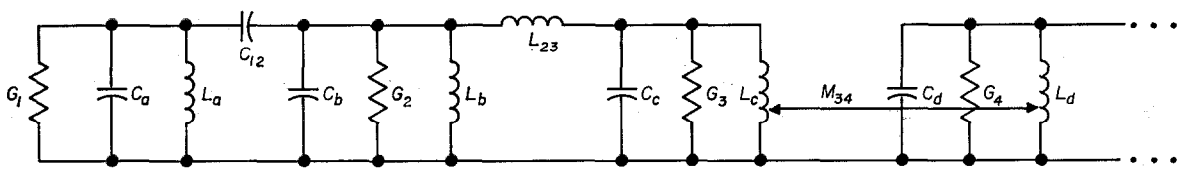

Figure 4A—Node networks using parallel resonant circuits. Each node Q is given by $Q_r = R_r/X_{0r}$ where the node capacitance (or inductance) is the capacitance or inductance existing across a node *when all other nodes are short-circuited.* For the three types of coupling shown: $K_{12} = C_{12}/(C_1C_2)^{1/2}$, $K_{23} = (L_2L_3)^{1/2}/L_{23}$, and $K_{34} = M_{34}/(L_3L_4)^{1/2}$. Any adjacent pair of resonators may be coupled by any of the three methods shown and then equivalent T's can be substituted for capacitive or inductive π's if advantageous. Each node must resonate at f_0 with all other nodes short-circuited.

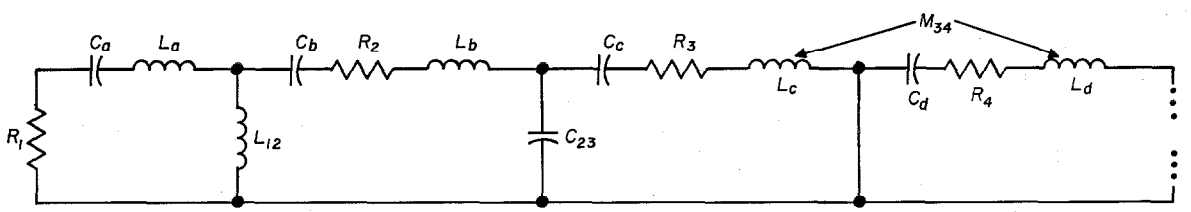

Figure 4B—For mesh networks using series resonant circuits. Each mesh Q is given by $Q_r = X_{0r}/R_r$, where the mesh inductance (or capacitance) is the resultant capacitance in series with a mesh when all other meshes are open-circuited. For the three types of coupling shown, $K_{12} = L_{12}/(L_1L_2)^{1/2}$, $K_{23} = (C_2C_3)^{1/2}/C_{23}$, and $K_{34} = M_{34}/(L_3L_4)^{1/2}$. Any adjacent pair of resonators may be coupled by any of the three methods shown; then, if advantageous, equivalent π's can be substituted for capacitive or inductive T's. Each mesh must resonate at f_0 with all other meshes open-circuited.

Figure 4—The small-percentage-band-pass ladders to which the design data of this paper can be directly applied and the relations between the 3-decibel-bandwidth normalized k's and q's and the L's, C's, M's, and R's. For both networks, $q = Q/(f_0/BW_{3db})$ and $k = K/(BW_{3db}/f_0)$.

When *n is odd*, this fraction is the short-circuited input impedance of the required reactance ladder, viewed from that end on which the loading is to be placed, and normalized to the value of this loading resistor; that is, for n odd, it is Z_{insc}/R. (By substituting the words open-circuited for short-circuited, admittance for impedance, and conductance for resistance, the dual input function for n odd will be obtained.)

When *n is even*, the fraction (8) is the normalized open-circuited input impedance of the required reactance ladder. (Again the dual words can be used to obtain the dual input function for n even.)

Next, (8) is expanded in continued-fraction form and the first resulting quotient of the continued-fraction expansion gives the necessary normalized impedance of the reactive part of the first arm of the ladder; the arm next to the loading resistor. The next quotient gives the normalized admittance of the susceptive part of the second arm of the ladder network. The third quotient gives the impedance of the reactive part of the third ladder arm, and so forth; impedance and admittance functions alternating with each other. (Again the dual words apply.)

The numerical part of the quotients produced by the above continued-fraction expansion are usually called normalized ladder-network coefficients, and will be symbolized by the letters a_1, a_2, a_3, ... To go from these a's to the normalized decrement-and-coefficient-of-coupling form of circuit constants, the following simple relations are used.

$$\left.\begin{aligned} d_1 &= (1/a_1) + d_0, \\ d_{2\to n} &= d_0 \\ k^2_{12} &= 1/a_1a_2 \\ k^2_{23} &= 1/a_2a_3 \\ k^2_{34} &= 1/a_3a_4 \\ &\cdots \end{aligned}\right\} \tag{9}$$

5.3 Resulting Numerical Design Data for Singly Loaded Ladders

5.3.1 Lossless-Element Design Data, n = 1 . . . 9

When the numerical work outlined by (7), (8), and (9) is accomplished, the design data of Table 2 is obtained *for lossless-element* ladders that produce gaussian magnitude approximations up to the 9th order. It will be noted that the normalized end-element Q is given; this is simply the inverse of the normalized decrement. Also, it must be realized that the actual required coefficients of coupling and end decrements are obtained by multiplying the normalized values given in Table 2 by the normalizing bandwidth variable $\omega_{3\text{db}}$ for low-pass filters, or $BW_{3\text{db}}/f_0$ for band-pass structures.

The last column of Table 2 gives the grid-to-grid gain that will be obtained for the small-percentage band-pass case, wherein C_1 and C_n are independently chosen, and a voltage-controlled current generator drives one end of the ladder with output voltage appearing across the other

TABLE 2

nTH-ORDER GAUSSIAN-FILTER DESIGN DATA FOR "LOSSLESS" LADDERS LOADED ON ONE END ONLY

Order n	q_1	k_{12}	k_{23}	k_{34}	k_{45}	k_{56}	k_{67}	k_{78}	k_{89}	q_n	Gain $\frac{G_m}{2\pi BW_{3\text{db}}(C_1C_n)^{1/2}}$
1	1.0	—	—	—	—	—	—	—	—	—	1.000
2	0.3877	1.396	—	—	—	—	—	—	—	∞	0.7163
3	0.2334	2.452	0.9978	—	—	—	—	—	—	∞	0.5735
4	0.1638	3.532	1.561	0.9073	—	—	—	—	—	∞	0.4871
5	0.1237	4.688	2.112	1.356	0.8755	—	—	—	—	∞	0.4256
6	0.09796	5.923	2.680	1.767	1.277	0.8622	—	—	—	∞	0.3793
7	0.08018	7.234	3.276	2.176	1.625	1.241	0.8563	—	—	∞	0.3437
8	0.06727	8.618	3.899	2.594	1.960	1.556	1.223	0.8535	—	∞	0.3146
9	0.05754	10.07	4.552	3.027	2.296	1.850	1.520	1.214	0.8521	∞	0.2911

end of the ladder. Notice the interesting point that for constant end-resonator capacitances, transfer gain drops appreciably as the gaussian approximation order is raised.

For the low-pass and large-percentage-band-pass case, no zero-frequency gain column is given, since with infinite-Q elements the open-circuit voltage of the equivalent Thévenin generator will always appear across the output terminals.

5.3.2 *Uniformly Lossy Element Design Data, $n = 5$ and 8*

For the case of 5- and 8-pole singly loaded networks made up of *uniformly lossy elements*, Tables 3 and 4, respectively, give the normalized K's and Q's required to make the lossy networks produce 5th- and 8th-order gaussian approximations. To conserve space, the required q_1 and k's are presented for specific values of the normalized unloaded Q of the network elements that the engineer plans to use. Obviously, to obtain design data for any other values of normalized unloaded Q, the reader can interpolate between these values by constructing a graph from these data.

It is worth noting that elements having normalized unloaded Q's as low as 0.7 or 0.8, say, can be used practicably to build filters approximating gaussian response shapes.

The last two columns of Tables 3 and 4 give the resulting maximum transfer impedance $(V_{out}/I_{in})_0$ of the lossy network; the next-to-the-last column is normalized in a way making it most useful for small-percentage-band-pass circuits; whereas the last column is normalized in a way making it most useful for low-pass ladders.

In the next-to-the-last column, which gives the grid-to-grid gain for the small-percentage-band-pass case, C_1 and C_n are the independently chosen node capacitances of the first and last resonators and G_m is the transconductance of the driving generator.

In the last (low-pass-gain) column of Table 3, R_1 is the *total* required resistance shunting the loaded copacitor in the $n = 5$ low-pass ladder. In the corresponding column of Table 4, R_a is the *added* resistor placed in series with the end inductor in the $n = 8$ low-pass ladder.

A simple procedure that will guarantee correct connection of the driving generator and the load to ladders that have a shunt element at one or both ends is as follows:

(A) Completely design the ladder network including loading resistor with no consideration as to the actual generator or load configuration.

(B) An infinite-impedance current generator is drawn across the resistor at *either* end of the net-

TABLE 3

5TH-ORDER GAUSSIAN FILTER DESIGN DATA FOR UNIFORMLY DISSIPATIVE LADDERS LOADED ON ONE END ONLY*

$q_{2,3,4,5}$	q_1	k_{12}	k_{23}	k_{34}	k_{45}	Gain $\frac{}{G_m/2\pi B W_{3db}(C_1C_5)^{1/2}}$	$\frac{V_{out}/I_{in}}{R_1}$
∞	0.1237	4.688	2.112	1.356	0.8754	0.4255	1.000
5.877	0.1351	4.219	1.931	1.267	0.8354	0.3122	0.6974
2.938	0.1488	3.752	1.755	1.184	0.7991	0.2256	0.4786
1.469	0.1866	2.831	1.422	1.049	0.7416	0.1124	0.2158
0.9795	0.2501	1.938	1.139	0.9482	0.7116	0.05392	0.09508
0.8396	0.3014	1.506	1.029	0.9405	0.7144	0.03770	0.06493
0.7346	0.3792	1.056	0.9156	1.003	0.7778	0.02731	0.04842
0.6905	0.4368	0.7250	0.4752	0	1.563	0	—

* To conserve space, this design information is presented for specific values of normalized unloaded Q. To obtain the design data for any normalized unloaded Q, the reader should construct a graph (from these data) for q_1 and each $k_{r(r+1)}$ versus $q_{2,3,4,5}$.

work and open-circuit output voltage terminals are then drawn across the resistor appearing at the other end of the network; it is the ratio of this open-circuit output voltage to this infinite-impedance input current that is given in the last two columns of Tables 3 and 4.

(C) The actual equivalent current generator to be used will almost always have some shunt resistance and shunt capacitance associated with it: therefore divide the shunt R and C of the input node into two parts, one part equal to that which of necessity will be supplied by the generator to be used, the remaining part to be supplied by the circuit designer. An equivalent procedure is used at the load end of the network to find that part of the last node or mesh that the circuit designer must supply.

6. *Reflection Coefficient and Its Application to the Design of Networks Loaded at Both Ends*

In his classic 1935 paper[1] Darlington presented a basic procedure for synthesizing reactive networks resistively loaded on both ends (in fact, it is one of the limiting cases of this general Darlington procedure that is the basis for that given in section 5 for singly loaded networks). One way of describing the fundamentals of the Darlington procedure is given below.

It is a basic fact that if one knows the equation for the required phasor voltage or current reflection coefficient of a purely reactive ladder terminated by a resistor, it is possible to obtain from this equation the much-simpler expression for the short-circuited (or open-circuited) input impedance (or admittance) of this same network. Then, if there are no finite-frequency points of infinite attenuation, a simple continued-fraction expansion of this input immittance will give, consecutively, the required element values for each reactive arm of a ladder network that will satisfy the originally specified phasor reflection coefficient.

With the above tool available, then to synthesize a network producing the gaussian magnitude approximation, the problem that must be solved is: How does one start with the shape of the magnitude of a desired relative attenuation and obtain from it the corresponding phasor reflection coefficient of a terminated reactive network?

6.1 Formation of Reflection Coefficient Magnitude

Because a purely reactive terminated network is specified, the solution of this problem is straightforward in principle—all the power accepted by the input terminals of the network must appear across the resistive load, where the desired relative attenuation shape must be produced; one can thus use the well-known relation between the following three quantities: the power

TABLE 4

8th-Order Gaussian Filter Design Data for Uniformly Dissipative Ladders Loaded on One End Only*

$q_{2\to 8}$	q_1	k_{12}	k_{23}	k_{34}	k_{45}	k_{56}	k_{67}	k_{78}	Gain $\frac{G_m/2\pi BW_{3db}(C_1C_8)^{1/2}}{}$	$\frac{V_{out}/I_{in}}{R_a}$
∞	0.06727	8.618	3.899	2.594	1.960	1.556	1.223	0.8535	0.3146	1.000
5.877	0.07313	7.847	3.575	2.404	1.841	1.483	1.179	0.8295	0.2042	0.6106
2.938	0.08011	7.077	3.253	2.218	1.727	1.414	1.139	0.8080	0.1301	0.3647
1.469	0.09901	5.544	2.621	1.863	1.522	1.300	1.076	0.7723	0.05047	0.1219
0.9795	0.1296	4.023	2.012	1.546	1.365	1.230	1.039	0.7469	0.01849	0.03702
0.8396	0.1532	3.268	1.718	1.410	1.320	1.225	1.035	0.7380	0.01109	0.01968
0.7346	0.1874	2.508	1.418	1.278	1.312	1.272	1.057	0.7347	0.006679	0.01017
0.6675	—	—	—	—	—	—	0	—	0	—

* To conserve space, this design information is presented for specific values of normalized unloaded Q. To obtain the design data for any normalized unloaded Q, the reader should construct a graph (from these data) for q_1 and each $k_{r(r+1)}$ versus $q_{2\to 8}$.

P_g *available* from a resistive generator, the power P accepted by a complex input immittance, and the magnitude squared of the reflection coefficient between this resistive generator and this complex input immittance; namely,

$$|P/P_g| = 1 - |\Gamma|^2. \qquad (10)$$

Simple manipulation of (10) results in the important form,

$$|\Gamma|^2 = \frac{|P_p/P| - |P_p/P_g|}{|P_p/P|}, \qquad (10A)$$

where P_p is the power accepted by the network at that frequency at which *peak* power is accepted.

Since both P, the accepted power at any frequency, and P_p, the accepted power at the peak frequency, are delivered to identically the same load resistance, their ratio is of course also equal to $|V_p/V|^2$, which is the equation for the magnitude squared of our desired relative attenuation shape. The equation $|P_p/P|$ in (10A) is thus known because the desired magnitude shape is specified.

The quantity $|P_p/P_g|$ in (10A) is the ratio of accepted power at the peak response frequency to the maximum power available from the resistive generator and is, therefore, a simple ratio that must be chosen; any value between unity and zero may be used. Usually, for networks resistively loaded on both ends, it is desired that the peak-frequency output be equal to the maximum power available from the generator and $|P_p/P_g|$ is set at unity. For networks resistively loaded on one end only, no power is delivered to the load; here, $|P_p/P_g|$ is set at zero. (This case was considered in section 5.)

The above explains the transformation from the specified gaussian-approximation relative-attenuation-shape equation (6) to the corresponding magnitude squared of the voltage or current reflection coefficient that must be possessed by a purely reactive resistively terminated network. It is worth rewriting (10A) in a form stressing the important role that $|\Delta|_{\min}$ of (5) plays in the numerator of (10A); by using the form of (5) for the denominator of (10A), it can be written

$$|\Gamma|^2 = \frac{M^2 - |\Delta|^2_{\min}\,|P_p/P_g|}{M^2}. \qquad (10B)$$

6.2 Determination of Phasor Reflection Coefficient

The next problem is to obtain the *phasor* reflection factor associated with the magnitude (10B). The phasors for the denominator and numerator of (10B) can be considered separately.

First taking the denominator of (10B), a solution is needed for the X/X_β roots of the denominator (there are $2n$ of them), they must be multiplied by j, and then, because this denominator is the polynomial part of (5), the physically realizable transfer function, the n *left*-half-plane jX/X_β roots must be chosen to form the n root factors to be multiplied out for the phasor denominator. For the case of infinite-Q elements, these denominator roots are, of course, those already given in Table 1; for uniformly dissipative network elements, these denominator roots are the predistorted roots formed by reducing the magnitude of the real part of the Table-1 roots by the normalized decrement of each element.

Next consider the numerator of (10B); this equation indicates that its numerator is obtained by first forming the magnitude of the already-obtained predistorted phasor-denominator polynomial. The minimum value $|\Delta|_{\min}$ of the polynomial part of this equation must be found and then from this polynomial, the product $|\Delta|^2_{\min} \times |P_p/P_g|$ must be subtracted. Now a solution can be found for the X/X_β roots of this new polynomial. These roots are then multiplied by j, and n of the resulting jX/X_β roots are chosen to form the required n root factors. Here a slight complication arises—since this numerator is not a physical transfer or input function, these n roots can be chosen in a variety of ways, always keeping in mind, however, that the phasor formed from the roots must have the original numerator of (10A) as its resulting magnitude. In this paper there will first be chosen all the n right-half-plane roots to form a phasor corresponding to the numerator of (10B).

When the above root factors are multiplied out, a phasor reflection factor corresponding to (10B) can now be written as

$$\Gamma = \frac{\left(j\frac{X}{X_\beta}\right)^n - V_{n-1}\left(j\frac{X}{X_\beta}\right)^{n-1} + V_{n-2}\left(j\frac{X}{X_\beta}\right)^{n-2} - V_{n-3}\left(j\frac{X}{X_\beta}\right)^{n-3} + \ldots V_0}{\left(j\frac{X}{X_\beta}\right)^n + U_{n-1}\left(j\frac{X}{X_\beta}\right)^{n-1} + U_{n-2}\left(j\frac{X}{X_\beta}\right)^{n-2} + U_{n-3}\left(j\frac{X}{X_\beta}\right)^{n-3} + \ldots U_0}, \qquad (11)$$

where the U's and V's are the numerical coefficients that result when the n root factors of the denominator and numerator, respectively, are multiplied out.

6.4 Determination of Short- or Open-Circuit Input Immittance

From the above phasor voltage or current reflection coefficient, the corresponding *terminated* normalized input impedance or admittance can immediately be written; it is the ratio of the denominator *plus* numerator of (11) to the denominator *minus* numerator of (11).

The expansion of this terminated input immittance is quite tedious compared to expansion of the corresponding short- or open-circuit immittance and it is therefore highly desirable to form the latter function directly from (11)—this is accomplished by omitting the 2nd, 4th, 6th, . . . terms in the numerator and the 1st, 3rd, 5th, . . . terms in the denominator of the terminated input immittance; the resulting expression is (12), which can be formed directly from (11).

$$\frac{2\,(jX/X_\beta)^n + (U_{n-2} + V_{n-2})(jX/X_\beta)^{n-2} + \ldots}{(U_{n-1} + V_{n-1})(jX/X_\beta)^{n-1} + (U_{n-3} + V_{n-3})(jX/X_\beta)^{n-3} + \ldots}. \qquad (12)$$

When n is *odd*, this fraction is the short-circuited input impedance of the required reactance ladder, viewed from one end of the ladder, and normalized to the value of loading resistor R_a that will be used at this end; that is, for n odd, (12) is Z_{insc}/R_a. (By substituting the words open-circuited in place of short-circuited, admittance in place of impedance, and conductance in place of resistance, the dual input function for n odd will be obtained.)

When n is *even*, (12) is the normalized open-circuited input impedance of the required reactance ladder. (Again the dual words can be used to obtain the dual input function for n even.)

Next, (12) is expanded in continued-fraction form and the first resulting quotient of the continued-fraction expansion gives the normalized impedance that must be possessed by the reactive part of the first arm of the ladder (the arm next to the R_a loading resistor); the next quotient gives the normalized admittance of the susceptive part of the second arm of the ladder network; the third quotient gives the impedance of the reactive part of the third ladder arm, et cetera; impedance and admittance functions alternating. (Again the dual words apply.)

The numerical part of the quotients produced by the above continued-fraction expansion are usually called normalized ladder-network coefficients, which we will symbolize by a_1, a_2, a_3, ... To convert these a's to the normalized decrement and coefficient-of-coupling form of circuit constants, the simple relations of (13) are used.

$$\left.\begin{aligned} d_1 &= (1/a_1) + d_0 \\ d_{2\to(n-1)} &= d_0 \\ k^2_{12} &= 1/a_1a_2 \\ k^2_{23} &= 1/a_2a_3 \\ k^2_{34} &= 1/a_3a_4 \\ &\cdots \end{aligned}\right\} \qquad (13)$$

6.3 Determination of Short- (Open-) Circuit Input Immittance of Other End of Network

In the above procedure, the far-end loading resistor has in effect been removed by short- or

open-circuiting the ladder; it is therefore necessary to use an additional step to determine the required loading. A recommended procedure is as follows: To obtain the numerator of the phasor reflection factor (11), n of the $2n$ numerator roots of (10B) were picked in conjugate pairs. If the other n *mirror image* (with respect to the j axis) roots are now used to form the numerator of (11), the required phasor reflection factor and coefficients of coupling are obtained from:

$$\left.\begin{aligned} d_n &= (1/a_{\mathrm{I}}) + d_0 \\ d_{(n-1)\to 2} &= d_0 \\ k^2{}_{n(n-1)} &= 1/a_{\mathrm{I}}a_{\mathrm{II}} \\ k^2{}_{(n-1)(n-2)} &= 1/a_{\mathrm{II}}a_{\mathrm{III}} \\ &\cdots \end{aligned}\right\} \qquad (14)$$

the required loaded decrement of the last arm, d_n, was the desired information and, as a check

TABLE 5

nTH-ORDER ZERO-POWER-LOSS GAUSSIAN FILTER DESIGN DATA FOR LOSSLESS-ELEMENT LADDERS RESISTIVELY LOADED ON BOTH ENDS

n	q_1	k_{12}	k_{23}	k_{34}	k_{45}	k_{56}	k_{67}	k_{78}	k_{89}	q_n
1	1.0	—	—	—	—	—	—	—	—	—
2	0.4718	0.9870	—	—	—	—	—	—	—	2.176
3	0.2609	2.173	0.7460	—	—	—	—	—	—	2.213
4	0.1768	3.270	1.426	0.6929	—	—	—	—	—	2.240
5	0.1309	4.431	1.993	1.258	0.6748	—	—	—	—	2.249
6	0.1024	5.668	2.566	1.686	1.194	0.6674	—	—	—	2.253
7	0.08314	6.979	3.163	2.101	1.562	1.165	0.6641	—	—	2.254
8	0.06934	8.363	3.787	2.522	1.904	1.503	1.152	0.6626	—	2.255
9	0.05904	9.816	4.440	2.955	2.242	1.804	1.471	1.145	0.6619	2.255

seen looking into the other end of the network will be obtained, normalized to the loading resistor that must be used at this other end.

Identical numerical coefficients will result from either set of roots but, with the mirror-image set, the signs of the 2nd, 4th, 6th, . . . terms in the numerator of (11), will be opposite from those obtained with the original root set.

Thus, when the short- (open-) circuit input immittance function for this other end of the network is formed, it will be exactly in the form of (12) but the denominator terms will be formed by the *differences* instead of the sums of the indicated U's and V's.

Continued-fraction expansion of this new function will give the ladder network arm impedances normalized to the terminating resistor at this far end of the network. The numercial parts of the quotients of the continued-fraction expansion give a new set of ladder network coefficients a_{I}, a_{II}, a_{III}, . . . and the element decrements of the numerical work, the corresponding normalized k's of (14) should be identical with those of (13). It should be remembered that d_0 is the normalized uniform unloaded decrement of each network element; that is, $G_0/\omega_{3\mathrm{db}}C$ and $R_0/\omega_{3\mathrm{db}}L$ for the low-pass reactances and $Q_0/(f_0/BW_{3\mathrm{db}})$ for the band-pass resonators that are to be used.

6.4 NUMERICAL DESIGN DATA FOR DOUBLY-LOADED LADDERS PRODUCING MAXIMUM POWER TRANSFER

6.4.1 Lossless-Elements Design Data n = 1 . . . 9

When the numerical work outlined by (10B), (11), (12), (13), and (14) is accomplished, the design data of Table 5 are obtained for lossless-element ladders that produce gaussian magnitude approximations up to the 9th order.

As with all the design data presented in this paper, these are 3-decibel-bandwidth normalized values, for the band-pass case, the actual required end Q's are obtained by multiplying the q

values by the inverse of the desired BW_{3db}/f_0 and the actual required K's are obtained by multiplying the k values by the desired BW_{3db}/f_0. For the low-pass case, the normalizing bandwidth variable is ω_{3db}.

These designs all give zero midfrequency power loss; at the midfrequency of the pass band, all the power available from the equivalent resistive generator is delivered to the resistive load. From this fact, both band-pass and low-pass transfer impedances or gains can be simply calculated.

In practice, this lossless-element design data of Table 5 are mainly applicable to low-pass and large-percentage-band-pass filters because the assumption of infinite normalized unloaded Q is almost satisfied for these cases. (It will be remembered that the normalized unloaded Q for the inductors of a low-pass ladder is $q_0 = \omega_{3db}L/R_0$).

TABLE 6

5TH–ORDER MINIMUM–POWER–LOSS GAUSSIAN FILTER DESIGN DATA FOR UNIFORMLY DISSIPATIVE LADDERS RESISTIVELY LOADED ON BOTH ENDS*

$q_{01,2,3,4,5}$	q_1	k_{12}	k_{23}	k_{34}	k_{45}	q_5	Band-Pass Power Loss in Decibels	Low-Pass $\frac{V_{out}/I_{in}}{R_1}$
∞	0.1309	4.431	1.993	1.258	0.6748	2.249	0	0.500
5.877	0.1434	3.974	1.821	1.178	0.6459	1.667	3.30	0.349
2.938	0.1586	3.518	1.654	1.103	0.6201	1.322	6.84	0.240
1.469	0.2014	2.622	1.345	0.9795	0.5797	0.9300	14.5	0.109
0.9795	0.2762	1.770	1.098	0.9091	0.5583	0.7151	23.0	0.0493
0.8396	0.3382	1.379	1.016	0.9147	0.5613	0.6443	27.6	0.0348
0.7346	0.4323	0.9723	0.9267	1.028	0.6292	0.5933	32.4	0.0285
0.6905	0.4368	0.7250	0.4752	0	1.563	0.6905	∞	—

* To conserve space, this design information is presented for specific values of normalized unloaded Q. To obtain the design data for any normalized unloaded Q, the reader should construct a graph (from these data) for q_1 and each $k_{r(r+1)}$ versus $q_{01,2,3,4,5}$.

TABLE 7

8TH–ORDER MINIMUM–POWER–LOSS GAUSSIAN FILTER DESIGN DATA FOR UNIFORMLY DISSIPATIVE LADDERS RESISTIVELY LOADED ON BOTH ENDS*

$q_{01\to8}$	q_1	k_{12}	k_{23}	k_{34}	k_{45}	k_{56}	k_{67}	k_{78}	q_8	Band-Pass Power Loss in Decibels	Low-Pass $\frac{V_{out}/I_{in}}{R_a}$
∞	0.06934	8.363	3.787	2.522	1.904	1.503	1.152	0.6626	2.255	0	0.500
5.877	0.07552	7.600	3.467	2.336	1.789	1.433	1.112	0.6448	1.659	4.30	0.305
2.938	0.08292	6.837	3.150	2.155	1.681	1.370	1.076	0.6286	1.310	8.76	0.183
1.469	0.1032	5.318	2.530	1.813	1.487	1.264	1.019	0.6016	0.9204	18.3	0.0609
0.9795	0.1365	3.814	1.939	1.515	1.347	1.203	0.9848	0.5815	0.7078	28.6	0.0185
0.8396	0.1628	3.070	1.659	1.393	1.312	1.200	0.9791	0.5739	0.6341	34.1	0.00984
0.7346	0.2018	2.325	1.376	1.282	1.321	1.2478	0.9948	0.5695	0.5738	39.8	0.00508
0.6675	—	—	—	—	—	—	0	—	—	∞	—

* To conserve space, this design information is presented for specific values of normalized unloaded Q. To obtain the design data for any normalized unloaded Q, the reader should construct a graph (from these data) for q_1 and each $k_{r(r+1)}$ versus $q_{01\to8}$.

6.4.2 Uniformly-Lossy-Element Design Data
n = 5 and 8

For small-percentage-band-pass circuits, the normalized unloaded resonator q_0 is $q_0 = Q_0/(f_0/BW_{3db})$ and seldom is this q_0 greater than 10, in many practical cases the normalized value being as low as 2 or 3; thus the infinite-unloaded-Q assumption can definitely not be made. When the gaussian-approximation root positions of Table 1 are predistorted by $1/q_0$ and the synthesis procedure of section 6 is carried out, the design data of Table 6 results for 5th-order lossy gaussian ladders and the design data of Table 7 results for 8th-order lossy gaussian ladders that work between a resistive generator and a resistive load and produce minimum midfrequency power loss for the given unloaded element Q that is used. The type of gain information given in the last column of these tables is identical with that described in detail for Tables 3 and 4.

7. Design Examples

7.1 Low-Pass-Filter Example

7.1.1 Required: A 5th-order low-pass gaussian filter having a 3-decibel-down bandwidth of 1.32 megacycles per second.

7.1.2 It is economically and mechanically feasible to use inductors having an unloaded Q value, measured at the 3-decibel-down frequency, of 100; this is, of course, the low-pass normalized unloaded element Q, or q_0. From the first column of Tables 3 or 6 (which will be the abscissa for graphs that the reader can prepare from these tables), it is seen that a Q of 100 will result in a set of required k's and end q's that are negligibly different from the infinite-unloaded-Q set. [The exact required values can be read from the prepared graph (Figure 5), but for this example the infinite-unloaded-Q set will be used.]

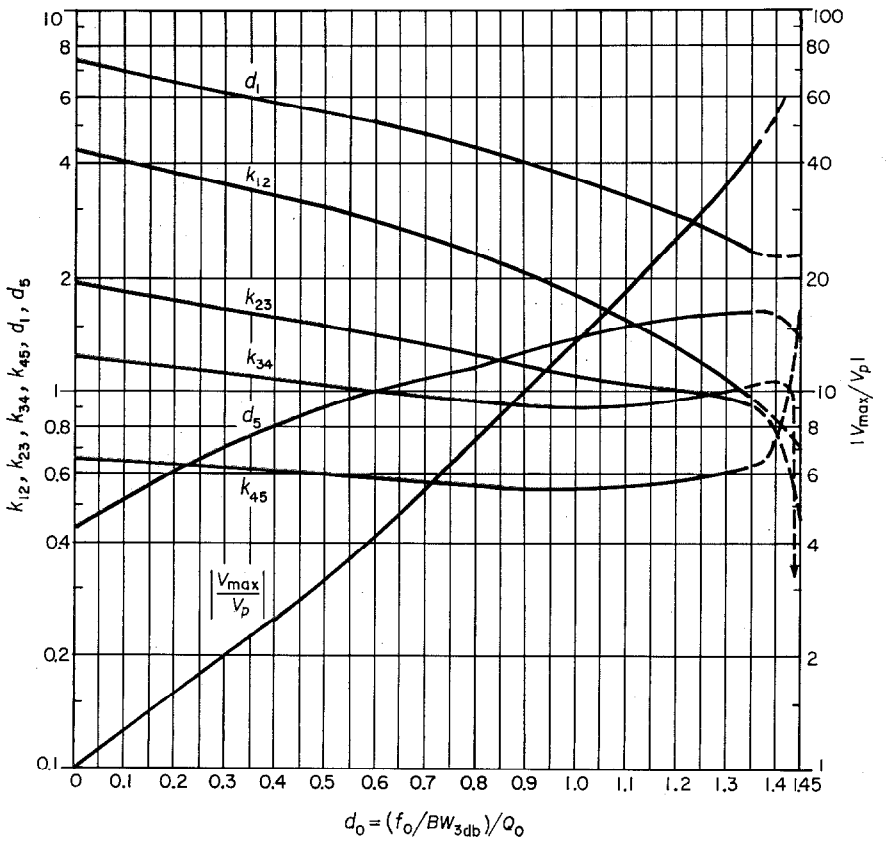

Figure 5—Minimum-transducer-loss 3-decibel-down normalized k's and q's required to produce an $n = 5$ gaussian-approximation amplitude shape. $d = (f_0/BW_{3db})/Q$ and $k = K/(BW_{3db}/f_0)$.

7.1.3 A filter loaded on only one end is more critically dependent for its proper operation on the exact adjustment of the single loading resistor and the k's than is a doubly loaded network. For this reason, the decision is made to use a doubly loaded design; Table 6 will be used.

7.1.4 To absorb the shunt capacitances associated with the equivalent generator, the low-pass ladder with a shunt capacitance for its first element will be used.

7.1.5 It is worth noting that if the equivalent generator and load resistances are produced by active components such as tubes or transistors, it is very important to make certain that their incremental output and input resistances stay truly constant in value over the whole driving signal cycle. Without the use of appreciable negative feedback around the individual active elements, this is hard to accomplish, and, in general, incremental output and input resistances at the low-current part of the signal cycle are appreciably higher than those at the high-current part. The safest procedure is to isolate the potentially nonlinear generator and load from the ends of the network and to use true resistors to provide the generator and load resistances.

7.1.6 At the point in the system where the filter is to be inserted, signal amplitude and gain considerations demand that the over-all low-pass filter have a transfer impedance of at least 75 ohms. From the low-pass transfer impedance column of Table 6, this requires that R_1 (the resultant loading resistance across C_1) be 150 ohms.

7.1.7 The low-pass design is now accomplished by starting with R_1 and working to the right, element by element.

(A) For low-pass ladders with a shunt capacitance for the first element,

$$q_1 = \omega_{3db} C_1 R_1.$$

Therefore,

$$\begin{aligned} 1/R_1C_1 &= (1/q_1)\,\omega_{3db} \\ &= (1/0.1309) \times 2\pi \times 1.32 \times 10^6 \\ &= 2\pi \times 10.1 \times 10^6. \end{aligned}$$

Therefore,

$$C_1 = 105 \text{ picofarads.}$$

$1/R_1C_1$ is of course the 3-decibel-down radian frequency of the R_1C_1 combination by itself; thus the 3-decibel-down frequency of this RC combination must equal 10.1 megacycles.

In the finished filter, a good test that C_1 and R_1 are correct is to experimentally measure the 3-decibel-down frequency of this combination alone.

(B) For this low-pass ladder,

$$k_{12} = 1/\omega_{3db}(C_1L_2)^{1/2}.$$

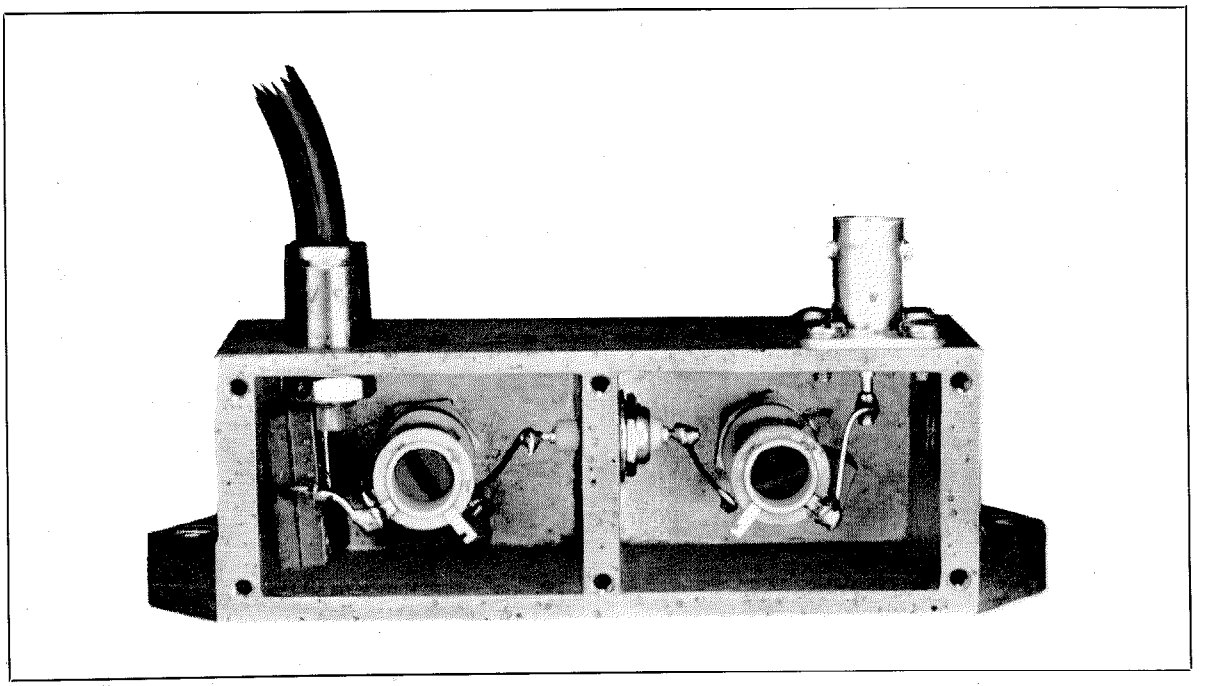

Figure 6—An embodiment of the low-pass gaussian-approximation filter synthesized in the low-pass design example of section 7.1. The illustration is actual size.

Therefore,

$$1/(C_1L_2)^{1/2} \times k_{12}\,\omega_{3db} = 4.431 \times 2\pi \times 1.32 \times 10^6 = 2\pi \times 5.85 \times 10^6.$$

Therefore,

$$L_2 = 7.05 \text{ microhenries.}$$

$1/(C_1L_2)^{1/2}$ is, of course, the resonant radian frequency of the C_1L_2 combination considered by itself; thus L_2 must resonate with the now-known C_1 at 5.85 megacycles.

In the finished filter, the best procedure for ascertaining that L_2 is correct is to experimentally measure the resonant frequency of C_1 and L_2.

(C) To obtain the third low-pass element,

$$1/(L_2C_3)^{1/2} = k_{23}\,\omega_{3db} = 2\pi \times 2.64 \times 10^6.$$

Thus, C_3 must resonate with L_2 at 2.64 megacycles;

$$C_3 = 520 \text{ picofarads.}$$

(D) and (E) Consecutive application of the k_{34} and k_{45} columns give the required adjacent arm resonant frequencies and element values as

$f_{034} = 1.66$ megacycles; $L_4 = 17.8$ microhenries,

$f_{045} = 0.89$ megacycles; $C_5 = 1780$ picofarads.

(F) Finally, the q_5 column gives the required 3-decibel frequency of the C_5R_5 combination alone as

$f_{3db5} = 0.588$ megacycles; $R_5 = 150$ ohms.

The design of the low-pass filter is now complete. Figure 6 is a photograph of an embodiment.

The experimentally observed performance of such a filter is of interest and Figure 7 is a composite picture showing some of the response characteristics of a filter similar to the above-designed unit but with a 0.84-megacycle 3-decibel-down bandwidth.

7.2 Band-pass-Filter Example

7.2.1 Required: A 5th-order band-pass gaussian-approximation filter for a carrier-centered double-sideband system. The required midfrequency is

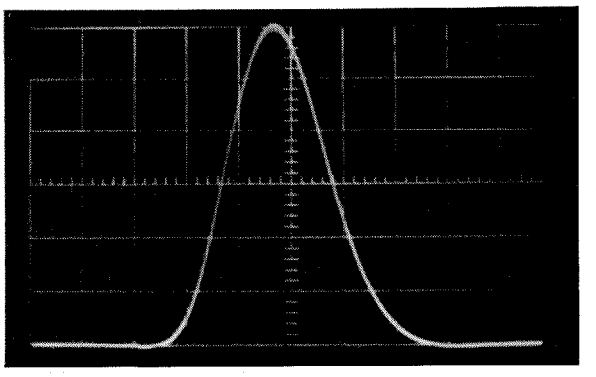

Figure 7A—The filter 3-decibel-down bandwidth was 0.840 megacycles and the sweep speed was 0.18 ± 10 percent microsecond per centimeter. A 0.18-microsecond pulse was the driving function.

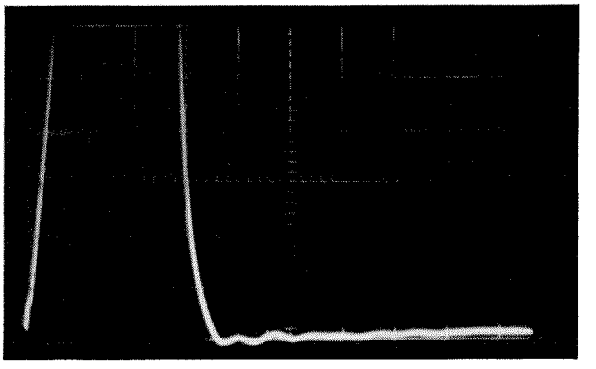

Figure 7B—Same impulse output as Figure 7A but with oscilloscope gain increased so that one vertical division is 1/100 of the peak impulse output; the undershoot and ringing shown are approximately 60 decibels down from peak output.

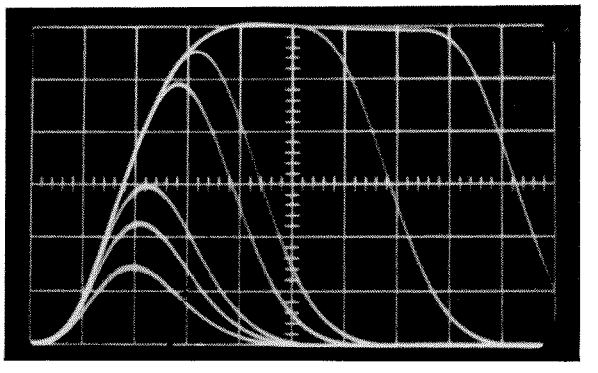

Figure 7C—Filter output as a function of pulse input width (constant input amplitude). The input pulse widths are 1.5, 1.0, 0.50, 0.40, 0.20, 0.15, and 0.10 microsecond. Sweep speed was 0.18 ± 10 percent microsecond per centimeter.

70 megacycles and the required 3-decibel-down bandwidth is 2.75 megacycles. The fractional 3-decibel bandwidth to which all the decrements and coefficients of coupling are normalized is therefore 1/25.5.

7.2.2 At 70 megacycles, it is practical and economical to use in the resonators commercial ferrite-slug-tuned solenoids having unloaded Q's in the 150-to-200 region. The silvered-mica capacitors to be used have Q's of approximately 1000. Therefore, the net resonator unloaded Q will be in the 130-to-170 region. To obtain the actual resonator unloaded Q, it is important to place the actual inductor and capacitor in the shielding compartment that will be used in the embodiment of the filter and then measure its unloaded 3-decibel bandwidth using a generator and detector very-loosely coupled to the shielded resonator. If the measured unloaded resonator Q were 150, say, the normalized unloaded Q would be 150/25.5 = 5.88. The design data given in the second row of Tables 3 and 6 could thus be used directly. As previously mentioned, the k's and end-element q's for any value of available resonator unloaded Q can be obtained by graphing the proper region of the tables.

7.2.3 The filter is to work between pentode tubes, and therefore a loading-on-one-end-only design could be used; however, because the resulting response shape is less sensitive to element-value changes when a loaded-on-both-ends design is used, this latter design will be adopted.

7.2.4 A 75-ohm resistor will be put between grid and cathode of the driven tube because transit-time and space-charge input impedance variations at the grids of vacuum tubes due to bias changes and aging are appreciable. If response shapes are to be reproduced with close tolerances, it is highly desirable not to have a filter resonator associated with this grid-to-cathode impedance. It is also decided to use an inductor between the grid and cathode to neutralize the input capacitance (approximately 13 picofarads) at this port. The bandwidth of the resulting single-tuned circuit it so broad that over the band of the filter it may be considered a pure 75-ohm resistive termination for a length of 75-ohm cable that can be used to connect the filter proper to the grid. Because it is properly terminated, the length of this cable is not critical.

7.2.5 A practical alignment procedure for multiple-resonant-circuit filters is as important as correct design—a recommended procedure[3] is available in the literature. The alternating maximums and minimums used in this procedure are more easily observed when the low-Q end of a filter is connected to the generator. In Table 6, resonator *1* is at the low-Q end of the filter; therefore, for alignment reasons, this end will be driven by the generator and the 75-ohm load will be transformed into the high-Q end (fifth) resonator of the filter (the transformation procedure will be discussed later).

7.2.6 System considerations require that a grid-to-grid voltage gain of at least unity be supplied by the tube-plus-filter circuit. Simple manipulation of the equation for load power over available generator power results in

$$\left|\frac{V_{\text{out}}}{E_{gk}}\right|_0 = G_m \frac{(R_L R_g)^{1/2}}{2}\left(\frac{P_L}{P_a}\right)^{1/2}, \qquad (15)$$

where R_g is the equivalent generator resistance and the ratio $|P_L/P_a|$ is the power gain (less than unity) that is given in decibels in the power loss column of Tables 5, 6, and 7. For the normalized unloaded Q of 5.88, Table 6 shows a midfrequency power loss of 3.3 decibels or P_L/P_a = 0.468. If the driving tube has a G_m of 12 000 micromhos, (15) shows that the generator impedance must be 820 ohms to obtain a grid-to-grid gain of unity.

7.2.7 For two reasons it is decided to place the first resonator of the filter directly in the plate circuit of the driving tube.

(A) The 820-ohm generator resistance is shunted by the tube-and-wiring output capacitance, approximately 4 picofarads or 570-ohms reactance. Thus, when resonated, the equivalent generator will have a Q of 1.44, or a normalized Q of 0.056. From Table 6 the normalized singly loaded Q of

[3] M. Dishal, "Alignment and Adjustment of Synchronously Tuned Multiple-Resonant-Circuit Filters," *Proceedings of the IRE*, volume 39, pages 1448–1455; November, 1951: Also, *Electrical Communication*, volume 29, pages 154–164; June, 1952. (Addendum, volume 29, page 292; December, 1952.)

resonator *1* must be 0.1309; the generator normalized Q is thus certainly not zero compared to this value and therefore one cannot consider the generator to be purely resistive and attempt by impedance transformation to couple it to this end resonator.

(B) Even if it were a truly resistive generator, it is probably impracticable to construct, as a separate entity, a transformer that would have negligible frequency response; that is, negligible normalized Q compared to the low singly loaded Q required for this end resonator.

7.2.8 In small-percentage-bandwidth filters, the midfrequency reactance of the inductance (or capacitance) of the *internal* resonators may be chosen independently of the response-frequency requirement or gain requirements—the choice of reactance level can be based on the desire to obtain maximum unloaded resonator Q and practical mechanical construction.

An inductor of 85-ohm reactance, requiring a total node capacitance of 27 picofarads will be used for these internal resonators.

With reference to the *end* resonators of a small-percentage-bandwidth filter the following applies:

(A) If a resistive generator or load is to be impedance transformed to load properly the first and/or last resonator, then here also the resonator reactance can be chosen on the basis of practical mechanical construction and high unloaded Q.

Since the 75-ohm resistive load is to be transformed to load properly the fifth resonator, this end resonator can be similar to the internal resonators; an inductor requiring a 27-picofarad total resonating capacitance.

(B) However, if the generator or load is to be connected directly across the first or last resonator, then the ratio of generator resistance to resonator reactance must be exactly such that the q_1 (or q_5) column in Table 6 is satisfied; a specific resonator reactance must be used if the generator resistance is fixed, or vice versa.

In the present example, the generator resistance has been fixed at 820 ohms and is to be placed directly across the first resonator. Realizing that $d_1 = d_g + d_0$, where d_g is the normalized decrement due to placing the generator resistance alone across the resonator, (16) can be simply derived and gives the required relation between the resonator reactance and the generator resistance.

$$X_{01}/R_g = (d_1 - d_0)\, BW_{3db}/f_0, \qquad (16)$$

where d_0 is the inverse of the q_0 column of Table 6 and d_1 is the inverse of the q_1 column.

Substitution of values in (16) results in $X_{01} = 220$ ohms, or $C_1 = 10$ picofarads.

7.2.9 Now that the total capacitances of each node have been set, it is necessary to decide the coupling mechanism to be used between adjacent nodes. Firm rules as to coupling mechanism choice are hard to make—in general, the designer's ingenuity, governed by the mechanical construction, can lead to a variety of choices. We will use capacitance coupling between the first and second nodes, a combination of capacitance coupling and aiding mutual-inductance coupling between the second and third nodes, capacitance coupling between the third and fourth nodes, mutual-inductance coupling between the fourth and fifth nodes, and high-side capacitance impedance transformation to load properly the fifth resonator by the 75-ohm resistive load.

7.2.10 Using the design data of the second row of Table 6, the network can now be designed.

In the steps below, the calculations give the coupling capacitance or mutual inductance necessary to produce a required coefficient of coupling. However, it is imperative that it be understood that the proximity of ground planes due to the shielding enclosures used in the embodiment of the filter network can appreciably affect the value of direct capacitance supplied by a capacitor and can even-more-strongly affect the value of self or mutual inductance supplied by an inductor or pair of inductors. Therefore, particularly when small values are called for, the actual coupling capacitors and/or inductors required in a filter cannot usually be directly obtained by Q-meter (for example) measurement of components; a recommended procedure[3] for experimentally setting each coefficient of coupling and each end Q is detailed in the literature. Because the referenced procedure

measures the bandwidth between two sharply defined response peaks with the filter components in the exact position they will occupy in the final embodiment, it is practical to set each coefficient to within 1 percent of its required value. Once the correct values have been obtained, Q-meter or physical-configuration measurements can then be used to *duplicate* these correct values.

(A) The required Q_1 is

$$Q_1 = q_1 (f_0/BW_{3db}) = 0.1434 \times 25.5 = 3.65.$$

We have already satisified this requirement by the use of (16) in step 7.2.8.

(B) The required coefficient of coupling between the first and second nodes is

$$K_{12} = k_{12} (BW_{3db}/f_0) = 3.974 \times 1/25.5 = 1/6.40.$$

The required high-side coupling capacitor is therefore

$$C_{12} = K_{12} (C_1C_2)^{1/2} = (1/6.40) (10 \times 27)^{1/2} = 2.57 \text{ picofarads.}$$

(C) The required coefficient of coupling between the second and third nodes is

$$K_{23} = k_{23} (BW_{3db}/f_0) = 1.821 \times 1/25.5 = 1/14.0 = 0.0714.$$

With the inductors as close together as the mechanical layout allows, the measured resulting coefficient of mutual inductance coupling is 0.0344 (this K_M is measured by the peak-bandwidth method[3]). The required capacitance coupling is therefore

$$K_{c23} = K_{23} - K_{M23} = 0.0714 - 0.0344 = 0.0370.$$

The required high-side coupling capacitor is therefore

$$C_{23} = K_{c23} (C_2C_3)^{1/2} = 0.0370 (27 \times 27)^{1/2} = 1.00 \text{ picofarad.}$$

(D) The required coefficient of coupling between the third and fourth nodes is

$$K_{34} = 1.178 \times 1/25.5 = 1/21.6.$$

Since only high-side capacitance coupling is to be used,

$$C_{34} = (1/21.6) (27 \times 27)^{1/2} = 1.24 \text{ picofarads.}$$

(E) The required coefficient of coupling between the fourth and fifth nodes is

$$K_{45} = 0.6459 \times 1/25.5 = 1/39.5 = 0.0254.$$

Since this coefficient is to be supplied by mutual-inductance coupling, a peak bandwidth measurement[3] is the recommended method for setting the physical spacing between inductors *4* and *5* to obtain this K_{45} value.

Because this particular coefficient has a major effect on the over-all filter 3-decibel-down bandwidth, the designer may wish to make the position of inductor number five slightly adjustable so that production-line adjustment of K_{45} can be used to set exactly the 3-decibel bandwidth of the filter.

(F) Finally Q_5, the singly loaded Q of the end resonator, must be set. From Table 6,

$$Q_5 = q_5 (f_0/BW_{3db}) = 1.667 \times 25.5 = 42.5.$$

This Q_5 is the resultant Q due to both the unloaded Q of the fifth resonator and the effect of the transformed resistance of the 75-ohm load. Simple manipulation of this relation leads to (17) for the required transformed resistance R_b:

$$X_{05}/R_b = (d_5 - d_0) (BW_{3db}/f_0). \quad (17)$$

Substitution of the present values in (17) leads to the required transformed resistance of R_b = 5030 ohms. Large impedance transformation as required here can be simply accomplished by connecting between the 75-ohm load R_L and top of the fifth resonator a high-side capacitor of reactance

$$X_t = (R_bR_L)^{1/2} = (5030 \times 75)^{1/2} = 613 \text{ ohms,}$$

therefore

$$C_t = 3.71 \text{ picofarads.}$$

With this simple transforming method, the voltage delivered to the load is slightly asymmetrical with respect to frequency, the high-frequency skirt of the response falling off less sharply than the low-frequency skirt—for small-percentage

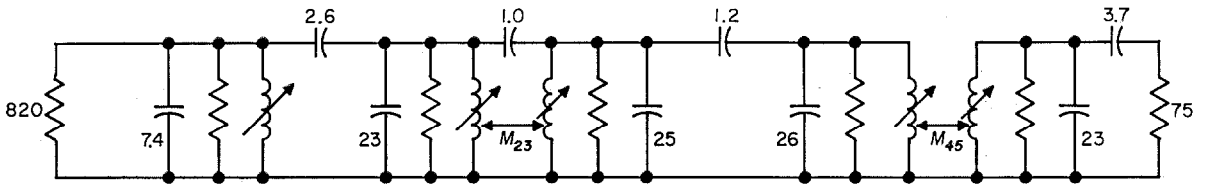

Figure 8A—The node network that was directly synthesized.

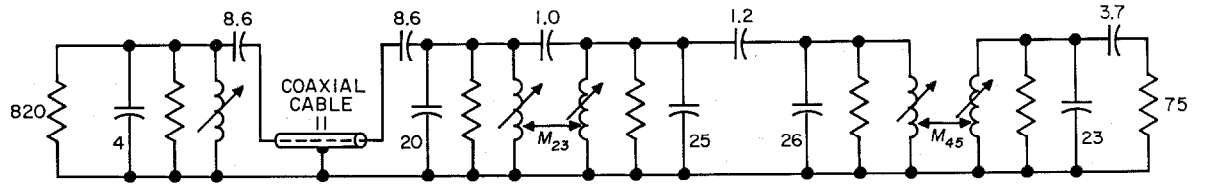

Figure 8B—An exactly equivalent network described in section 7.2 enables a piece of coaxial cable to be incorporated in the K_{12} circuit.

Figure 8—The electrical schematic of the 70-megacycle-midfrequency 5th-order-band-pass gaussian-approximation filter synthesized in the band-pass design example of section 7.2. Capacitances are in picofarads and resistances in ohms. The unlabeled resistors represent the equivalent losses of the unloaded resonators. The element values given show only two significant figures, whereas 2-to-5-percent accuracies are normally required for coefficient-of-coupling tolerances. This is done to stress the fact that the exact adjustment of these coefficients of coupling cannot usually be accomplished by measurements on components that are not in the exact physical position they will occupy in the finished filter. Instead, these K's must be set by a procedure equivalent to the peak-bandwidth-measuring procedure[3]. Similarly, an adequate alignment procedure must be evolved similar for example to that described[3] and illustrated in Figure 10 of this paper.

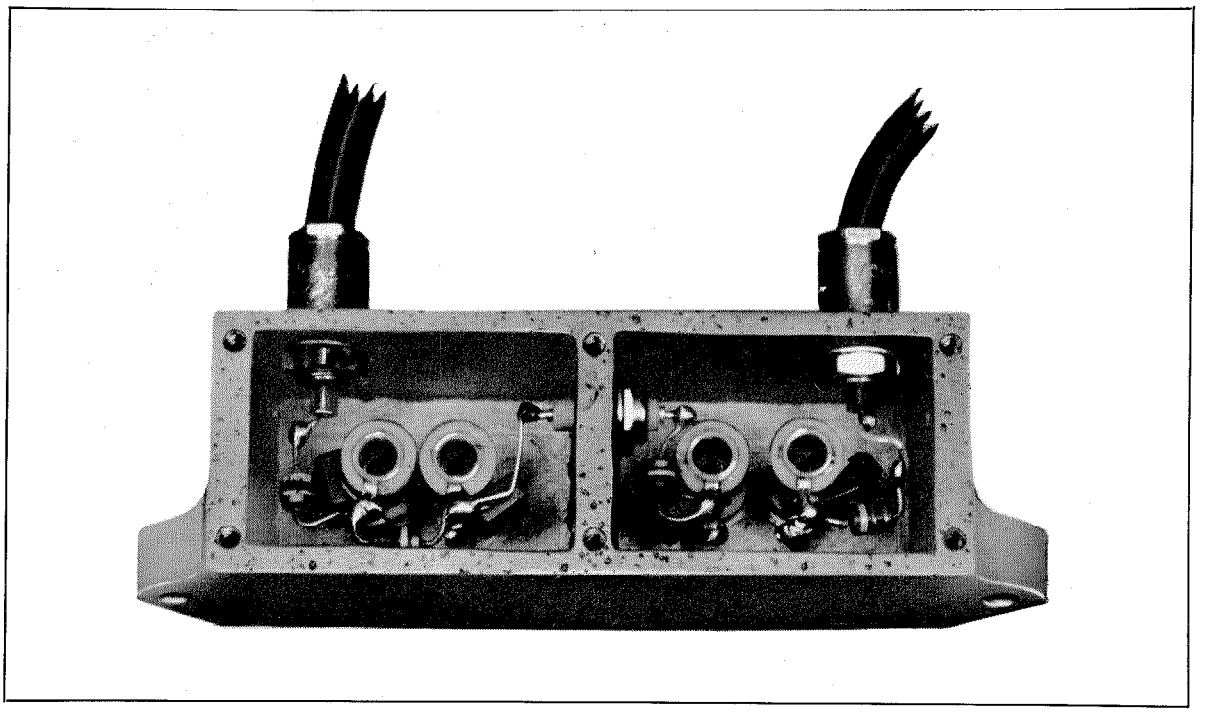

Figure 9—An embodiment of the 70-megacycle band-pass 5th-order gaussian-approximation filter synthesized in the band-pass design example of section 7.2. The first resonator of this filter is contained in another unit.

bandwidths, the resulting asymmetry can usually be neglected.

Figure 8A is a schematic of the resultant filter.

7.2.11 For manufacturing purposes, it is desirable that the filter be a separate passive entity. By using a 75-ohm cable connector on the load end of the filter, it is possible to physically separate this end from the rest of the equipment (see section 7.2.4). However, because the first resonator of the filter is connected directly to the plate of the driving tube, it is obviously not possible to separate physically this end of the filter from the rest of the equipment. If it is desirable to embody the last four resonators as a separate unit connected by a cable to the unit containing

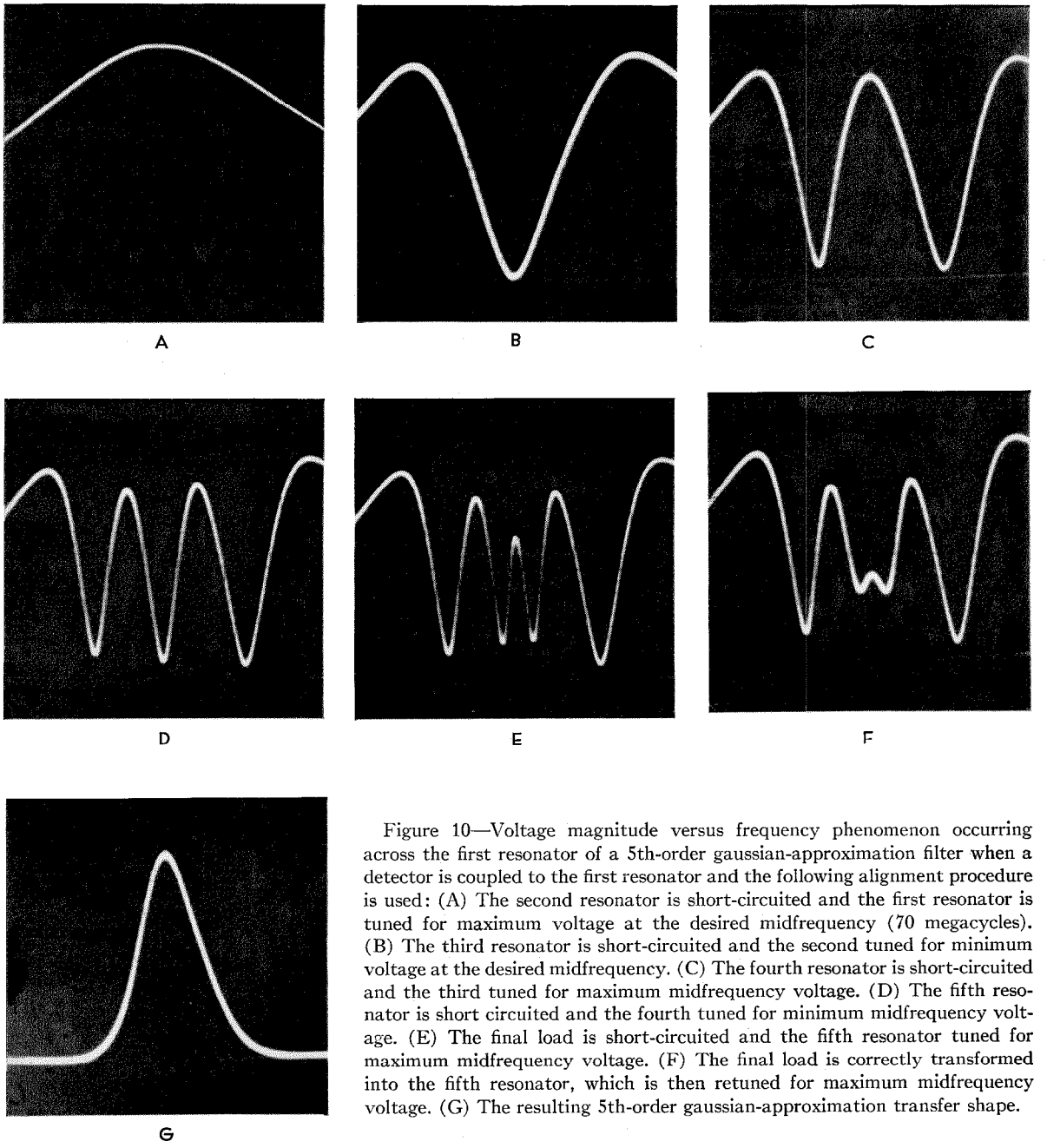

Figure 10—Voltage magnitude versus frequency phenomenon occurring across the first resonator of a 5th-order gaussian-approximation filter when a detector is coupled to the first resonator and the following alignment procedure is used: (A) The second resonator is short-circuited and the first resonator is tuned for maximum voltage at the desired midfrequency (70 megacycles). (B) The third resonator is short-circuited and the second tuned for minimum voltage at the desired midfrequency. (C) The fourth resonator is short-circuited and the third tuned for maximum midfrequency voltage. (D) The fifth resonator is short circuited and the fourth tuned for minimum midfrequency voltage. (E) The final load is short-circuited and the fifth resonator tuned for maximum midfrequency voltage. (F) The final load is correctly transformed into the fifth resonator, which is then retuned for maximum midfrequency voltage. (G) The resulting 5th-order gaussian-approximation transfer shape.

the first resonator, the following procedure can be used.

(A) Part of the node-to-ground capacitance of the first and second nodes in conjunction with the total C_{12} (2.57 picofarads) are used to form a capactive π.

(B) Transform this capacitive π to a capacitive T.

(C) Embody the shunt arm of this T by a piece of cable whose length (which must be very short compared to a wavelength, of course) is such as to supply the required shunt capacitance.

Figure 8B shows the filter schematic with this "coefficient-of-coupling cable" incorporated.

As will be noted, 4 picofarads of capacitance have been left across the 820-ohm generator resistance; this is the output capacitance of the driving tube. Thus the π that has been transformed into the T consisted of shunt legs of 3.4 picofarads and a high-side leg of 2.6 picofarards.

It is worth stressing once again that the capacitance values arrived at in step 7.2.10 and given to only two significant figures on Figure 8 are for guidance only—the coefficients of coupling and the end Q's should be experimentally adjusted and checked to plus-or-minus 2-percent accuracy by the procedures detailed elsewhere[3].

Figure 9 is a photograph of an embodiment wherein the last four resonators of an $n = 5$ gaussian intermediate-frequency filter are contained in one casting. The cable entering at the left supplies the 11 picofarads required by Figure 8B to satisfy K_{12} and the cable at the right leads to a 75-ohm resistive load.

Exact tuning of each node to the desired mid-frequency (70 megacycles) is, of course, imperative for proper filter operation. Figure 10 shows the resulting output voltage observed across the first resonator (by a loosely coupled detector) when the recommended tuning procedure[3] is applied; the last photograph shows the resulting transfer magnitude of the correctly aligned filter —no tuning controls were retouched to obtain this transfer picture.

Recent Telecommunication Development

Award for Automatic Radio Direction Finders in Aircraft

THE Professional Group on Aeronautical and Navigational Electronics of the Institute of Radio Engineers has given its 1959 Pioneer Award jointly to Henri G. Busignies and Francis L. Moseley "for their individual pioneering efforts to bring about the adoption of automatic radio direction finders for employment on aircraft."

Mr. Busignies, now president of ITT Laboratories, has spent practically his entire professional career in companies associated with the International Telephone and Telegraph Corporation. The first of over a hundred patents issued to him was on a direct-reading radio direction finder. His inventions predominantly concern direction finding, navigation, radar, and instrument landing, although many are in other branches of electronics.

Mr. Moseley, who is now president of F. L. Moseley Company, has received over 35 patents covering not only air navigation but also servo systems, control apparatus, data transmission, flight indicators, and electronics in general.

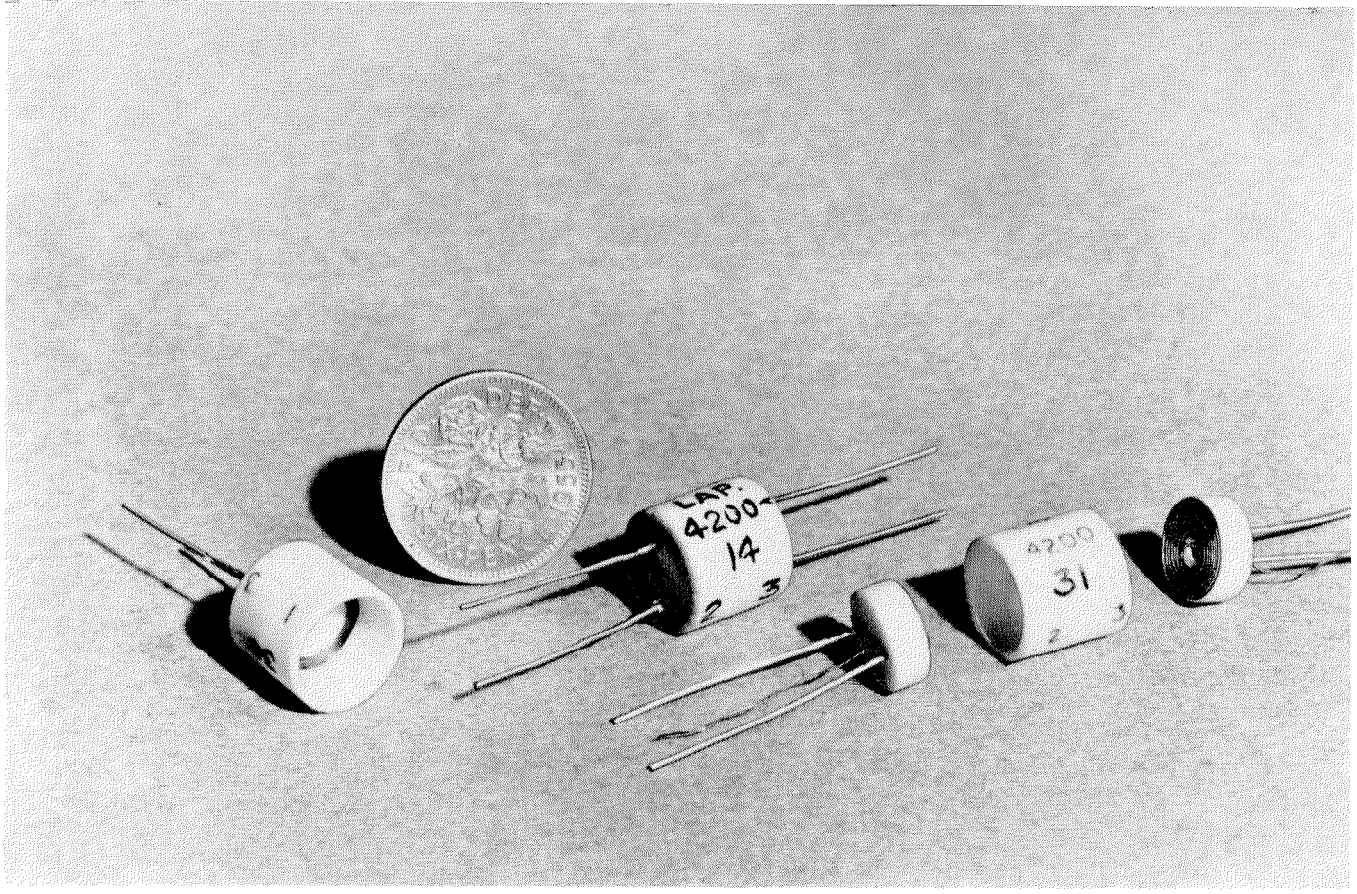

Figure 1—Constructional features of the transformer design.

Transformers for 70-Megacycle Intermediate-Frequency Amplifiers

By W. F. GLOVER and E. D. PEAKALL

Standard Telephones and Cables, Limited; London, England

REQUIREMENTS for wide-band intermediate-frequency amplifiers centred on 70 megacycles per second for microwave systems have created a demand for small transformers that can be manufactured to close limits of self-inductance and coupling coefficient.

1. Construction

The stability and accuracy necessary in transformers that were to be installed in amplifiers without subsequent adjustment led to the adoption of a ceramic tube and disc construction.

The two coils are spirally wound and mounted on ceramic discs that carry the terminal wires. One of the discs is then inserted at each end of the ceramic tube.

The inductance of each coil is adjusted to a precise value by withdrawing the inner end of the spiral winding through the hole in the ceramic disc. Fractional-turn adjustment is possible, and inductance changes of 0·003 microhenry can be made.

Figures 1 and 2 illustrate the transformer construction and Figure 3 the method of adjusting the inductance.

The coupling coefficient is adjusted on a test jig embodying the test circuit in Figure 4 and illustrated in Figure 5. In effect, the leakage inductance of the transformer is series-resonated with a capacitive load provided by the test jig.

The final adjustments are made permanent by sealing the discs with an epoxy resin.

The overall dimensions of the transformers are 0·437 inch (11·1 millimetres) in diameter and 0·406 inch (10·3 millimetres) long.

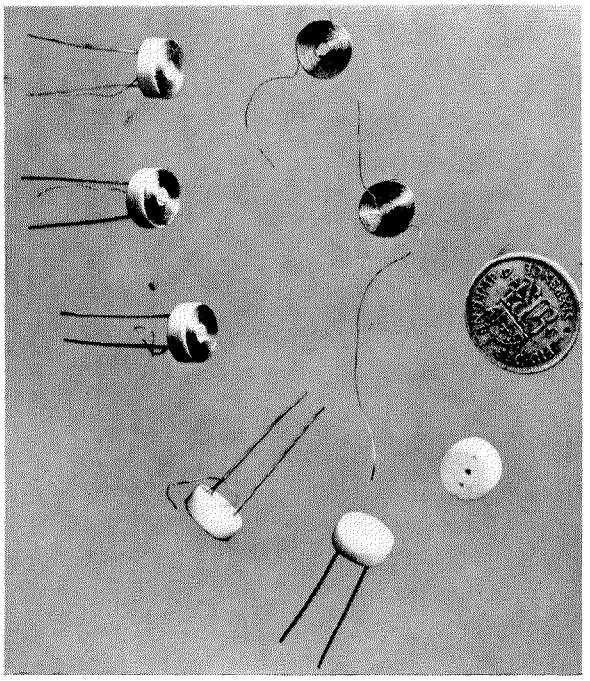

Figure 2—Coils, end discs, and assemblies.

2. *Electrical Performance*

Each spiral winding can be wound to an inductance in the range of 0·14 to 3·5 microhenries. The Q of the windings at 70 megacycles

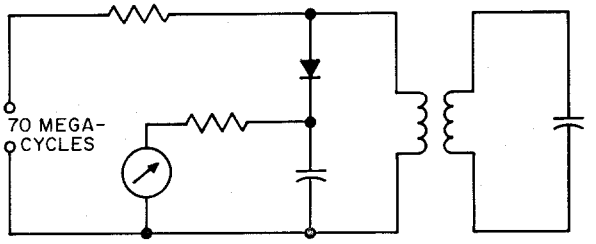

Figure 4—Test circuit used to adjust the transformer for coupling coefficient.

is about 50, but in general this is insignificant in relation to the circuit Q. The transformers can be made with coupling coefficients in the range 0·33 to 0·70.

The effect of capacitance between windings is reduced by using the same gauge wire for both windings and by mounting them in the tube so

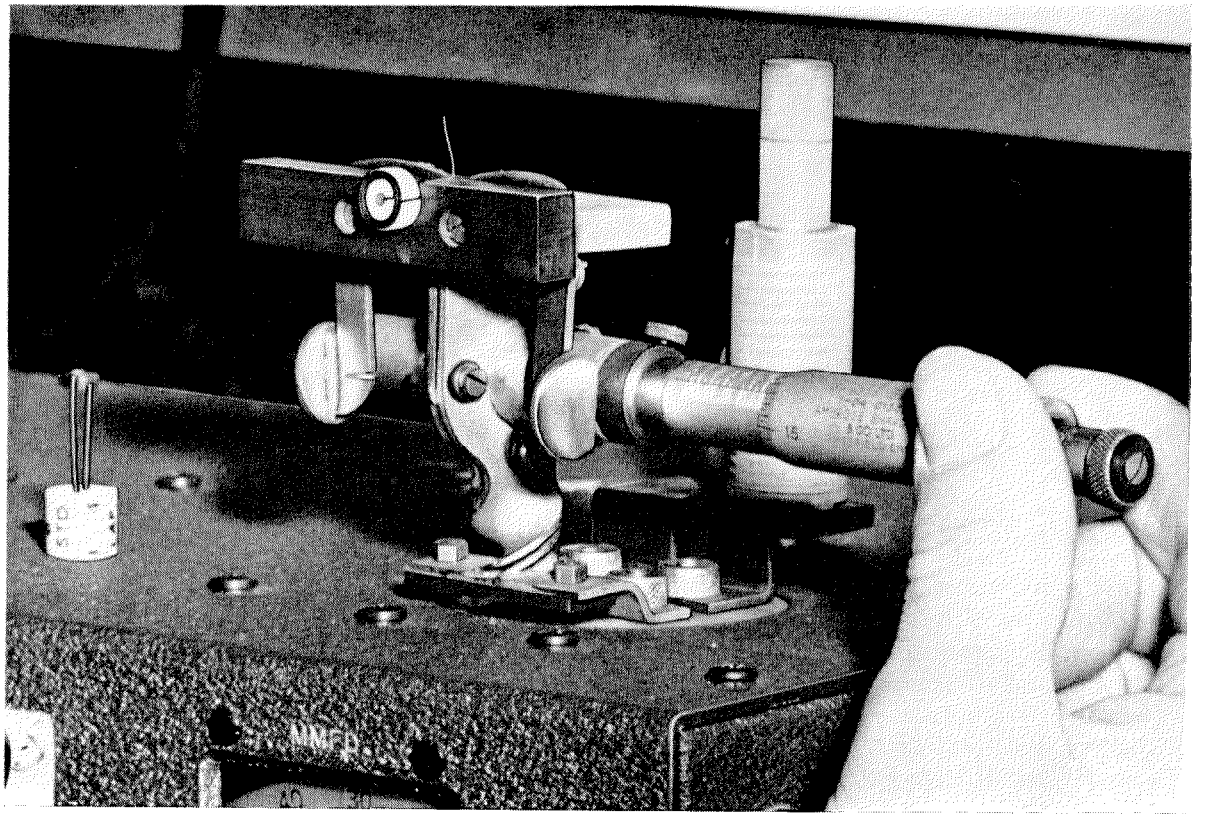

Figure 3—Adjusting self-inductance.

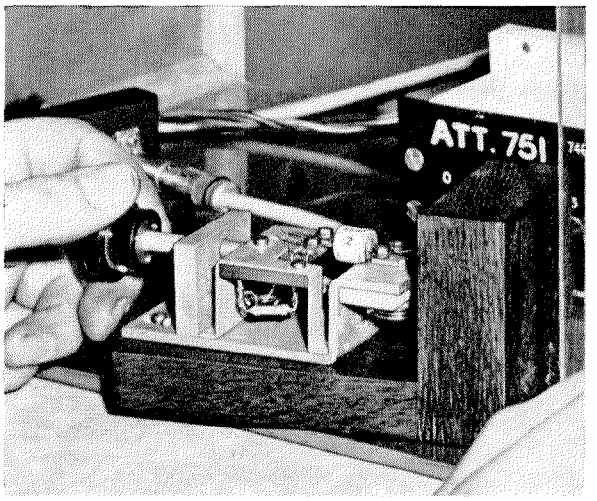

Figure 5—Adjusting coupling coefficient.

that the direction of winding is the same. The coils are always wound to the same outside diameter but the inside diameter varies according to the number of turns required. It follows, therefore, that if the outer ends of the two windings are at the same potential, the corresponding turns in each winding will be at approximately equal potentials.

In practice it is found that this condition is realised sufficiently to make interwinding capacitance effects of no circuit significance.

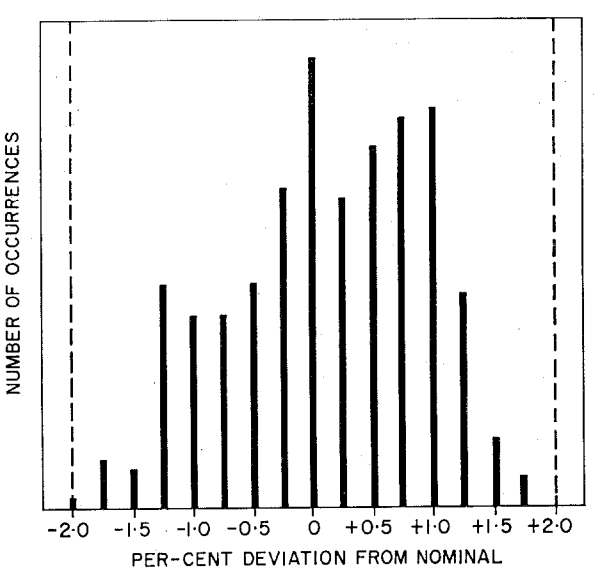

Figure 6—Histogram showing the per-cent deviation from the nominal value of self-inductance of the primary. The limits are set at 2 per cent.

3. Manufacture

Histograms showing the results of a production run on one type of transformer are shown in Figures 6, 7, and 8. This performance is typical of the product and indicates that the construction and method of manufacture are capable of close control.

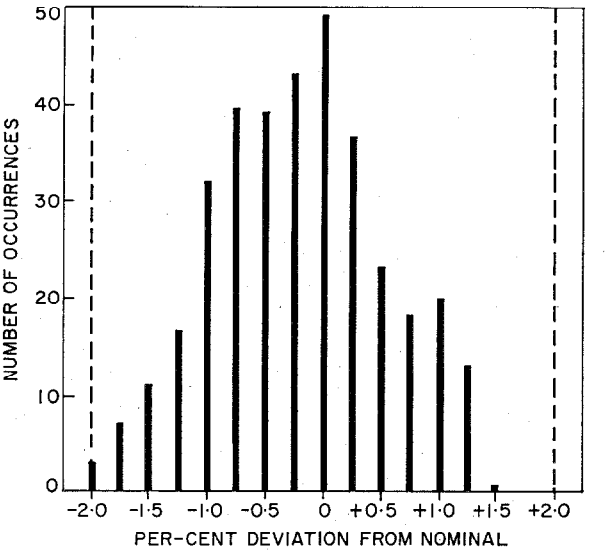

Figure 7—Histogram showing the percentage deviation from the nominal value of coupling factor. The limits of 2 per cent are shown.

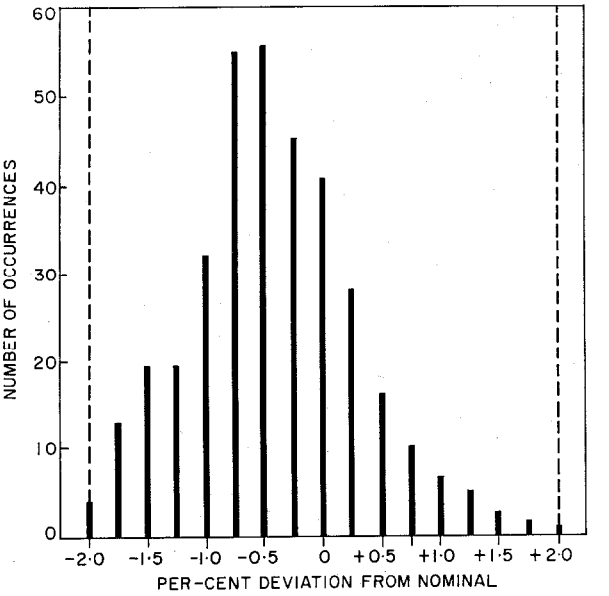

Figure 8—Histogram showing the percentage deviation from the nominal value of self-inductance of the secondary.

On the Design of Some Rhombic Antenna Arrays*

By A. A. DE CARVALHO FERNANDES

Standard Eléctrica, S.A.R.L.; Lisbon, Portugal

THE EXPRESSION of the field radiated by a rhombic antenna, taking into consideration both the vertical and the horizontal polarization components, is used to establish the theory of the array of two stacked rhombics and of the array of four rhombics in a stacked and interlaced arrangement. The main conclusions obtained are that for convenient values of the vertical and horizontal spacings between the antennas of the array, there is a greater concentration of power radiated along the directions of the main lobe of the pattern and, as a result, these arrays show an appreciable gain over a conventional rhombic. Practical rules for the design of these arrays for point-to-point and broadcasting are given in some detail.

• • •

1. List of Symbols

H = average height of a horizontal antenna or array above ground.

l = side of the rhombus.

s_h = horizontal spacing of the partial arrays of stacked rhombic antennas of a stacked interlaced array.

s_v = vertical spacing between the two antennas of a stacked rhombic array.

ϕ = tilt angle.

Δ = angle formed by the direction of radiation with the plane of the antenna (angle of elevation or angle of fire in horizontal antennas).

ψ = angle formed with the main diagonal of the rhombus by the projection of the direction of radiation on the plane of the antenna (azimuth angle in horizontal antennas).

λ = wavelength.

* Reprinted from *IRE Transactions on Antennas and Propagation*, volume AP-7, pages 39–46; January, 1959.

2. Horizontal Antenna in Presence of Ground

Rhombic antennas and rhombic antenna arrays are still a very-convenient solution for many radio communication problems both in the high- and in the very-high-frequency fields. The theory of the rhombic antenna has been described in several papers[1,2] and the arrays of perhaps greatest practical interest were described by Christiansen.[3–5]

Using the symbols summarized above and referring to Figure 1, one can obtain the equation,[6]

$$E = 480\ (I/R)\cos\phi\,|\,F_1(\Delta, \phi - \psi) \cdot F_2(\Delta, \phi + \psi)\cdot F_H(\Delta)\,|, \quad (1)$$

which gives the far field (taking into consideration both the horizontal and the vertical polarization components) due to the radiation from a horizontal rhombic antenna situated at height H above ground. Factors F_1, F_2, and F_H are given, respectively, by (2)–(4).

$$F_1(\Delta, \phi - \psi) = \frac{\sin\left\{\frac{\pi l}{\lambda}\left[1 - \cos\Delta\sin(\phi - \psi)\right]\right\}}{\left[1 - \cos\Delta\sin(\phi - \psi)\right]^{1/2}}. \quad (2)$$

[1] E. Bruce, "Developments in Short-Wave Directive Antennas," *Proceedings of the IRE*, volume 19, pages 1406–1433; August, 1931.

[2] E. Bruce, A. C. Beck, and L. R. Lowry, "Horizontal Rhombic Antennas," *Proceedings of the IRE*, volume 23, pages 24–46; January, 1935.

[3] W. N. Christiansen, "Directional Patterns of Rhombic Antennae," *AWA Technical Review*, volume 7, pages 33–51; September, 1946.

[4] W. N. Christiansen, W. W. Jenvey, and R. D. Carman, "R.F. Measurements on Rhombic Antennae," *AWA Technical Review*, volume 7, pages 131–144; December, 1946.

[5] W. N. Christiansen, "Rhombic Antenna Arrays," *AWA Technical Review*, volume 7, pages 361–383; October, 1947.

[6] A. A. De C. Fernandes, "Teoria e Projecto de Antenas Rômbicas," Coimbra Editora, Lda., Lisbon, Portugal, 1955. [See Sections 9.2, 9.3, and 9.4, where the basic assumptions underlying (1)–(7) are stated. For (1)–(4), it is assumed and justified that the current distribution can be considered without attenuation, and the ground can be taken as an infinite plane of a perfect conductor.]

$$F_2(\Delta, \phi + \psi) = \frac{\sin\left\{\frac{\pi l}{\lambda}[1 - \cos\Delta \sin(\phi + \psi)]\right\}}{[1 - \cos\Delta \sin(\phi + \psi)]^{1/2}}. \quad (3)$$

$$F_H(\Delta) = \sin\frac{2\pi H \sin\Delta}{\lambda}. \quad (4)$$

To calculate I in (1), one must know the power supplied to the antenna at its input terminals and the terminal impedance of the antenna. The theoretical derivation for the self and mutual impedances for rhombics is very complex and has recently been made by Channey.[7–9] However, the equations obtained seem to be so complicated that they are of little practical use. On the other hand, it is relatively simple to measure the terminal impedance of a rhombic antenna, and experience shows that in most practical cases the mutual impedance between the antenna and its image is small compared with its self-impedance Z_{11}. Experience also shows that the terminal impedance Z_1 has a resistive component that varies slightly with frequency (values of 600 and 700 ohms are representative[10] for 3-wire and 2-wire rhombics, respectively), and a reactive component that varies more widely with the frequency although its value is usually only a fraction of the resistive component. In Figure 2, are represented on a partial Smith chart the values of Z_1/Z_0 (for $Z_0 = 700$ ohms) obtained experimentally with a 2-wire rhombic over a frequency range from 6 to 22 megacycles.

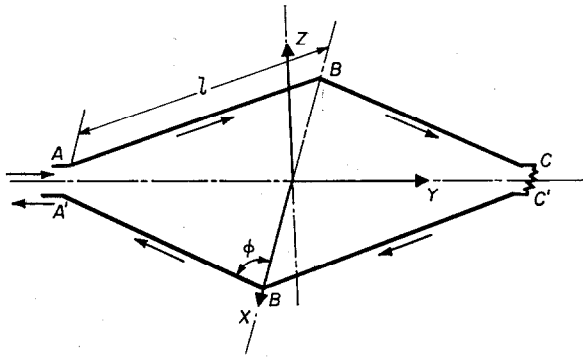

Figure 1—Schematic representation of a rhombic antenna. l is the side of the rhombus and ϕ is the angle made by the side with the transverse diagonal (tilt angle).

For approximate field intensity or gain calculations, one may consider the terminal impedance Z_1 reduced to its resistive component R_1 and the root-mean-square value of I could be obtained from approximation (5), where P represents the power supplied to the antenna at its terminals.

$$I = (P/R_1)^{1/2} \approx (P/R_{11})^{1/2}. \quad (5)$$

3. *Stacked Rhombic Array; Vertical Spacing Factor*

If two rhombics are stacked, as shown in Figure 3, and if they are driven in parallel, as

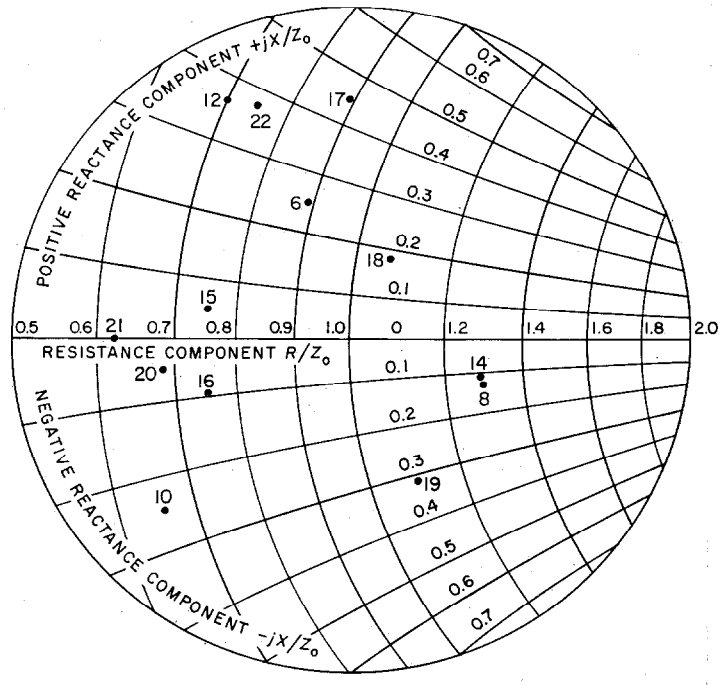

Figure 2—On the central portion of the Smith chart, where the standing-wave ratio is less than 2, are plotted values of normalized terminal impedance (in relation to $Z_0 = 700$ ohms) in a 2-wire rhombic antenna with $l = 200$ feet (61 meters), $\phi = 60$ degrees, $H = 82$ feet (25 meters), spacing between wires at side poles = 6.56 feet (2 meters). The numbers indicate frequency in megacycles.

[7] J. G. Channey, "Free-Space Radiation Impedance of Rhombic Antenna," *Journal of Applied Physics*, volume 24, pages 536–540; May, 1953.

[8] J. G. Channey, "Simplifications for Mutual Impedance of Certain Antennas," *Journal of Applied Physics*, volume 24, pages 747–750, June, 1953.

[9] J. G. Channey, "Mutual Impedance of Stacked Rhombic Antennas," *IRE Transactions on Antennas and Propagation*, volume AP-2, page 39; January, 1954.

[10] A. E. Harper, "Rhombic Antenna Design," D. Van Nostrand Company, Incorporated, New York, New York, 1941; sections 12–15. See also footnote reference 6, section 9.4.

indicated in Figure 4, we have a typical case of a uniform broadside array since the currents at the input terminals of both antennas can be considered approximately of the same magnitude and phase. The magnitude of the radiated field can therefore be obtained by multiplying (1) by the vertical spacing factor, which can be derived from conventional array theory and is given by (6), s_v being the vertical spacing of the two antennas.

$$2F_{vs}(\Delta) = 2\left|\cos\left[(\pi s_v/\lambda)\sin\Delta\right]\right|. \quad (6)$$

The magnitude of the radiated field due to an array of two stacked rhombics is therefore given by (7),

$$E = 960(I/r)\cos\phi\,|F_1(\Delta, \phi - \psi) \cdot F_2(\Delta, \phi + \psi)\cdot F_H(\Delta)\cdot F_{vs}(\Delta)|, \quad (7)$$

where I is the input current to each of the an-

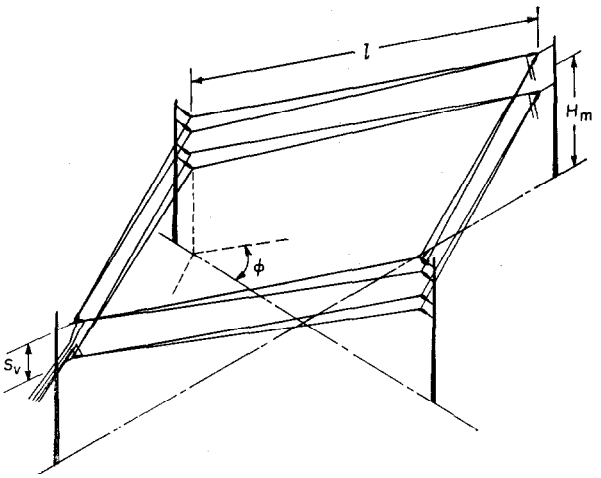

Figure 3—Schematic representation of a stacked rhombic array. s_v is the vertical spacing between the two antennas of the array; H_m is the average height above ground.

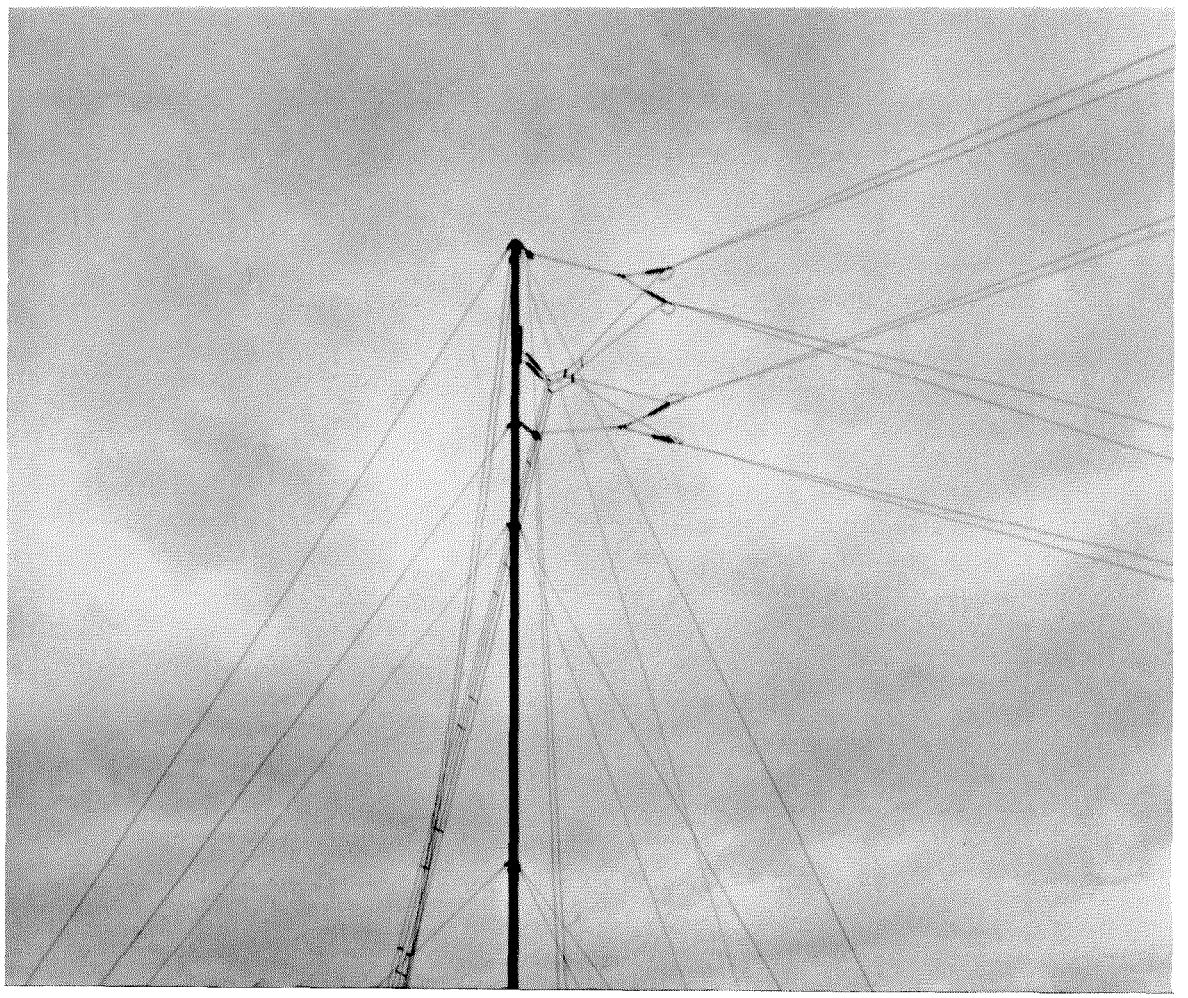

Figure 4—Four-wire down-lead transmission line and driving arrangement in stacked rhombic array.

tennas of the array. To calculate the height factor $F_H(\Delta)$, (4) is used, where H now represents the average height of the array above ground.

The calculation of current I is now more complicated than for a single rhombic because one must take into consideration the mutual impedances between the two antennas of the array and between them and their images.

It is fortunate, however, that the influence of the mutual impedance in the terminal impedance of the array seems to be small if the two antennas of the array are reasonably separated. In Figure 5 are represented on a partial Smith chart the values of Z_1/Z_0 (for $Z_0 = 320$ ohms) obtained experimentally with an array of two 2-wire stacked rhombics over the frequency range from 6 to 26 megacycles. The measurements were made at the end of the downlead 4-wire tapered transmission line matching the theoretical 350-ohm driving-point impedance to the value of 320 ohms used as characteristic impedance of the transmission line. The analysis of Figure 5 shows that the terminal impedance of the array is remarkably constant over such a wide frequency range. On this basis the approximate equation is

$$I \approx (P/2R_{11})^{1/2}. \qquad (8)$$

where R_{11} can be taken as 600 ohms for 3-wire rhombics and 700 ohms for 2-wire rhombics. The root-mean-square value of I mentioned in (7), required for approximate field intensity or gain calculations, can therefore be obtained from (8).

The pattern diagram of this type of array can be obtained from (7) and, to make it easier to study the influence of the vertical spacing factor on the pattern diagram of the array, the values of $F_{vs}(\Delta)$ have been plotted in Figure 6 for different values of s_v/λ and of Δ. From this figure it can be seen that for values of s_v up to 35 percent of λ and for angles of elevation Δ less than 24 degrees, the value of $F_{vs}(\Delta)$ is above 0.9. It also can be seen that the smaller s_v/λ is, the closer $F_{vs}(\Delta)$ is to unity; but in fixing the value of s_v in practice, it must not be made too small; otherwise the mutual impedance between the two antennas may become of great importance. A good practical rule is to make s_v not smaller than twice the separation between the extreme wires of each rhombic at the side poles when 2-wire or 3-wire rhombics are used (this separation is normally of the order of 15 to 20 per cent of the average height of the antenna above ground). Following this criterion, one arrives normally at values of $F_{vs}(\Delta)$ that are reasonably close to unity for the main lobe of the radiation pattern. Under these circumstances, the influence of the vertical spacing factor on the form of the main lobe of the pattern is very small and in most cases negligible.

If, however, the position of the nulls of the diagram or the secondary lobes are to be taken into consideration, the graphs of Figure 6 can be of great assistance either to fix the most-convenient value of s_v or, once it is already determined, to study in detail the influence of the vertical spacing factor in the complete pattern diagram of the array.

It is also to be noted that the vertical spacing factor is not a function of the azimuthal angle ψ, which means that the form of the horizontal

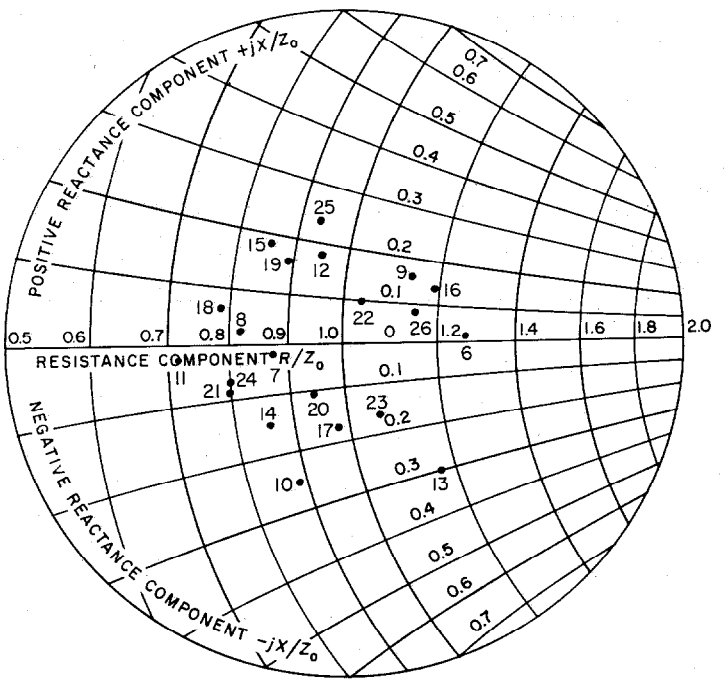

Figure 5—Values of normalized terminal impedance (in relation to $Z_0 = 320$ ohms) of a stacked rhombic array where $l = 295.3$ feet (90 meters), $\phi = 60$ degrees, $H = 140.1$ feet (42.7 meters), and $s_v = 19.7$ feet (6 meters).

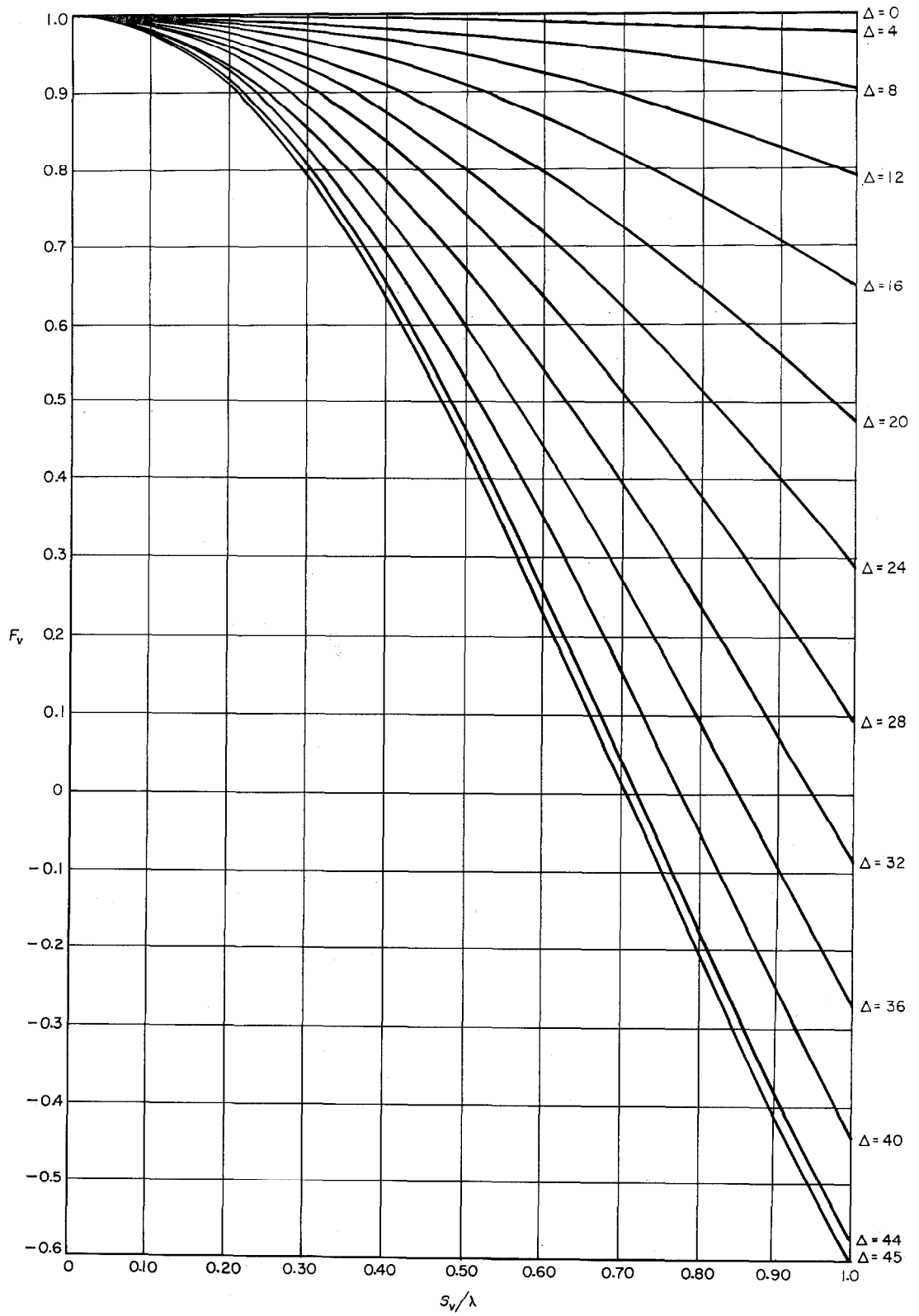

Figure 6—Variations of $F_{vs}(\Delta)$ as a function of the vertical spacing s_v for different values of the angle of elevation Δ in degrees.

radiation pattern of an array of stacked rhombics is the same as that of a single rhombic.

Comparing (7) and (1) and taking into consideration the values of I in both equations, it is concluded that when $F_{vs}(\Delta)$ is approximately equal to unity, an array of two stacked rhombics has a theoretical gain of 3 decibels over a single rhombic; in practice, when the ideal conditions on which the derivation of (1) and (7) depend cannot be completely met, a gain slightly smaller than 3 decibels is to be expected. The condition of $F_{vs}(\Delta)$ being approximately equal to unity will occur, as indicated above, for the directions of radiation covered by the main lobe in the majority of cases of practical interest. This circumstance leads to the conclusion that there is a greater concentration of radiated power in the main lobe, to which a reduction of the importance of the secondary lobes must necessarily correspond. In fact, by plotting the complete pattern diagrams using (7) and (1), this same conclusion can be reached.

As regards power dissipated in the terminating device, published data[11] seem to indicate that the dissipation is less in an array of stacked rhombics than in a conventional rhombic. This fact is, however, more difficult to take into consideration theoretically.

4. *Array of Interlaced Stacked Rhombics; Horizontal Spacing Factor*

If two arrays of stacked rhombics are interlaced as shown in Figure 7 and are driven with currents of the same magnitude but with a difference in phase equal to the phase delay in a wave traveling in the same direction along a distance equal to the horizontal spacing s_h, the two partial arrays are then associated as a typical uniform end-fire arrangement. The magnitude of the radiated field due to the complete array comprising the 4 rhombics can therefore be obtained by multiplying (7) by the horizontal spacing factor. This can be derived from conventional array theory and is given by (9) where Δ is the angle of elevation and ψ the azimuthal angle.

$$2F_{hs}(\Delta, \psi) = 2\left|\cos\left[(\pi s_h/\lambda)(1 - \cos\Delta\cos\psi)\right]\right|. \quad (9)$$

The magnitude of the radiated field due to an array of four rhombics in the stacked and interlaced arrangement described above is therefore

$$E = 1920(I/r)\cos\phi\,|F_1(\Delta, \phi - \psi) \cdot F_2(\Delta, \phi + \psi) \cdot F_H(\Delta) \cdot F_{vs}(\Delta) \cdot F_{hs}(\Delta, \psi)|, \quad (10)$$

where I is the input current at each of the antennas of the array.

In practice, the interlaced array has a driving point from which the transmission lines depart to each of the partial stacked arrays. It is essential that the standing-wave ratio in both lines be as close to unity as possible and that the input impedances of both lines at the driving point are the same. Also, to satisfy the requirement that the phase difference at the input of the two partial arrays be equal to the phase delay in a wave traveling a distance equal to s_h, it must be ensured that the difference in length of the two transmission lines from the common driving point to the input of each array be equal to s_h.

As regards the mutual impedances between the antennas of the array, experience shows that in

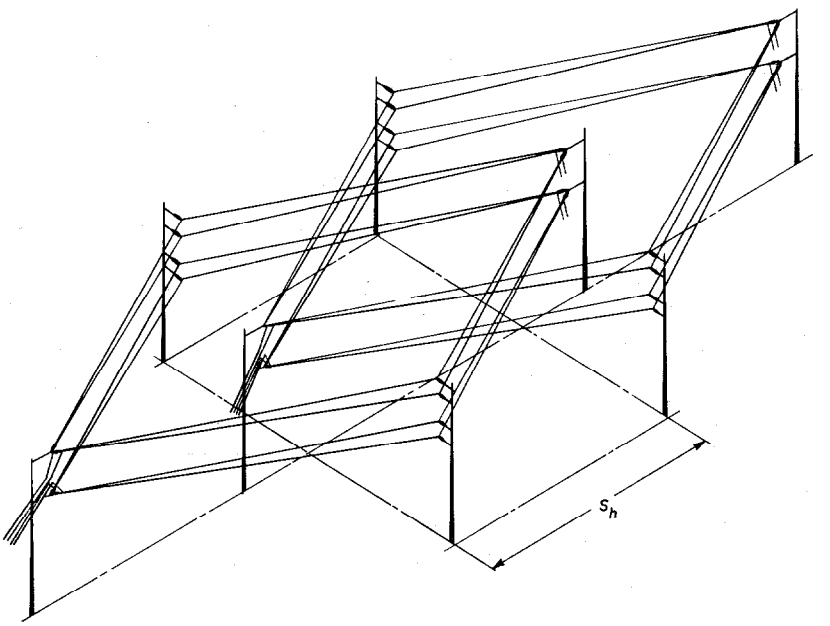

Figure 7—Schematic representation of an interlaced stacked rhombic array. s_h is the horizontal spacing between the two partial stacked rhombic arrays.

[11] Footnote reference 5, page 379.

most practical cases their influence on the terminal impedances of both partial arrays is small. The root-mean-square magnitude of the current I shown in (10) can therefore be calculated by approximation (11), where R_{11} has the value mentioned,

$$I \approx (P/4R_{11})^{1/2}, \quad (11)$$

apropos of (8). These equations can be used for approximate field intensity or gain calculations involving these types of arrays.

The influence of the horizontal spacing factor on the pattern of an array can be studied by using the graphs shown in Figures 8–11, each having been drawn for a certain value of s_h/λ from 1 to 4. From these graphs it can be seen that for the values of Δ and ψ usually covered by the main lobe of the radiation pattern, $F_{hs}(\Delta, \psi)$ is approximately equal to unity, which means that the form of that main lobe is not affected much by the interlacing if the value of s_h is within the limits covered by the above graphs. In these circumstances, and by comparing (10), (7), and (1), it is concluded that the interlaced array described has a theoretical gain of about 6 decibels over a conventional rhombic and of about 3 decibels over a stacked array with the same basic dimensions. This means that there is a greater concentration of power radiated in the

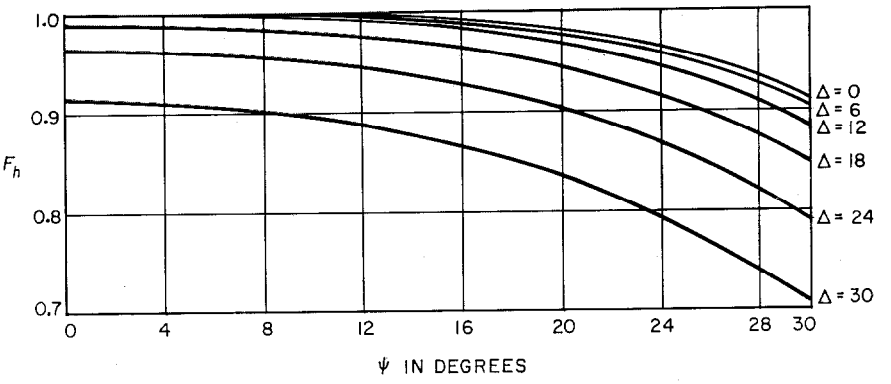

Figure 8—Variation of $F_{hs}(\Delta, \psi)$ as a function of the azimuthal angle ψ for different values of angle of elevation Δ in degrees and for $s_h/\lambda = 1$.

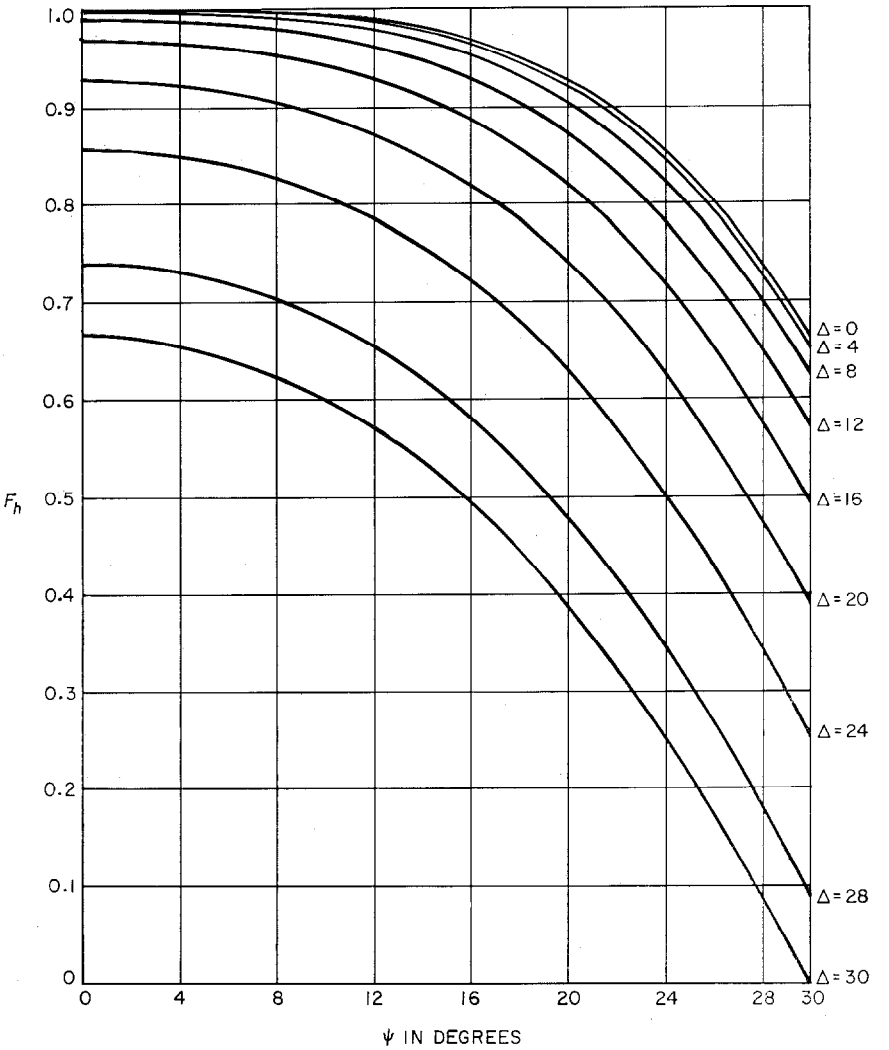

Figure 9—Variation of $F_{hs}(\Delta, \psi)$ as a function of the azimuthal angle ψ for different values of angle of elevation Δ in degrees and for $s_h/\lambda = 2$.

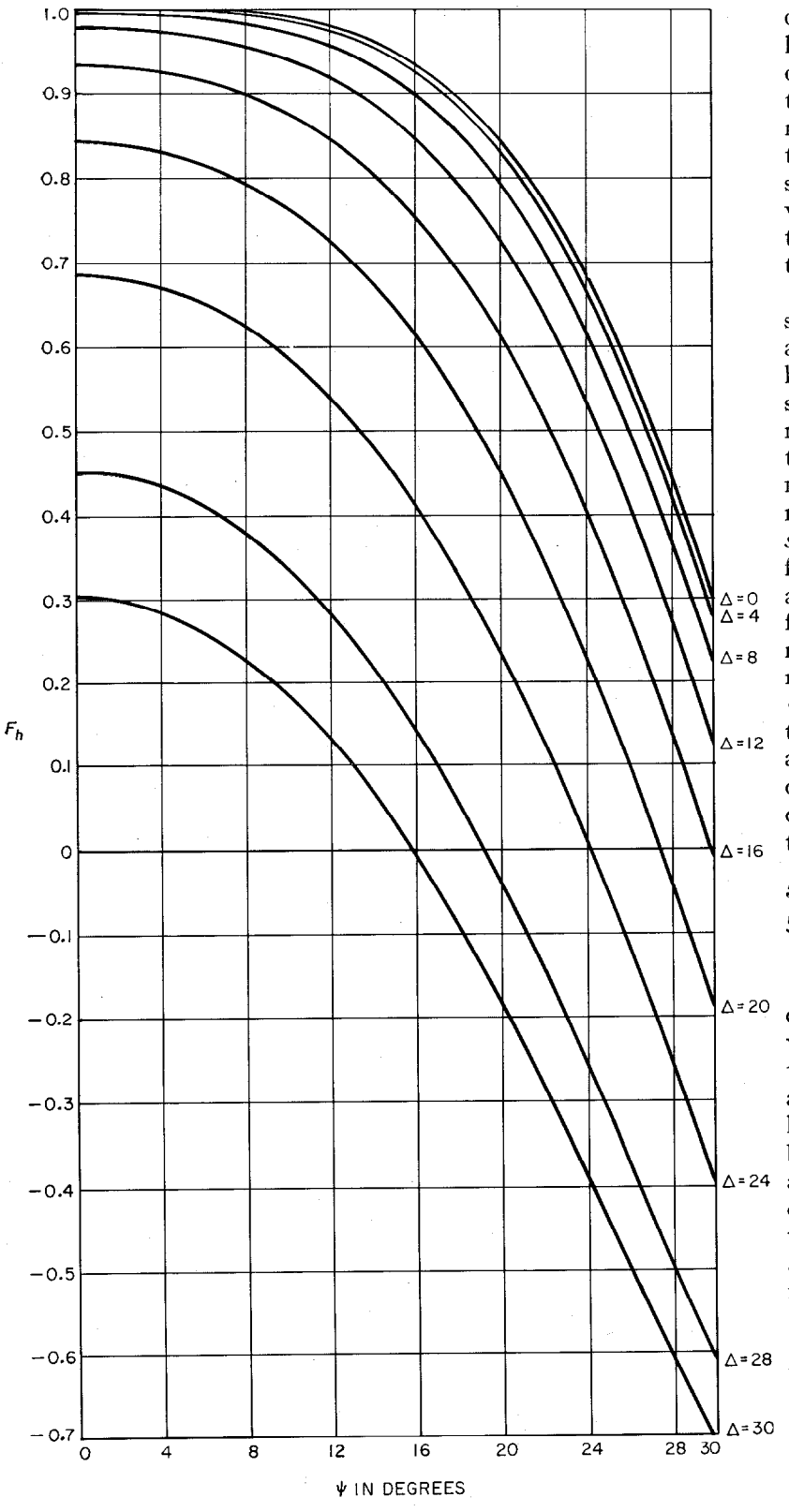

directions covered by the main lobe of the pattern, with the corresponding reduction in the secondary lobes. Furthermore, experience shows[11] that the percentage of power dissipated in the terminating devices of the rhombics is lower than in the case of a conventional rhombic.

In designing these both stacked and interlaced stacked arrays, the vertical and the horizontal spacings s_v and s_h should be large enough for the mutual impedances of the antennas of the array to have a negligible effect on the terminal impedance; but s_v and s_h should also be small enough for $F_{vs}(\Delta)$ and $F_{hs}(\Delta, \psi)$ to be as close to unity as possible for the useful directions of radiation. It is also to be noted that (6), (7), (9), and (10) assume that coupling between the antennas of the array has a negligible effect on the amplitude and phase of the current distribution in the antennas.

5. Practical Design

5.1 Field of Application of Rhombic Antennas

Among the antennas more-commonly used for high- and very-high-frequency directional radiation, the rhombics and the arrays of rhombics have an outstanding position because they offer a reasonably high directivity at low cost, with the additional advantage of being useful over a wide range (1:2 or 1:3) of frequencies.

With almost all types of antenna systems, cost increases with directivity (arrays of

Figure 10—Variation of $F_{hs}(\Delta, \psi)$ as a function of the azimuthal angle ψ for different values of angle of elevation Δ in degrees and for $s_h/\lambda = 3$.

dipoles are a typical example). In the rhombic antenna, the directivity varies with the geometric configuration of the antenna, the cost being only slightly affected; in consequence, the advantages of the rhombic antenna are accentuated with the increase of directivity.

One of the inconveniences of the rhombics is the dissipation of power in the terminating device, but more importance has been given to this point than it probably merits. Actually, when an antenna system is intended to provide a certain radiation beam, the main interest is in concentrating in that beam as much as possible of the available transmitter power; whether the wasted power is dissipated in the antenna or radiated in wrong directions is of no consequence to the main purpose of the antenna, the former case being obviously less harmful.

For point-to-point communications or for highly directional broadcasting (with a total beamwidth up to, say, 15 degrees to 20 degrees), the rhombic antenna is a very-convenient and, in general, the most-economical solution; the array of two stacked rhombics costs little more than a conventional rhombic (higher masts and more antenna wire, et cetera), but introduces many advantages over a conventional rhombic (greater concentration of the power in the main beam and therefore less power wasted in secondary lobes and in the terminating device). The signal gain that can be obtained with rhombic antennas is about 10 to 15 decibels over a horizontal half-wave dipole at the same average height, while the directivity gain[12] over a hypothetical isotropic antenna in free space is about 20 to 25 decibels. The use of arrays of stacked and interlaced rhombics introduces still-greater concentration of power in the desired beam, but it must be taken into consideration that the cost of an interlaced array is slightly more than twice the cost of a stacked array.

For broadcasting use and when a total beamwidth of about 20 to 30 degrees is required, conventional rhombic antennas have seldom been used because curtains of dipoles can ensure a higher gain for such a beamwidth. Actually, if an interlaced array is used, the same order of magnitude of gain can be obtained at appreciably lower cost, with the additional advantage of a wide frequency range.[13]

[12] Footnote reference 10, pages 50–60.

5.2 Geometric Configuration of Antenna System

The first step in the design of a rhombic antenna or of an array of rhombics is to calculate the optimum values of H (average height above ground), l (side of the rhombus), ϕ (tilt angle), s_v (vertical spacing), and s_h (horizontal spacing); the geometric configuration of the antenna system must be calculated. To check the values obtained, the radiation pattern diagram should then be calculated; in practice, it is usually sufficient to calculate and draw the so-called vertical diagram (varying Δ for $\psi = 0$) and the "horizontal" diagram (varying ψ for optimum Δ) for the different frequencies of interest. Additional steps involve the mechanical design of the antenna system and both the electrical and the mechanical design of the driving and terminating arrangements (including the wide-band impedance matching sections when required).

Several methods of calculating the geometric configuration of a rhombic antenna have been described in the available literature, but almost all of them ignore the horizontal beamwidth requirement that is essential when the antenna is intended for broadcasting use. This is especially important when calculating the length l and the tilt angle ϕ. Another requirement, which is often ignored, is the requirement for the antenna to operate in a certain frequency range. In the method described below, all these conditions are taken into consideration, enabling the most-convenient compromise solution to be obtained. However, this solution will need to be analyzed further, bearing in mind the mechanical limitations of the system, availability of ground space, and other factors affecting the particular case being studied.

To calculate the height H above ground, a simple criterion consists in obtaining the value that makes the factor $F_H(\Delta)$, given by (4), equal to unity (its maximum value) for the desired value of Δ (conditioned by the propagation path) and for the wavelength λ_0 corresponding to the

[13] The Portuguese Broadcasting Authority (Emissora Nacional de Radiodifusão) has in use, for the same service, curtains of 16 horizontal dipoles with reflectors (*HR4/4* arrays) and arrays of stacked and interlaced rhombics, giving a beamwidth of the order of 30 degrees and having approximately the same gain. The tilt angle (ϕ) of the rhombics is 40 degrees, which means that they are slightly foreshortened in the direction of radiation.

midfrequency of the range given by

$$\lambda_0 = (2\lambda_{min}\lambda_{max})/(\lambda_{min} + \lambda_{max}). \quad (12)$$

It can be easily seen that under these conditions, the value of $F_H(\Delta)$ will be the same at the two extreme frequencies of the range. H can therefore be calculated using (13), which follows directly from (4), if the minimum possible value of H, which makes $F_H(\Delta)$ equal to unity, is taken

$$H = \lambda_0/4 \sin \Delta. \quad (13)$$

To arrive at the most-convenient values for l and ϕ, two conflicting conditions must be taken into consideration: (A) The maximum possible field must be obtained in the main direction of radiation; (B) The horizontal beamwidth must be greater than the minimum given by the specifications laid down for the antenna.

From (1)–(3), for $\psi = 0$ (that is, in the plane of maximum radiation) and when $F_H(\Delta) = 1$, E is proportional to a factor termed gain factor,[14] given by

$$F_G = (\cos \phi)/(1 - \cos \Delta \sin \phi), \quad (14)$$

and to the length factor,[15] given by

$$F_l = \sin^2 [(\pi l/\lambda)(1 - \cos \Delta \sin \phi)]. \quad (15)$$

The maximum value of the length factor is obviously unity and the maximum value of the gain factor, for the desired value of $\Delta = \Delta_0$, is reached when $\cos \Delta_0 = \sin \phi$; for practical purposes, when $\phi = (\pi/2) - \Delta_0$. These conditions could be a basis for design, of course, if the beamwidth did *not* have to be considered.

However, if this is an important factor, and it normally is, even in point-to-point communications where it is sound to insure a certain beam-width to take care of variations of direction at reflection points, another criterion will have to be followed. For the desired angle of fire Δ_0, it must be insured that the ratio

$$E_{(\psi=0)}/E_{(\psi=\psi 0)}$$

is below a certain limit if the total beamwidth $2\psi_0$ is to be obtained. For instance, for a 6-decibel

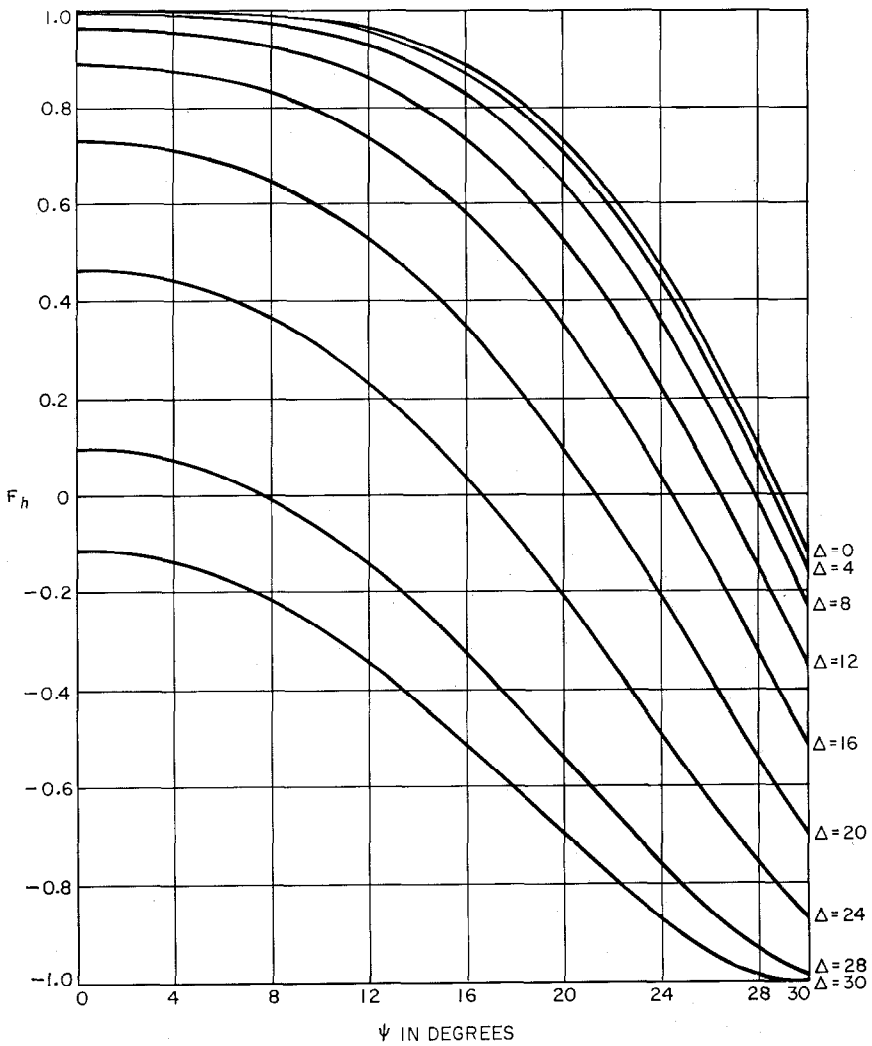

Figure 11—Variation of $F_{hs}(\Delta, \psi)$ as a function of the azimuthal angle ψ for different values of angle of elevation Δ in degrees and for $s_h/\lambda = 4$.

[14] A graph of F_G in function of Δ and ϕ can be found in H. P. Williams, "Antenna Theory and Design," Sir Isaac Pitman & Sons, Limited, London, England; 1950: page 287, Figure 6.44.

[15] Graphs of F_l in function of Δ and l/λ, for different values of ϕ can be found in footnote reference 14, pages 288–289, Figures 6.45(a)–6.45(d).

drop at the "edges" of the beam, that ratio should have a maximum value of 2 over the whole frequency range of the antenna.

Taking into consideration (1)–(3) and calculating the above ratio, the following approximate value is obtained

$$\frac{E_{(\psi=0)}}{E_{(\psi=\psi 0)}} = \frac{\sin^2\left[\frac{\pi l}{\lambda}(1 - \cos\Delta_0 \sin\phi)\right]}{\sin\left\{\frac{\pi l}{\lambda}[1 - \cos\Delta_0 \sin(\phi + \psi_0)]\right\}\cdot\sin\left\{\frac{\pi l}{\lambda}[1 - \cos\Delta_0 \sin(\phi - \psi_0)]\right\}}, \tag{16}$$

in view of the fact that (17),

$$\frac{[1 - \cos\Delta \sin(\phi - \psi)]^{1/2}\cdot[1 - \cos\Delta \sin(\phi + \psi)]^{1/2}}{1 - \cos\Delta \sin\phi}, \tag{17}$$

is roughly equal to unity for the directions of radiation of interest for the main lobe of the radiation pattern.

The values of l and ϕ should heretofore be calculated so that (16) is below the value previously fixed (2, in the example seen) for all the frequencies of the range and for the desired angle of fire Δ_0. Because, for a certain antenna, the beamwidth decreases when the frequency increases, it is usually sufficient to make this calculation for the highest frequency of the range. Of the possible pairs of values for l and ϕ, those that make higher the gain factor of (14) and the length factor of (15) should be selected. Tables or graphs[15] of F_G and F_l will be of considerable help in making these calculations.

Actually the process outlined above is much simpler than it looks at first glance and after a little practice it is very easy to follow. The most-convenient values for l and ϕ can then be obtained after one or two attempts.

When designing a stacked rhombic array, it is necessary to determine the value of the vertical spacing s_v; the criterion outlined in section 2 can then be followed.

For an interlaced array, the value of s_h will also have to be established. This is not critical and a sound criterion is to make it from 30 to 50 percent of the main diagonal of the rhombus; the exact value to be used may depend on the mechanical conditions affecting the erection of the masts and the interlacing of the antennas.

5.3 Driving Arrangement

It is well known that in a simple rhombic transmitting antenna it is common to have a 2-wire line with 600-ohm characteristic impedance, and in a receiving antenna the most-common solution consists of installing a wide-band impedance matching unit at the top of the end mast, the transmission line between it and the receiver being the coaxial type.

In a transmitting array of stacked rhombics where the terminal impedance at the driving point of the array is about 300 to 350 ohms, the down-lead transmission line should be of the 4-wire type (the two wires of each side at the same potential). When high-power transmitters are used (about above 50 kilowatts), it is convenient[16] to choose a 4-wire transmission line, and a value of the characteristic impedance from 300 to 350 ohms is a convenient one. It is of great interest to note that a slight impedance matching can be effected by varying conveniently the distance between the side conductors of the transmission line from top to "ground" level; thus, the terminal impedance offered to the transmission line at all working frequencies of interest is within the desired values. If, however, the line from the transmitter is of the 2-wire type with a characteristic impedance of about 600 to 700 ohms, the down-lead transmission line must match the 4-wire 350-ohm (when using 2-wire rhombics) driving point at the top to the 2-wire 600-ohm one at the bottom. An exponentially tapered line having a gradual variation (from top to bottom) in the separation of the side wires

[16] F. C. McLean and F. D. Bolt, "The Design and Use of RF Open-Wire Transmission Lines and Switchgear for Broadcasting Systems," *Proceedings of the Institution of Electrical Engineers*, volume 93, part 3; 1946: section 2.1.2, page 192, and section 6.1, page 204.

and the distance between the conductors will provide the wide-band impedance matching required.

In the case of an array of stacked and interlaced rhombics, exponential lines can also be used for impedance matching. In Figure 12 (at the bottom of the figure), is shown a common driving point for both stacked arrays of the interlaced array. Two 2-wire 640-ohm transmission lines depart from this point to each stacked array and parallel connection is made to the 320-ohm 4-wire line from the transmitter. The exponential transmission line matching the 2-wire 640-ohm line to the 4-wire 350-ohm line can also be seen in this figure.

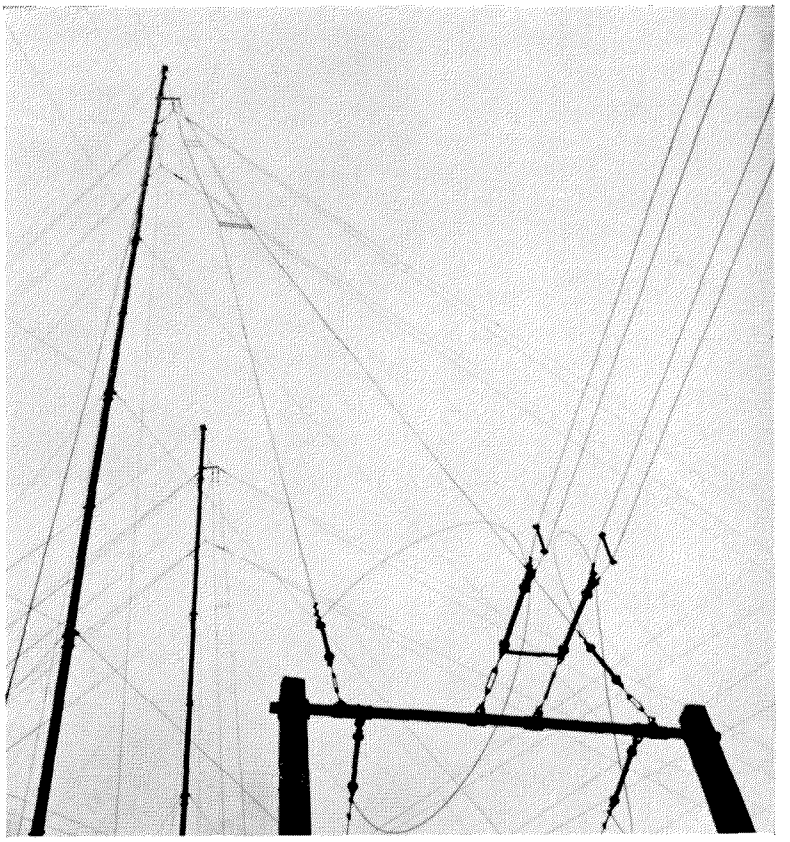

Figure 12—Detail of driving arrangement of an interlaced array.

5.4 Terminating Arrangement

To ensure a progressive-wave current distribution in the antenna conductors, a rhombic antenna must be terminated by a resistance of the order of 700 to 800 ohms in which a certain power will be dissipated. When this power is below about 5 to 10 kilowatts, it is easy to build a group of noninductive resistors in a convenient housing at ground level and connect it to the antenna terminating points by a dissipative transmission line. This last detail is very important since the line itself might dissipate almost as much power as the terminating resistors and an appreciable saving therefore can be made. For higher power, a greater length of dissipative line must be interposed between the terminating points of the antenna and the resistors. The most-economical solution consists of using a tapered dissipative line and in reducing progressively[17] the wire size so that a greater uniformity of power dissipated per meter of line is obtained. The line required is then much shorter than if it had constant characteristics.

In a stacked array, each rhombic can either be terminated separately or terminated together by a 4-wire dissipative line; in this case the tapering arrangement mentioned above can be of particular interest. In an interlaced array, the two partial stacked arrays will have to be terminated separately.

[17] Footnote reference 16, section 2.1.5, page 194.

6. Acknowledgments

In his work on design and construction of antenna systems, the author has greatly benefited from visits made to transmitting stations of and from conversations, years ago, with engineers of the British Broadcasting Corporation. Some of the constructional details illustrated in this paper have been mechanically designed with the cooperation of Standard Telephones and Cables Limited, and Coubro and Scrutton, of England. The author wishes to thank the Technical Director of the Emissora Nacional de Radiodifusão (Portuguese Broadcasting), of Lisbon, for permission to publish some of the photographs and diagrams shown in this paper.

Thermal Noise in Multisection Radio Links*

By B. B. JACOBSEN

Standard Telephones and Cables, Limited; London, England

MICROWAVE radio links are used for the long-distance transmission of large groups of telephone channels and for television signals. Thermal noise effects arise in each section of the link and the magnitude of the resulting noise in the overall circuit is one of the major parameters of the overall transmission circuit.

The paper outlines methods of calculating the thermal noise in a long radio link when the individual radio transmission sections are subject to fading. Various methods of expressing fading statistics are discussed and it is proposed that the statistics of the individual path shall be expressed in terms of the three first hourly moments of the fading ratio and the statistics of these moments.

A technique is described for combining the effects of fluctuating fading in successive (tandem-connected) paths to obtain the hourly fading moments of the overall circuit. A method is given of converting the overall moments into an overall circuit fading distribution; this is expressed in terms of an augmented log-normal distribution, which can readily be translated into the distribution of thermal noise in the overall connection.

The noise requirements for long-distance telephone circuits are specified for a 2500-kilometre (1550-mile) circuit, although any particular project will generally be much shorter. To avoid the difficulties involved in subdividing the noise permitted for 2500 kilometres, it is proposed instead to treat such path performance data as can be made available as if it were representative of all the sections that would enter into a 2500-kilometre circuit (synthetic overall circuit).

Thermal noise can be calculated for the synthetic circuit and compared with the requirements; this comparison will show whether the actual paths for which data are available are suitable to form part of an overall connection.

. . .

1. Introduction

Microwave radio relay links that provide large numbers of telephone channels and/or a television channel are coming into use. In current systems, the useful signal (base-band signal) is transmitted as phase or frequency modulation of the carrier frequency, modulation taking place at the transmitting terminal, repeater stations being provided at spacings of about 30 miles (48 kilometres). At these stations the received carrier signal is amplified and retransmitted along the route, usually with a change of carrier frequency. The carrier signal finally reaches the receiving terminal, where, after amplification and demodulation, it again provides the base-band signal. There may be terminal stations at several points along a long route.

The object of the paper is to give a method of calculating thermal-noise effects in multisection radio links. This calculation would be very simple but for the fact that the radio paths between the stations have a transmission loss that is continually varying (fading).

In most systems, the carrier power outputs from the transmitting terminal and the repeater equipment are held at specified values, independent of effects in the preceding sections. (There may be occasions when this is not true and these will need special consideration.)

The power is carried by the transmission line to the aerial, and via the space path reaches the aerial of the next station. From this aerial the received signal is taken to the repeater or receiving equipment. The loss between the transmitting equipment and the receiving equipment at the next station is the gross path loss, and this will be referred to as path loss.

The path loss in each section will vary with time, owing to fading, and as a result so will the carrier power received at the end of the section.

* Reprinted from *The Proceedings of The Institution of Electrical Engineers*, Part C, volume 105, pages 139–150; March, 1958.

At these end-points the carrier signal is of relatively low level and may be considered here to be exposed to thermal-noise effects. The thermal-noise power is uniformly distributed over most of the significant part of the frequency spectrum; its density is approximately −139 decibels below 1 milliwatt per 3-kilocycle-per-second bandwidth for an ideal receiver, but in practice this value must be increased by the noise factor of the equipment. The thermal noise at the input remains constant, but its relative value is increased when there is fading in the preceding path. The input circuit noise is added to the incoming wave and is amplified and transmitted with it into the next sections, where further noise additions occur. In practice, the total noise power over the radio-frequency bandwidth of one repeater is small compared with the lowest carrier-signal power received, so that threshold effects do not occur.

In phase- and frequency-modulation systems, it is normal to provide some limiting action in each repeater to prevent the accumulation of noise which, after several sections, could produce threshold effects. The limiters have no useful effect otherwise on the amount of noise found in the output signal after detection at the receiving terminal. The limiters at repeater stations remove the amplitude effect of the noise but incorporate the phase-modulation effect into the carrier signal itself, which may then be said to consist of the original signal plus phase noise.

Each repeater produces a phase-noise signal, although it will be incorporated into the signal proper only when a limiter is present. The phase noise that is effective in the whole link will be the power sum of the phase-noise power produced at the end of each space-transmission section. The noise will therefore consist of many contributions, each of the same quality (white phase noise), but the scale of each contribution will vary with the path loss of the section. The structure of the total noise will nevertheless be that of white phase noise, but the scale of the total will depend on the combined effect of the varying path losses of the space sections. Noise will therefore be taken to mean white noise; however, the fluctuations dealt with are not those of white noise *per se*, but rather are the fluctuations of the short-term mean power of the noise that arises from fading.

2. *Combination of Path-Loss Effects*

A useful concept borrowed from carrier telephony is that of the equivalent single section, which has a transmission loss such that, used by itself, it would produce the same noise as the actual tandem-connected sections. Two equal sections connected in tandem would, for instance, have an equivalent loss 3 decibels higher than the individual section, while for 50 equal sections, it would be 17 decibels higher than the loss of one section. If the losses in the individual sections vary with time, so will the loss of the equivalent single section. The equivalent single-section loss is

$$A_e = 10 \log_{10} \sum_{r=1}^{r=n} 10^{A_r/10} \text{ decibels}, \qquad (1)$$

where A_e is the equivalent single-section loss, A_r is the loss of the rth section, and n is the total number of paths connected in tandem (if diversity is used this will modify the A_r functions for the sections having diversity).

It is, of course, possible to extract from the A_r values a constant A_0; then (1) becomes

$$A_e - A_0 = 10 \log_{10} \sum_{r=1}^{r=n} 10^{(A_r - A_0)/10} \text{ decibels}. \qquad (2)$$

Each of the quantities after the summation sign in (2) will later be referred to as a fading ratio—the factor by which the power-transfer factor of a section is divided when the path loss increases from A_0 to A_r, and also that by which the phase-noise power due to the rth section is increased when the loss of that section is A_r instead of A_0.

Both equations imply that the A values for each section are taken at the same time; they may be either actual values that have occurred at a particular instant or values that are expected to occur at a future instant. In the following work, these quantities will be assumed to be only statistically defined and then A_e also will be statistically defined, but any instantaneous A_e value will be the result of a set of A_r values that by implicit assumption occur simultaneously.

2.1 Evaluation and Use of Combined Path Loss

There are three distinct problems in evaluating and using the equivalent-single-section loss in

(1) and (2). These are briefly stated here and the discussion of them occupies the major part of the paper.

(A) *First Problem*—Express statistically the fading properties of each radio section (sections 5 to 6.4). Functions A_r must be found to adequately describe in statistical terms the performance of each path at various times. In practice, this would mean making path-loss measurements over a long period and condensing the results without losing information in the process. It must be borne in mind that any test of path loss is, in effect, a sampling process, and only if the sample is large can it be relied upon to represent the path performance accurately.

(B) *Second Problem*—From the fading properties of individual sections, find the combined multisection fading effect (sections 8 to 10.2 and 13). Given suitable functions A_r, a method must be found for effecting the summation of (2). This, in effect, is a further sampling process; each A_r function describes a population, and the equivalent-single-section loss is the result of combining, according to (2), a sample from each of the n populations. By repeating such sampling indefinitely, the population A_e can be inferred.

(C) *Third Problem*—Calculate the thermal noise in an overall connection and compare it with the noise requirements (sections 6.5, 11, and 12). The thermal noise in the base-band is readily calculated from A_e and the parameters of the radio link, but the overall specification for noise is in terms of a 2500-kilometre (1550-mile) circuit. An actual project for which fading data are available will, in general, have a shorter length; it will therefore be necessary to translate either the specification or the expected performance, so that they can be compared.

Only one part of the overall requirement had been agreed to by the Comité Consultatif International Téléphonique; namely the maximum limit for the hourly mean noise power in a telephone channel during any hour. A further part, defining permissible values of noise during shorter periods, is being studied[1] by the Comité Consultatif International Télégraphique et Téléphonique. The permissible noise includes other effects; the thermal noise is only a part of the total.

It is obviously desirable that the terms in which (2) is expressed should be compatible with those in which the complete noise specification will eventually be stated. It will be assumed, in the absence of a final specification, that it is satisfactory to express the thermal noise effect in terms of its statistical distribution during any hour.

3. Sources of Fading Behaviour

The radio transmission paths used for microwave links are usually designed for line-of-sight transmission with first-Fresnel-zone clearance. There are three main sources of fading on such paths, namely:—

(A) *Atmospheric multipath transmission* occurs during still-air conditions and increases in severity and frequency of occurrence as the path length increases. The incidence and amplitude of this type of fading show strong diurnal and seasonal variations, but diversity is effective in reducing it. This type of fading tends to make the third source of fading more troublesome.

(B) *Abnormal refraction gradient with height* is particularly liable to cause trouble when the ground clearance of the path is small, since the beam then tends to be intercepted by the ground. Although this type of fading occurs less frequently when the path clearance is large, the clearance used in practice will rarely be sufficient to prevent occasional occurrence. This type of fading is not improved by diversity and oversea paths may on rare occasions suffer severely from it. This form of fading starts gradually, but it may persist for a considerable time at a high value.

(C) *Ground or water reflection*, when it is large, can give severe fading that on occasion can last for as long as an hour. When the ground reflection is small, it will be harmful only in the presence of the first type of fading. Diversity is very effective against these reflection effects.

4. Cyclic Effects

If the fading performance of a specific section is measured over many periods each of, say, an hour's duration, several different types of hourly

[1] "Red Book" of the Comité Consultatif International Télégraphique et Téléphonique, First Plenary Session, volume 1, page 104, question 7 of Study Group 1.

distribution are obtained and diurnal and annual effects become noticeable. Cyclic effects are in some measure common to all the sections and constitute correlation between the fading events in the individual sections.

When the test results are subsequently sampled for the purpose of inferring the equivalent-single-section loss of a multisection system, it is necessary that the populations from which the samples representing each of the individual sections are drawn shall be typical of the actual path performance likely to apply at the time of day for which the sample is taken.

If cyclic effects are present it will be necessary to define populations to represent different parts of the cycle; the fading statistics for the individual paths must be given for periods short enough to ensure that they are mutually at random inside the period.

4.1 Consequences of Ignoring Cyclic Effects

The statement that "fading in all paths is liable to be high between the hours of 6 and 8 A.M." expresses correlation between the path losses. If only a single path were involved, it would not be completely unreasonable to give the distribution for a long period including the hours 6–8 A.M. This distribution would indicate that the path was liable to bad fading for a fraction of the time, and it might be considered a matter of indifference if this liability occurred at one time or another. But if several path performances are to be combined, as in (1), it would be wrong to use long-term distributions that do not explicitly include the important fact (in the example) that all paths are liable to fading at the same time of day and that, *per contra*, they are all less liable at other times. Even if it is a matter of indifference whether liability to high noise occurs at one time or another, the fact that all the sections are liable at the same time cannot be disregarded.

To illustrate this point more clearly, assume that, in fact, all of 50 sections have a fixed loss for 22 hours but have 6-decibels extra loss (fading) for 2 hours. If the sections now have full fading correlation, the extra loss will occur in all sections simultaneously and the equivalent loss will be 23 decibels for 2 hours and 17 decibels for 22 hours. If, however, the losses are mutually at random, they will occur in each section at times that are quite independent of occurrences in other sections and without any restriction except that the total time of fading in each path is 2 hours; the equivalent loss will in this case be within 18 ± 1 decibels (for 98 per cent of the time).

If, in fact, the first assumption of correlation is correct, the consequency of ignoring the correlation would be to overestimate the equivalent loss by 1 ± 1 decibel most of the time; but for 2 hours the consequence would be to underestimate the loss by 5 ± 1 decibel, which would be a serious error.

This example is a simplified version of correlation effects that can occur with real links, but it shows clearly that path performances must not be averaged if cyclic effects that are likely to be common to many paths are thereby concealed. Annual cyclic effects are well known and must be taken into account.

4.2 Noncyclic Covariation

It should be mentioned that noncyclic covariation between path losses could occur; it might, for instance, be caused by common weather conditions. This covariation, however, is likely to be infrequent and small and will hardly ever extend over groups of more than two sections. For this reason it is not likely to be significant when a large number of sections are considered together.

5. Path Performance Data

The overall noise performance or expectation for a multisection link is required to be in terms of the noise during any hour. In section 4.1 it was apparent that cyclic effects make it necessary not to combine the path performance data for periods having cyclic differences. It is therefore proposed that all path loss data should be expressed on an hourly basis.

Collecting data is a sampling process and unless sampling is carried on for a long time there will be uncertainty, particularly about the true proportion of rare events. Rare events, in this connection, mean not only considerable fading in the hourly data, but also abnormal average monthly fading for a period of the day during a particular month. The average may vary from

year to year, but this cannot, of course, be seen from the results unless testing has been carried out over many years. Usually it will not be possible to collect data over very-long periods, but in the preparation of condensed data, all the available facts should be included.

Data may be presented in several ways; as level recordings against time (raw data), histograms giving for each hour the fraction of time during which the path loss falls within each of a number of ranges (frequency data), or a distribution curve derived from other data and expressing the probability of a certain level of fading being (or not being) exceeded. The data should be given for separate periods of an hour.

5.1 Path Performance in Terms of Fading Moments

A new method of presenting hourly path performance data will now be considered. It consists of calculating or measuring directly the hourly statistical moments of the fading ratio [defined in (2)].

The first hourly crude moment (about zero fading ratio) is the mean fading ratio over the hour, while the second is the mean-square fading ratio, and so on. The crude moments can be calculated from an hourly distribution curve or they can be measured directly (a practical method of measurement would have to be developed).

The hourly fading distribution is precisely defined by its moments. If only the three lowest moments are used, the definition is less precise and no-longer unique. The lower moments contain less information than the hourly curve, but they contain the most-essential information. It will be seen later that this statement is particularly accurate when the path data are required only for finding the overall effect of using several paths in tandem [addition according to (2)].

Section 17.2 shows a convenient method of computing the crude moments from the fading distribution curve. The sloping ordinate scale used for this computation is generally a useful one for presenting distribution functions of highly fluctuating quantities for which a logarithmic scale for the variant is appropriate. In Figures 7 and 8, the data are plotted with reference to the sloping lines, which apply a weighting allowance for the relative frequency of occurrence of the various parts of the original distribution. The area under the curve, when the logarithmic ordinate is allowed for, is the first moment of the fading ratio distribution. The second and third moments are found in the same way, but by plotting double or treble the distribution-curve values. The performance of a path during an hour may therefore be given by three figures. Such figures must be obtained for a large number of hours and tests must be made over a whole year—ideally over several years.

The expression of path loss data in terms of moments is a considerable advance over other methods that do not give a simple numerical result. It offers the possibility of making the hourly performance (in terms of moments) the subject for statistical treatment.

6. Classification and Condensation

The hourly results expressed by moments can be considered as a condensation of one hour's fading information into a set of three quantities. Before condensing the test results further, it will be necessary to divide the totality of results into classes of results that belong to different parts of the diurnal cycle.

This could be done by averaging separately each of the three hourly moments or their logarithms for each hour of the day over, for instance, a month. If these (hour-class) averages are plotted against the hour of day, the resulting curves will show the diurnal cyclic effect. Data for all periods of day having similar performance as shown by these curves may be provisionally classed together.

It is not desirable to have too many classes and similar performance in the above should be interpreted rather broadly. It should, in particular, be remembered that the third moment depends on the third power of the fading ratio, so that a difference of 2:1 (3 decibels) in third moments corresponds roughly to a fading difference of only 1 decibel. It may thus be convenient to plot the second and third moments in terms of their square and cube roots, respectively.

6.1 Final Classification

The purpose of this section is to determine the grouping of the path data into classes. The problem of expressing the class performance will be dealt with separately. While it is desirable to

have only a few classes, it is also important not to class together data having systematic differences.

Sets of 30 hourly results are small samples and so liable to sampling error, and it is therefore very desirable to combine as many single-hour sets as appropriate. It may be quite proper in this case that the frequency of occurrence of a single bad hour is reduced. This may be an improvement in the data due to the larger (combined) sample, but in combining data in this way it is implicitly assumed that a very-bad event that actually occurred in only one part of the sample (hour class) did so by sampling effect, but that if testing could be extended it would be found in all parts of the data to the average extent. In other words, it is assumed that the hour classes put into one class are samples of the same population. This assumption should be borne in mind in selecting the hour classes for a class.

It is not easy to distinguish sampling differences between hour classes (which do not bar the hours from being classed together) from systematic differences between hour classes (which make it improper to put them into a class). To answer such questions, it will be desirable to consider the statistics of the moment distributions. In each particular hour class there will be (for one month) 30 sets of crude hourly fading moments, the variates being m'_1, m'_2, and m'_3, each of which should be considered separately. When these distributions are very skew, the comparison between hour classes is best carried out in terms of the logarithms of the moment rather than of the moments themselves. Two methods of comparison will now be described.

The distribution of $\frac{1}{2} \log m'_1$ has moments t'_{11} and t'_{12}, which are its first and second crude moments. Each hour class defines such a set of parameters and each set applies to a sample of 30 items from a parent (class) population. The problem is to decide which sets of parameters belong to the same parent population.

The individual hour-class values t'_{11} have a theoretical variance that for a sample of 30 items will be approximately 1/30 of the variance t_{12} of the sample (hour class) itself[2]; $t_{12} = t'_{12} - t'^2_{11}$.

[2] For a description of the necessary tests see, for instance, G. U. Yule and M. G. Kendall: "An Introduction to the Theory of Statistics", fourteenth edition, Griffin, London, England; 1950: Chapter 22, "The Analysis of Variance."

The standard error of the sample mean t'_{11} is the square root of the theoretical variance. The parent mean (which it is desired to find) and the sample mean are not likely to differ by more than 3 times the standard error. This rule is fully accurate only when m'_1 is log-normally distributed. Similarly, if two samples have been drawn from the same parent population, the theoretical variance of the difference of their mean will be 1/30 of the sample variances. The difference should not exceed 3 times the square root of the theoretical variance of the difference.

To be more sure that two samples were taken from the same parent population it is also necessary to compare the parameters t_{12}, the sample variance of each hour class.[2]

What has been said about the distribution of m'_1 also applies to m'_2 and m'_3, but the higher moments arise largely from rare events and are therefore subject to large sampling effects. When the parent population is nonuniform or patchy, sampling variations will be particularly severe and this is likely to be the case with fading effects.

An alternative method of deciding which hour classes can be classed together consists of plotting the (discontinuous) log-moment distribution curve for each hour class on the special coordinate system described in section 17.2. For 30 results, the increments in p may conveniently be taken as 3.2 per cent per result.

The curve is a very-unusual type of histogram that gives prominence to high values of the variate without giving them undue weight. By comparing the histograms of different hour classes it should be possible to decide which may be classed together.

If an overall fading problem involving many sections is to be solved, the small errors in classification of the separate section data will not be serious. In section 13, however, the data for a single path will be used to represent many sections and in such a case it is particularly important to classify correctly.

6.2 Class Performance

It would seem reasonable to express the result of the statistical summation in (2) in terms of overall moments. Such moments have been formulated and it was found that all the expressions are simplified if both the individual section moments and the overall moments are expressed

in terms of central moments rather than as crude moments. (The central moments are taken with respect to the mean of the hourly distribution.) The result is quoted without proof[3]: the moments of the sum are equal to the sum of the moments of the quantities being added. This is true for second and third central moments.

The central moments are very simply related to the crude moments.[3] The first moment is left as a crude moment but obeys the moment addition rule (the first central moment being always zero). The data for a class will consist of a set of crude hourly fading ratio moments for each individual test hour. In a class there will be 30 such sets for each hour class. The results for each single hour should now be translated from crude into central moments.

The next problem is to find suitable ways of condensing the central moment data for a class into a simple statement. One method is to plot the distribution of each central moment for the whole class, there being three such curves for each class. It should be noted that these curves contain no information about correlation between the three central moments. In using them it will be assumed that there is a high degree of correlation between the three moments. This should be verified at this stage. Another method is to express each of the three moment distributions by its central moments. For clarity, these moments of moments will be called central distribution parameters of the central fading ratio moments.

The method of parameters is preferred for general purposes; the path performance for a class will then be given by three groups of three figures. The first group describes the hourly first-moment distribution m'_1 by its distribution parameters, which are: x_{11} for the first moment (mean); x_{12} for the second central moment; and x_{13} for the third central moment.

The second group similarly describes the hourly second central-moment distribution m_2 by its central parameters x_{21}, x_{22}, and x_{23}, while the third group describes the hourly third central moment distribution m_3 by its central parameters x_{31}, x_{32}, and x_{33}. It will generally be found convenient to state the parameters logarithmically.

All the figures depend on the arbitrary quantity A_0 in (2), but they can readily be translated into terms of a different constant. If A_0 is reduced by A_1 decibels, for instance, the moments and their distribution parameters will change as shown in Table 1.

TABLE 1

INCREASE OF MOMENTS AND DISTRIBUTION PARAMETERS WHEN REFERENCE LOSS A_0 IN (2) IS REDUCED BY A_1 DECIBELS

Quantity	m_1	x_{11}	x_{12}	x_{13}
Decibels increase	A_1	A_1	$2A_1$	$3A_1$
Quantity	m_2	x_{21}	x_{22}	x_{23}
Decibels increase	$2A_1$	$2A_1$	$4A_1$	$6A_1$
Quantity	m_3	x_{31}	x_{32}	x_{33}
Decibels increase	$3A_1$	$3A_1$	$6A_1$	$9A_1$

The quantities m'_1, m_2, and m_3 are variates (hourly central moments) and a particular set of these values describes the hourly fading behaviour of one section for one class. The quantities x_{11}, x_{12}, and x_{13} are the distribution parameters of the first hourly moment; similarly, the other x values define the parameters of the higher hourly moment distribution. These parameters are characteristic of the fluctuation of the m values of their class. More particularly, it can be said that an m'_1 value is the mean fading ratio for an hour (this is the power mean, sometimes referred to as root-mean-square fade). The following serves to clarify the significance of some of the parameters:—

x_{11} = mean fading ratio for the whole class (period of day).

x_{12} = variance of the hourly mean fade for the whole class.

x_{21} = mean hourly fading variance for the whole class.

x_{22} = variance of the hourly fading variance for the whole class.

The variance is the second moment about the mean value of the variate and is equal to the square of the standard deviation.

It may be appropriate to select only a few classes of data for further work. These might for instance include such classes as: the worst period of day during the worst month and the worst

[3] This rule is a special case of a more-general rule, namely that the cumulants of a summation equal the sum of the cumulants of the quantities being added. The cumulants (or Thieles' seminvariants) are described by M. G. Kendall, "The Advance Theory of Statistics," volume 1, fifth edition, Griffin, London, England; 1952: see page 60.

[4] Footnote reference 3: page 290 and following pages.

period of day that coincides with the busy hour. These may be used to represent the performance of the particular path when computing in section 10 the equivalent-single-section loss distribution. It is, of course, essential that the classes taken for the individual paths shall be consistent; that is, they must apply to the same time of day.

6.3 Validity of Condensed Results

In using the condensed results for prediction, the implicit assumption is made that further tests, if they were made in subsequent years, would give results statistically equal. This assumption cannot be avoided, but the probability of the prediction being accurate becomes greater as the volume of results on which the prediction is based increases. But however carefully the available results are treated, they are only the results for a particular test period and the possibility cannot be excluded that in the future there may be years when the statistical performance will be rather different from that of the test year. The overall error to which this may lead in practice is lessened by the fact that the single path is only one of a large number that make up the overall circuit. If, however, there are long-term effects common to all the paths, the error could be substantial. Other methods of reducing the volume of results are less appropriate than that described. It would, for instance, be incorrect to base the work on the fading performance for periods of several hours; such data would not necessarily be valid for prediction of hourly performance, but rather for the performance over several hours together.

The condensation method proposed includes all the available path information, provided that the extent of averaging is limited, as discussed in section 6.1.

Although the discussion has been in terms of hourly results, the methods could be applied equally for other lengths of time, provided that cyclic effects were not concealed. Data expressed for a certain period of time can often be used for calculating performance over a greater length of time, but generally they cannot be used for accurate prediction of the performance over much-shorter periods. It is therefore very important that the basic data should be available in terms that are closely related to the terms of the overall noise performance specification.

6.4 Comparison Between Different Radio Paths

An important advantage of the condensed form of path-performance statement (section 6.2) is that it permits comparison of the performance of different paths on a realistic and numerical basis. It is expected that with experience of such data, it may become possible to associate the various x parameters with detailed properties of the individual paths, as length, local climate, clearances, and reflection factors. It may also be found possible to isolate the effect of antenna directivity on the path loss performance. Knowledge of such effects would be a great help in planning future radio paths.

6.5 Recommendation for Overall Noise Specification

The full benefit of such knowledge of path performance will be effective only if the overall noise requirements for a complete 2500-kilometre (1550-mile) circuit are stated in such a form that they can be translated into terms of x parameters for the overall permitted noise. These can then be subdivided to provide for various sources of noise and particularly to provide for thermal noise in terms of x-parameter requirements for a single path or for a few paths used in tandem.

With this in view, it is recommended that the overall noise requirements for long-distance telephone circuits should be stated in terms of moment parameters.

7. Time Structure of Fading

The type of data discussed so far gives information about the distribution of fading; that is, for what fraction of time certain values are exceeded. It does not give a complete and unambiguous answer to questions about the short-time structure of fading events; that is, the length of time a fade remains in excess of a certain value or the number of occasions when fading passes through a certain value. The time structure for very-short periods may be of interest for the overall link with many paths connected in tandem, but the interest will mainly be in the time structure of high values of fading in the equivalent single section. These will arise largely from very-high fading in a single link; only very rarely will they

be caused by a combination of fading in several links.

When time-structure information is required, it may be sufficient to know the time structure of only the very-highest fading in the individual paths and to measure the number and length of periods during which the path loss of individual sections exceeds a particular single large value.

An alternative way of obtaining more information about the time structure is to express the path performance in terms of the moments of fading for intervals much shorter than an hour. These moments will fluctuate much more than the hourly ones, but the overall result of using such data may give sufficient detail of the time structure.

8. Simple Tandem-Section Fading Problem

In this section a method will be described of calculating the equivalent-single-section loss (2)

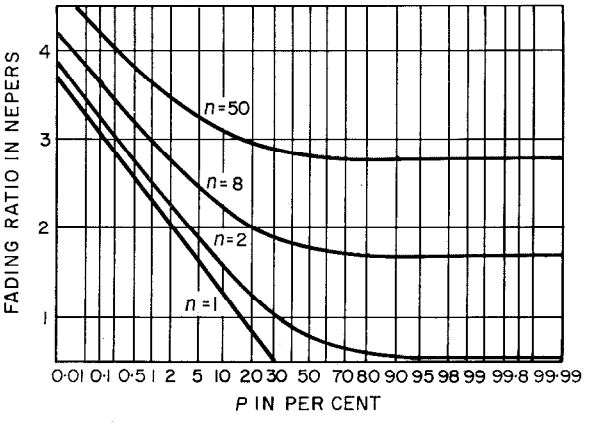

Figure 1—Addition of log-normal distributions for σ = 1 neper. Curve $n = 1$ is the parent population; the other curves represent the sum of 2, 8, and 50 items from curve $n = 1$.

when n sections are connected in tandem. All sections are assumed to have a log-normal fading-ratio distribution. This case is not likely to arise in practice, but its solution is a useful stage in the approach to the problem of finding a distribution function having specified moments.[5]

[5] The solution is also very useful in dealing with the addition of intermodulation noise products in multichannel telephone systems. See, for instance, B. B. Jacobsen, "Probability Theory in Telephone Transmission," *Teleteknik* (English edition), volume 1, number 1, pages 83–85; 1957: also, *Electrical Communication*, volume 35, number 4, pages 266–268; 1958.

Log-normal fading-ratio distribution means that the fading loss (in logarithmic measure) is normally distributed. The curve for $n = 1$ in Figure 1 is an example of such a distribution when the standard deviation is 1 neper. These curves are always straight lines when plotted on the probability scale used in Figure 1, the slope of the curve indicating the standard deviation of the logarithmic quantity. The single-path loss, A, in this case is given by

$$A = A_0 + y\sigma \text{ nepers}, \tag{3A}$$

where A_0 is the median path loss, σ is the standard deviation, and y is the normalized variate common to all normal distributions. (In Figure 1, the probability scale could be replaced by a linear y scale having $y + 3{\cdot}72$ at the left-hand edge (0·01 per cent), $y = 0$ in the middle at 50 per cent, and $y = -3{\cdot}72$ at the right-hand edge (99·99 per cent).) The frequency function for this distribution is

$$dP = \{1/(2\pi)^{\frac{1}{2}}\}(\exp -y^2/2)dy. \tag{3B}$$

The fading ratio is W, where

$$W = \exp 2y\sigma \text{ units}. \tag{4}$$

It is required to find the equivalent-single-section loss A_e in (2) when n sections are used in tandem (neper measure is used to simplify the equations). Equation (2) can now be rewritten as

$$A_e - A_0 = \tfrac{1}{2} \log \sum_1^n W_r \text{ nepers}. \tag{2A}$$

The W values from the different sections are log-normally distributed and mutually independent, and the addition will be carried out in terms of the central moments of W (see section 6.2). It is easiest first to determine the crude moments.

The rth crude moment of W is

$$m'_r = \int_0^1 W^r \, dP. \tag{5A}$$

Substituting from (3B) and (4) and rearranging gives

$$m'_r = (1/2\pi)^{\frac{1}{2}}(\exp 2r^2\sigma^2) \times \int_{-\infty}^{+\infty} \exp -(1/2)(y - 2r\sigma)^2 dy \tag{5B}$$

$$= \exp 2r^2\sigma^2 \quad \text{or} \quad r^2\sigma^2 \text{ nepers}. \tag{5C}$$

The first moment is the mean fading ratio of the distribution (root-mean-square fade). Allowing now for the median value A_0, the first moment will be the median value plus the square of the standard deviation (in nepers). The second and third central moments, m_2 and m_3, are related to the crude moments by

$$m_2 = m'_2 - m'^2_1 \tag{6}$$

$$m_3 = m'_3 - 3m'_1m'_2 + 2m'^3_1. \tag{7}$$

The sum-moments, that is, the moment of $\sum W_r$ in (2A), are n times the moments for a single section. To simplify the expressions, the following substitution is made:—

$$(\exp 4\sigma^2) - 1 = p. \tag{8}$$

Table 2 shows the result.

TABLE 2

MOMENTS OF LOG-NORMAL DISTRIBUTIONS WITH ZERO MEDIAN

Order of Moment	Crude Moments	Central Moments	Central Moments (n Combined)
1	$\exp 2\sigma^2$	—	n ($\exp 2\sigma^2$)
2	$\exp 8\sigma^2$	$(\exp 4\sigma^2)p$	n ($\exp 4\sigma^2)p$
3	$\exp 18\sigma^2$	$(\exp 6\sigma^2)(p^3+3p^2)$	n ($\exp 6\sigma^2)(p^3+3p^2)$

The central moments of the sum distribution given in Table 2 may in some cases be a sufficient answer—at least when the overall noise specification can be expressed in moment form. It is particularly convenient to retain the moment form if other noise contributions have to be added. If these also are expressed in central-moment form, the addition is direct. It may, however, be required to find the distribution function for A_e or other related variables of similar properties; the following section deals with this problem.

9. *Finding a Distribution Function Having Specified Moments*

Strictly speaking, all the moments should be taken into account to define a distribution function, but in practice it is often sufficient if the first three moments are correctly represented by the solution. A distribution function based on the first three moments is not unique and the higher moments are not necessarily correctly represented.

A function has been found that is particularly appropriate when W is a log-normal quantity (4). In selecting this function, it has been borne in mind that the upper values of the distribution for the summation (2A) will be rather similar in general character to that of the original distribution, but with increased occurrence, and that the lower values are not required to be very exact.

The chosen function will be referred to as an augmented log-normal distribution, defined by

$$W = (1 - a) + a \exp(2y\sigma_s - 2\sigma_s^2) \text{ units}, \tag{9}$$

where W is the variate (later to be used to represent the sum variate W_n), σ_s and a are auxiliary constants, and y has the definition used in (3B). The central moments of this function are found to be

$$\left.\begin{aligned} M'_1 &= 1 \\ M_2 &= a^2p_s \\ M_3 &= a^3(p_s^3 + 3p_s^2), \end{aligned}\right\} \tag{10}$$

where p is defined as before in (8). It should be noted that this is for a distribution function of unit mean power and it will therefore be necessary to increase W in (9) to obtain the required mean power; the second and third moments (10) must then be increased respectively by the square and cube of the multiplier k.

The required constants are obtained by equating the increased moments with the central sum-moments from Table 2. This gives

$$n \exp 2\sigma^2 = k \tag{11A}$$

$$n (\exp 4\sigma^2)p = a^2k^2p_s \tag{11B}$$

$$n (\exp 6\sigma^2)(p^3 + 3p^2) = a^3k^3(p_s^3 + 3p_s^2). \tag{11C}$$

If (11A) is substituted in the others,

$$p/n = a^2p_s \tag{12}$$

$$(1/n^2)(p^3 + 3p^2) = a^3(p_s^3 + 3p_s^2). \tag{13}$$

If (13) is divided by (12) raised to the power 3/2,

$$\left.\begin{aligned} \frac{1}{n^{1/2}} C &= \frac{p^{3/2} + 3p^{1/2}}{n^{1/2}} \\ &= p_s^{3/2} + 3p_s^{1/2} = C_s. \end{aligned}\right\} \tag{14}$$

This quantity has the advantage of being independent of a. (The quantities C and C_s indicate skewness of the distributions. C is the square root of Pearson's β_1 coefficient.)

Equation (14) is conveniently solved by a graphical method. Figure 2 shows C and p as functions of σ. The value of C is found first by entering the graph with the value of σ given in (3A). C is then divided by $n^{1/2}$ to give C_s. By entering the graph with this value, σ_s is found. Equation (12) then yields a^2 as the ratio p/np_s (the p values are read from Figure 2 by using σ and σ_s). k is most conveniently found as $n \exp 2\sigma^2$.

The required distribution of W_n is obtained by combining the two parts of (9), each multiplied by k. It will generally be desired to express W_n in log measure as A_e. The required sum distribution plotted to a scale of linear probability has an asymptote corresponding to each of the two components. The horizontal asymptote is

$$\tfrac{1}{2}\log(1-a) + \tfrac{1}{2}\log n + \sigma^2 \text{ nepers.} \quad (15)$$

The other asymptote is a log-normal distribution, with median

$$\tfrac{1}{2}\log a + \tfrac{1}{2}\log n + \sigma^2 - \sigma_s^2. \quad (16)$$

and standard deviation σ_s.

The final curve may be calculated by plotting the two asymptotes and adding for each probability the power values corresponding to the asymptotes. Figure 1 shows the result of a particular example in which $\sigma = 1$ neper; curves are shown for $n = 1$, 2, 8, and 50 sections, while Figure 3 is for $\sigma = 0{\cdot}5$ neper. (In the original publication, Figures 3 and 5 were transposed.)

The statistical summation of log-normal distributions expressed in augmented log-normal form will in most cases be accurate at the higher levels of fading but less accurate at the lower and lowest levels.

Possibly a better function could be found for the special case of log-normal summation, but the augmented log-normal form is very simple in use and, it is believed, sufficiently accurate where accuracy is needed.

9.1 Distribution Curve Representing Moment Summations

The augmented log-normal distribution can be used more widely to find distribution functions corresponding to sets of statistical moments that are the result, not of the addition of log-normal distributions, but of other distributions approximately log-normal only in their upper ranges.

In the general case, the path losses to be combined are unlikely to be log-normally distributed, but they may still be expressed in terms of their fading-ratio moments, and these may be added and the sum distribution A_e, (2), determined from the sum-moments.

If the three moment sums are M_1', M_2, and M_3, then

$$\left.\begin{aligned} M'_1 &= k \\ M_2/(M'_1)^2 &= a^2 p_s \\ M_3/(M_2)^{3/2} &= p_s^{3/2} + 3p_s^{1/2}. \end{aligned}\right\} \quad (17)$$

These correspond respectively to (11A), (12), and (14) and thus define an augmented log-normal distribution representing the three moments. In this case there is no restriction to addition of path losses all having the same distribution; the equations apply quite generally where the sum-moments are available, but the result is, of course, an approximation to the true distribution curve.

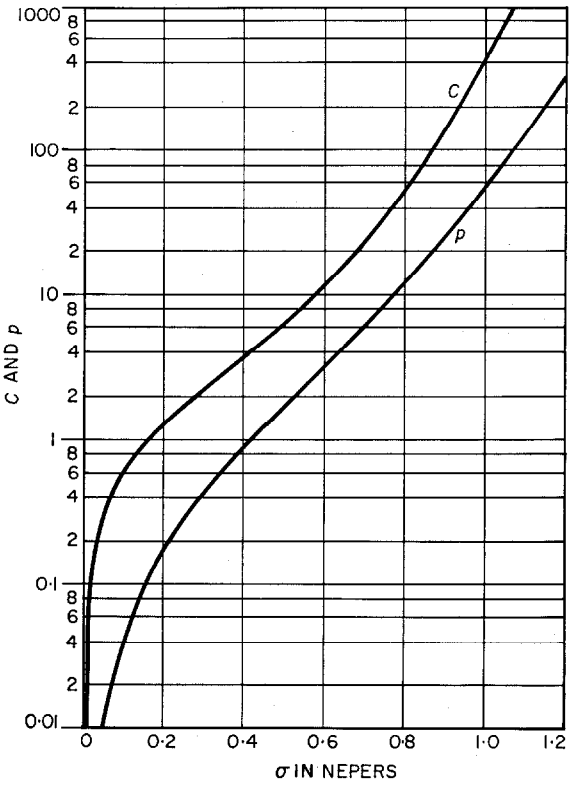

Figure 2—The constants p and C used for log-normal distributions. $p = (\exp 4\sigma^2) - 1$, $C = p^{3/2} + 3p^{1/2}$.

10. *Calculation of Multisection Fading Effects*

In section 6.2, the path performance was expressed in terms of the distribution parameters of the hourly central moments of the section fading ratio. Each transmission section in a multisection link has 9 such parameters for each class of performance. In this section, the statistical addition of the fading effects in the individual tandem-connected sections will be carried out in terms of these parameters.

The first step is to determine 9 parameters X_{rs} of the equivalent-single-section loss. These describe the hourly moment distributions of the equivalent-single-section loss (or overall fading ratio):—

$$X_{rs} = \sum_{1}^{n} {}_{1}x_{rs} + {}_{2}x_{rs} + \ldots + {}_{n}x_{rs}. \qquad (18)$$

By applying the X values in (17) in place of M, augmented log-normal curves can be found describing the three first hourly moments of the equivalent single section (or overall circuit fading-ratio hourly moments) for a particular class of performance. The X values themselves, or the moment distribution curves, may in some cases be a sufficient final answer; if this is not the case, a further stage of calculation is required.

In the next step it is necessary to determine levels of probability at which the overall moment distribution curves will be read. If, for instance, the data apply for three hours of each day during a month, this particular prediction will cover nearly 100 hours in a month; if the readings for a probability of 99 per cent are taken on the sum-moment distribution curves, the sum-moments indicated will be exceeded for (on the average) one hour in the 100 hours for which the class is valid. The distribution of the equivalent-single-section loss is next found by using (17) again. The result is the hourly distribution that is likely to obtain for one hour in the class considered. This is one final answer. It will generally be appropriate to repeat this process for other assumed probability values and later to deal with other sets of data (classes) in the same way. The precise procedure will depend on the exact form in which the information is required.

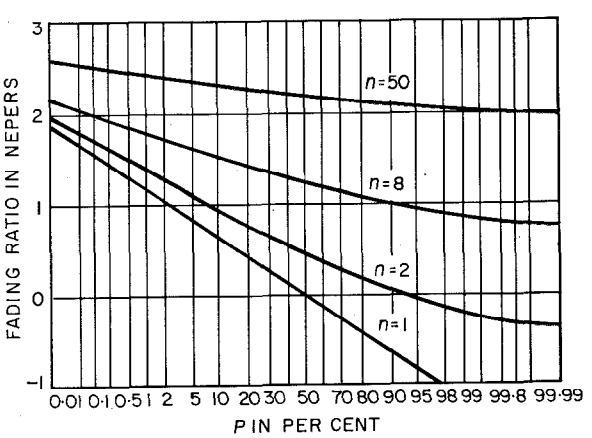

Figure 3—Addition of log-normal distributions for $\sigma = 0{\cdot}5$ neper.

When using the sum-moment distribution curves, the same probability value is taken for all three moments—a compromise necessary to make the method workable. It is not an exact procedure because the three moments are somewhat independent of each other, but it is believed that the error resulting from this simplification will be very small, particularly when the sum-moments have many component moments, as will usually be the case.

The first sum-moment will show a relatively small fluctuation, and therefore will not change very greatly with the level of probability taken. It has been found that the higher region of a loss distribution curve as determined from the moments is not very sensitive to moderate changes in either the second or the third moment by itself. The assumption that the moments vary together is thus not likely to lead to serious errors.

10.1 Combination of Classes of Overall Performance

The sum-moment parameters X may be used in a different way. Instead of considering X values separately for each class, they may be combined into a single statement covering many classes. Combination of this nature must be carried out in terms of crude parameters (of the central moments). The X values for each moment distribution must therefore first be converted to the crude values X'. Each separate type of X' value must then be averaged over all classes, the individual values being weighted according to the size of the class. This results in 9 parameters X', which should now be converted to central X parameters. There will be 9 such

parameters similar to the X parameters in section 10, but in this case they describe the moment distribution over all the classes that have been combined.

They may conveniently cover the performance over a month, but could cover longer periods if the corresponding classes were included. The data for a month will thus cover about 700 hours, and the corresponding moment distribution curves can be determined as before by using (17).

These curves can now be read to determine the moments of the hourly overall fading distribution that is exceeded only during, for instance, the worst 7 hours (1 per cent). What was said in section 10 about using the same probability values when reading the three moment curves applies here also, but probably the consequences are more serious in the present case, since the combined statistics contain classes of very-different performance, whereas in section 10, there was only a single class of relatively uniform performance.

10.2 Practical Limitation

The practical value of the methods just described may be restricted for lack of necessary data. As a rule, only a small number of transmission sections are installed at any one time, and test results can at best be obtained for only a few sections. It is, nevertheless, necessary to be able to check whether such sections as are available for test are suitable for forming part of an overall connection to the full 2500-kilometre (1550-mile) planning length. The problem has received some attention and two methods of making the necessary comparisons will be dealt with in sections 11 and 12 respectively.

11. Subdivision of Overall Noise Specification

One method is to find the equivalent specification for a fraction of the overall circuit (partial circuit). If the overall specification can be translated into terms of moments, there is little difficulty in defining the permissible moments for partial circuits or in translating these moments into limiting path-loss-distribution curves, but it is not possible to define fluctuation for the partial-circuit moments unless the overall criterion itself contains a moment-fluctuation allowance. In the absence of a fluctuation clause, the requirements tend to become unnecessarily severe for the partial circuit.

It is therefore very desirable that the overall specification should contain a moment fluctuation clause, at least for the third moment, which is most sensitive to high fading values of short duration. A more-satisfactory form for the overall criterion would be one that specified a distribution curve for the hourly moments during the month, or the parameters of such a distribution as proposed in section 6.5.

The present Comité Consultatif International Télégraphique et Téléphonique noise specification in effect gives a maximum limit for the first moment in any hour; it would therefore remain necessary to define limits for the second and third moments and it is for these that a specification in terms of hourly-moment distributions would be more suitable than mere maximum values.

12. Synthetic Overall Circuit Based on a Partial Circuit

According to the second method, a synthetic overall circuit is produced by imagining the real partial circuit in question to be tandem connected with itself a sufficient number of times to reach the full planning distance. This device is available only for statistical approach: it would be incorrect to make such a tandem connection on an actual circuit, for this would amount to the assumption that the path losses in the partial circuits are completely covariant—an assumption that is quite unwarranted. But, statistically it is possible to make proper use of this device. In the sampling process that is normally used for computing overall performance, it is only necessary in (18) to take all n items in the samples from the data of the actual partial-circuit sections instead of from n different sets of path data. The data must, of course, apply to a particular class.

In an extreme case, this can even be carried out for a single radio path. A procedure that can be carried out with so little data is more likely to find practical application than the more-complete one and it will therefore be described in more detail. A very-convenient method has been found for calculating the sum-moment distributions for this special case.

13. *Synthetic Overall Circuit Based on a Single Path*

The path data consist of the moment distributions for various periods of the day (classes). The rth moment is represented by a function $M_r(p)$, where p is the probability that $M_r(p)$ will not be exceeded. It is required to find the distribution of the sum of n values chosen at random from $M_r(p)$. The resulting distribution is $M(z_n)$, for which the following approximate equation has been derived:—

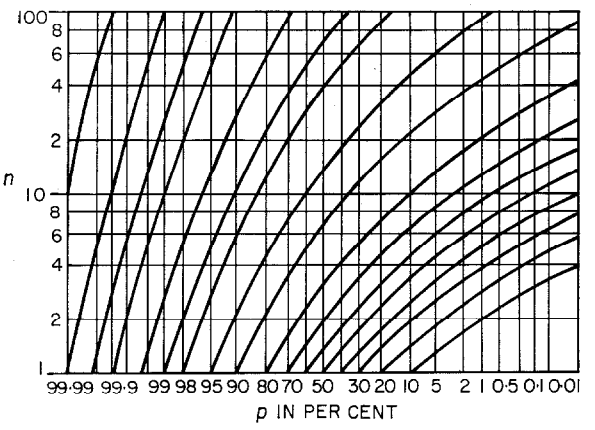

Figure 4—Curves for transforming probability scales. Used in connection with (19) for statistical summation; $z_n = p^n$.

$$M(z_n) = (n-1)\frac{1}{p_1}\int_0^{p_1} M(p)\,dp + M(p_1), \tag{19}$$

where $z_n = p^n$. Figure 4 shows z_n in graphical form.

In the special case of a distribution with unit first moment, the function

$$\frac{1}{p_1}\int_0^{p_1} M(p)\,dp$$

goes from 0 to 1 as p_1 goes from 0 to 1, and the function shows promise of being important for the sampling of distributions. It may be said to indicate the running mean value of the distribution over the range 0 to p. This function is easily calculated either directly from the data or from $M(p)$ in graphical form; in the latter case, the method described in section 17.2 is useful for the integration process.

For the purpose of a check, (19) has been applied to the summation of log-normal distributions. It is more accurate than the augmented log-normal method, but the results of the two summations agree accurately at the higher levels. Figure 5 shows the result of this computation; it should be compared with Figure 1.

For the purpose of the present section, $M(z_n)$ should be determined from (19) for each of the three moment distributions. If the final result is required in terms of equivalent-single-section distribution, (17) may be used as before (section 10) to find augmented log-normal distributions for a number of levels of probability in the $M(z_n)$ functions. The distributions thus found describe the equivalent-single-section loss of the synthetic overall circuit and from this the thermal agitation noise in any given system is readily calculated.

For an alternative calculation of synthetic overall circuit performance, the x values in (18) may all be taken from the available single-path data instead of from n separate paths; the work can then proceed exactly as in the general case (section 10). However, the method just described is the more accurate.

14. *Acceptance Test for a Radio Path*

The results of sections 12 and 13 show what fading would result in an overall circuit if it were built up by using sections with fading statistics identical with those of the actual single section for which fading results are available. This is a very-important result that would make it possible to decide whether the section in question was suitable to be one of the sections in an overall circuit.

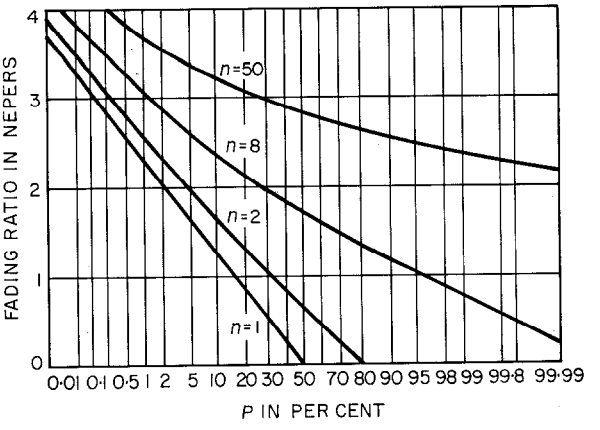

Figure 5—Addition of log-normal distributions for $\sigma = 1$ neper. Addition carried out by (19).

The final step of comparing the noise calculated for the synthetic circuit and the specified overall noise cannot be taken until a complete overall noise specification is available. A recommendation for the form of such a specification is made in section 6.5.

15. Conclusions

In calculations of the thermal noise for a multisection radio link, it is very important to take proper account of cyclic effects common to the fading statistics of many of the sections. It is recommended that fading data shall be expressed in terms of hourly performance and that the hourly fading performance shall be expressed in terms of the first three statistical moments of the fading ratio.

The moments for a particular hour of the day (during, perhaps, a month) may be grouped into a class with the moments for other hours of the day that appear to have similar performance. In each class, the moments of individual samples of hourly fading performance will fluctuate. It is therefore also necessary to calculate the statistics of the moments in each class. The path information for each class will then be specified by 9 parameters. Separate classes will also be needed for different parts of the year.

When these parameters are available for all the sections of an overall circuit, the hourly overall circuit fading effect can be evaluated in terms of either the overall fading-ratio moments or the overall fading distributions that will not be exceeded for specified fractions of the periods covered by a class of fading behaviour.

The full data needed for such an overall computation will rarely be available, but in the light of the principles of this computation a synthetic overall circuit is proposed that may be based on the performance data of even a single path. The performance computed for this circuit makes it possible to judge whether the single path is suitable for use as one of the paths in the hypothetical reference circuit used to define the noise-performance objectives for long-distance transmission.

An equation is given for the summation of log-normal distributions as well as a more-general sampling function. Methods are described for converting distribution data to moment form and a formula is given for finding an approximate distribution function from the first three moments of a variant.

It is recommended that the overall noise specification for a long-distance circuit shall be expressed in terms of the distribution parameters of the hourly central moments of the noise.

16. Acknowledgment

The author wishes to thank Mr. F. O. Roe for help in preparing the paper for publication.

17. Appendices

17.1 Phase Noise

Assume that the carrier frequency is ω_p radians per second and consider as a noise element a sine wave differing by ω_q radians per second in frequency and of a times the carrier-frequency power. The sum of these two voltages has the following approximate form when a is very small:—

$$(1 + a^{\frac{1}{2}} \sin \omega_q t) \sin (\omega_p t + a^{\frac{1}{2}} \cos \omega_q t).$$

The carrier frequency appears to be modulated in amplitude and phase. The effect of a limiter is to suppress the amplitude modulation, but the phase-modulation information remains and is equivalent to what could have been produced by a useful input signal of frequency ω_q. The effect of the carrier noise element is therefore to produce phase noise. In the example, the phase noise is of $(a/2)^{\frac{1}{2}}$ root-mean-square radians amplitude. It is convenient to express the square of the phase noise amplitude in decibels referred to an amplitude of 1 root-mean-square radian.

For the noise element of power $A = 10 \log a$ decibels referred to that of the carrier, the phase noise will be $(A - 3)$ decibels referred to 1 root-mean-square radian.

If a number of single small noise elements are present, the phase noise effects will combine on a power basis when the noise elements are of differing frequencies.

If the carrier-frequency noise is of uniform spectral density, the phase noise also will be of uniform density (white noise). Since noise bands above and below the carrier frequency are operative, the phase noise density per unit bandwidth at base-band frequency will equal the radio-frequency noise density relative to the carrier

power. If the radio-frequency noise density per unit bandwidth is A decibels referred to the received carrier level, the phase noise per unit bandwidth at base-band frequency will be A decibels referred to 1 root-mean-square radian. This equation is true also when the carrier frequency is modulated in phase or frequency.

Phase noise will be translated into base-band noise at the receiving terminal, but the exact translation will depend on the phase-modulation constant of the system at the various base-band frequencies. This constant is the phase signal (in decibels referred to 1 root-mean-square radian) that results when a base-band signal of 0 decibels relative to 1 milliwatt is applied.

If, for example, the phase-modulation constant for a particular telephone channel is -16 decibels referred to 1 root-mean-square radian and the phase noise per 4-kilocycle-per-second bandwidth is A decibels referred to 1 root-mean-square radian, the circuit noise will be $(A + 16)$ decibels relative to 1 milliwatt at a point of zero relative level, and in practice a psophometric weighting allowance may be required.

In a frequency-modulated system, the phase-modulation constant will vary over the base band: in a phase-modulated system it is constant. Actual systems tend to use frequency modulation at the lower frequencies but to approach phase modulation at the upper base-band frequencies.

The phase noise in all systems will tend to be of uniform density and for this reason it is convenient to work in terms of phase noise.

17.2 Determination of Crude Moments from Distribution Curves

When a logarithmic scale is used for the variate, it is particularly easy to determine graphically the moments of a distribution function. The principle adopted is to weight the distribution curve by its own "frequency". When the variate is in logarithmic terms, this is done by subtracting from the log-variate a quantity proportional to the logarithm of the frequency of occurrence. The frequency of occurrence is the differential of the probability and a suitable constant must be selected to determine the scale of the crude moment integral.

The method will be explained with reference to Figure 6, which shows a distribution curve A. The variate is the fading with respect to free-space transmission. The probability scale is logarithmic; p is the probability of the variate not being exceeded. The x scale is a transformed probability scale, where $x = 5 \log_{10} (1 - p)$.

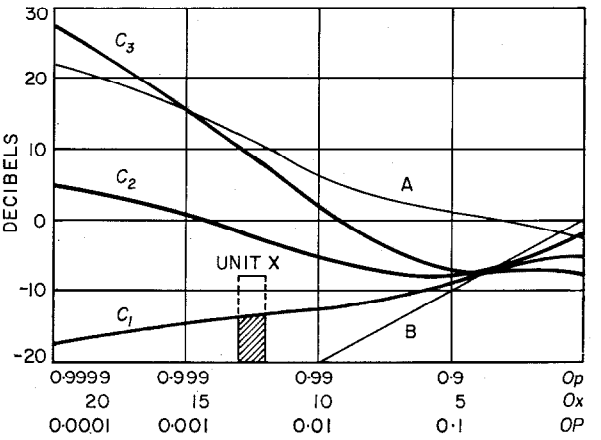

Figure 6—Graphical determination of moments and a special presentation of probability curves. Multiply moment result by 0·46 ($-$ 3·36 decibels).

Curve B shows the weighting function used, and has a slope of 10 decibels per decade in $(1 - p)$. For convenience, the curve applies zero weighting at $x = 0$. This introduces a scale error when the curve is integrated, but this is readily corrected by multiplying the moment results by 0·461 ($-$3·36 decibels). This correction applies when the integration is made in terms of unit x values.

The curve C_1 is obtained by adding the weighting values to curve A. To determine the first moment of curve A, the ordinates of curve C_1 should, in principle, be transformed into fading ratios, the area under the transformed curve then being the first moment. In practice, however, it is easier to proceed in a different way. Consider the shaded column. This is of unit width, and its moment contribution is therefore the mean fading ratio corresponding to the segment of curve C_1.

For small slopes of the segment, its mean height is very-nearly equal to the linear mean in log measure. For greater slopes, it is recommended to make a table of the linear mean in log measure with respect to the upper end point of the segment. The first moment is the sum of the

mean fading ratios of all segments multiplied by 0·461. The second (third) crude moment is worked out in precisely the same way, except that the variate values of curve A must be doubled (trebled). The resulting curves corresponding to C_1 are marked C_2 and C_3. Figure 7

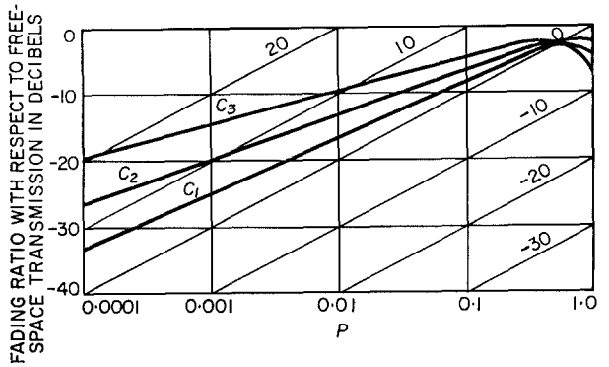

Figure 7—Path-loss curves and their moments (250 hours). 4000 megacycles per second. Path = 40 miles (64 kilometres). 1500–2100 hours.

shows a more-convenient way of plotting curves C directly. Sloping weighting lines are drawn at 10-decibel intervals and the fading distribution C_1 is plotted with respect to these lines, thereby applying the weighting automatically. The area under the resulting curve is determined as for Figure 6, using the horizontal ordinate lines in Figure 7. For the second (third) moment, two (three) times the fading distribution values have been plotted on the sloping coordinate system (curves C_2 and C_3).

The data actually used for Figure 6 were obtained[6] from a 1000-hour test in the Arncliffe Wood–Tinshill section of the Manchester–Kirk o'Shotts system in the course of a general check of path performance.

Those used for Figure 7 were obtained for the same path and period, but taking the results for the hours 1500–2100 only. Figure 8 applies to the same path, but covers only a single 6-hour period that showed exceptionally severe fading. Unfortunately, data are not available beyond 30-decibel fading and the complete evaluation of the second and third moments, in particular, is impossible. The path in question is nearly 64-kilometres (40-miles) long and therefore particularly liable to abnormal refraction fading (see section 3.2). Another difficulty is that the data are for a 6-hour period rather than the 1-hour period proposed in the present paper. For 1-hour distributions, the weighted curves would be more likely to bend over and so define the moments.

There are, however, distributions for which the moments are not finite: if "complete" fading occurs for even a very-short time, the moments will be infinite. Such distributions are not acceptable for long-distance links; or, at the worst, they can be accepted on only very-few occasions. By determining hourly fading distributions separately and condensing each hour's performance into the first three crude moments, the way is open for dealing properly with rare effects. This is done in terms of the distribution of the

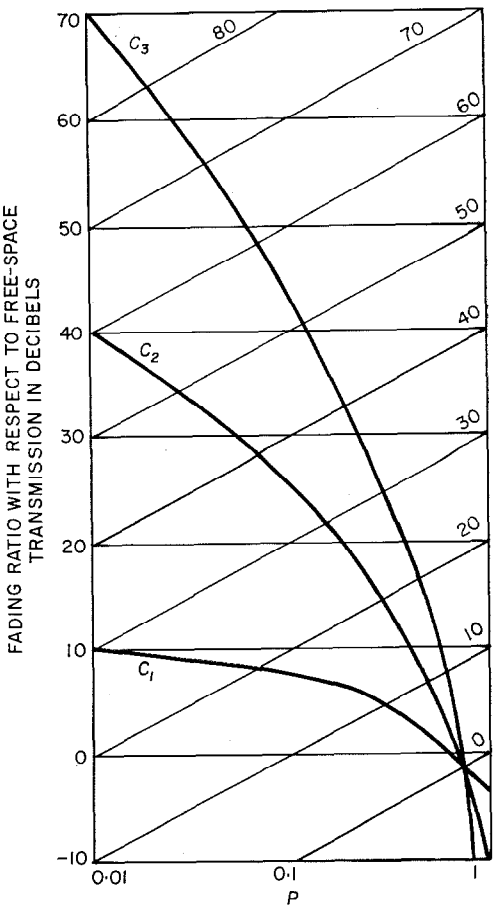

Figure 8—Path-loss curves and their moments (worst 6-hour period).

[6] G. Dawson, L. L. Hall, K. G. Hodgson, R. A. Meers, and J. H. H. Merriman, "The Manchester-Kirk o'Shotts Television Radio-Relay Systems," *Proceedings of the Institution of Electrical Engineers*, part 1, volume 101, pages 93–114; May, 1954.

hourly moments for a particular hour of the day over, for instance, a month.

In evaluating the higher moments, particularly the third, it should be remembered that an error in the third moment has less effect than might at first be expected. An error of 3 decibels, for instance, will for many purposes correspond to an error of only 1 decibel in the variate. Also there should not be too much concern about that part of the moment line that falls outside $p = 0{\cdot}01$ per cent, and which, in any case, represents only a very-small time (2·2 seconds in Figure 8, but for an hourly curve only, 0·36 second).

The first three moments can, in general, be adequately summed, provided that the distribution curves cover sufficiently short periods of time. The period of one hour seems suitable.

It is clear from curve C_1 of Figure 6 that the first moment arises largely from fading of less than 2 decibels with respect to the free-space path loss. Curves C_2 and C_3 show that the second and third moments arise largely from fading that lasted for perhaps 10 minutes during a 1000-hour test period. The presentation in Figures 6–8 gives a better indication of the relative importance of various levels of fading than does an ordinary distribution curve.

Curves such as C_1 in Figure 6 can also be used to determine, for a particular fading distribution, the integral in (19). The integral is the moment up to a certain p value on the curve divided by p (the probability of not exceeding). The resulting function may be said to represent the linear mean of all variate values below that for which the probability of its not being exceeded is p.

It should be noted that in Figure 4 the probability figures are in terms of p, where $p = 1 - P$.

Recent Telecommunication Development

Metal Rectifier Engineering

A BOOK entitled "Metal Rectifier Engineering" has recently been published. The author, E. A. Richards, was chief rectifier engineer of Standard Telephones and Cables. His sudden death when the manuscript was almost finished required that his son, W. A. Richards, complete it and handle the problems of publication.

The book is divided into the following 11 chapters.

Chapter 1—Introductory
Chapter 2—Construction and Characteristics
Chapter 3—Basic Rectifier Calculations
Chapter 4—Rectifier Losses and Efficiencies
Chapter 5—Electrical Design of Stacks
Chapter 6—Mechanical Design of Stacks
Chapter 7—Transformers for Use with Rectifiers
Chapter 8—Design of Rectifier Equipments
Chapter 9—Rectifier Harmonics and Smoothing
Chapter 10—Methods of Voltage Control
Chapter 11—Special Applications

There are 206 pages of text, 110 figures, 6 reproductions of photographs, 8 tables, and numerous equations. The dimensions are $5\frac{3}{4}$ by $8\frac{3}{4}$ inches (14.6 by 22.2 centimeters).

The book is published by Sir Isaac Pitman & Sons, 39 Parker Street, Kingsway, London, W.C. 2 and is priced at 37/6. It may also be ordered from Pitman Publishing Corporation, 2 West 45th Street, New York 36, New York, at $7.75 per copy.

Refractive Index of the Atmosphere as a Factor in Tropospheric Propagation Far Beyond the Horizon*

By R. E. GRAY

ITT Laboratories, a division of International Telephone and Telegraph Corporation; Nutley, New Jersey

TROPOSPHERIC beyond-the-horizon radio-link planning presently necessitates transmission tests to establish the median path loss and to determine the magnitude and duration of the path loss variations. Recent measurements indicate, however, that the relation existing between transmission loss and the refractive index of the atmosphere may enable estimates to be made, from climatic data alone, of the transmission characteristics of any particular path. Extreme values of transmission loss are believed to be chiefly due to exceptional variations with height of the refractive index, while the monthly median values of path loss have been found to be a function of the average surface values of the refractive index of the atmosphere on the transmission path. Curves are given showing the relation found on various paths between radio transmission loss and the refractive index of the atmosphere.

. . .

1. Introduction

No completely satisfactory theory has yet been advanced to explain tropospheric radio transmission far beyond the horizon, but it is known that the so-called scatter field is many orders of magnitude larger than the normal diffraction field at distances far beyond the horizon.

Path loss measurements made with ultra-high-frequency transmissions beyond the horizon show wide variations in received signal level from hour to hour, from day to day, and in some cases from month to month; in addition, the median path loss at these frequencies varies considerably with latitude. These variations in path loss are believed to be due entirely to changes occurring in the characteristics of the lower atmosphere, the most important meteorological factors being temperature and humidity, which, with pressure, determine the refractive index of the atmosphere.

In general, it has been found that the atmospheric conditions at any instant are not uniform along the transmission path; the average conditions at any particular time are, therefore, difficult to determine. However, the weather differences occurring along the path tend to average out during a period of a few weeks, so that daily meteorological measurements made at the two ends of a path, when averaged over, say, a four-week period, are likely to represent the average weather conditions along the transmission path during that month.

Measurements indicate that the monthly median path loss is, in general, a function of the monthly average value of surface refractivity on the transmission path; but the day-to-day variations do not, as a rule, show the same close correlation.

Although it has been shown that there is a close correlation between the long-term median path loss and the average surface value of the refractive index of the atmosphere, tropospheric radio propagation is influenced by several other meteorological factors. For example, the formation of reflecting and refracting layers[1] in the lower atmosphere may have a considerable effect on path loss, and superrefraction can reduce the path loss to less than the free-space value. In addition, atmospheric turbulence can produce scattering of radio waves in the troposphere.[2]

Tropospheric radio propagation far beyond the horizon is thus a complex phenomenon influenced by several different meteorological factors; however, a recently established fact of some practical importance is that the median

* Reprinted from *1957 IRE National Convention Record*, Part 1, pages 3–11.

[1] J. R. Bauer, "Suggested Role of Stratified Elevated Layers in Transhorizon Short-Wave Radio Propagation," Massachusetts Institute of Technology Technical Report 124; September, 1956.

[2] F. Villars and V. F. Weisskopf, "On the Scattering of Radio Waves by Turbulent Fluctuations of the Atmosphere," *Proceedings of the IRE*, volume 43, pages 1232-1239; October, 1955.

path loss, when averaged over a period of several weeks, is closely correlated with the average value of surface refractivity.

2. *Refractive Index of Atmosphere*

The refractive index of the atmosphere is given by

$$(n-1)=\frac{79}{T}\left(P-\frac{e}{7}+\frac{4800e}{T}\right)10^{-6}, \quad (1)$$

where

n = refractive index,
T = absolute temperature in degrees Kelvin,
P = total atmospheric pressure in millibars (1000 millibars = 29.5 inches = 749.3 millimeters of mercury), and
e = partial pressure of water vapor in the atmosphere in millibars = $0.00161PS$, where S = grams of water per kilogram of air.

The refractive index of the atmosphere at sea level varies between a value of about 1.000240 and 1.000400. Thus, expressed in N units where $N = (n-1)10^6$, the practical limits of N at the surface of the earth lie between about 240 and 400. Under normal atmospheric conditions, N decreases with height above the surface of the earth; and it has been shown, by Strickland[3] and others,[4] that this decrease is approximately logarithmic.

Figure 1 shows the change in the value of N with height, the normal variations in the refractive index at the earth's surface decreasing to almost zero at a height of 30 000 feet (9144 meters). The ordinate on the right of this figure shows the path length in statue miles corresponding to a height H of the volume defined by the intersection of the two tangent antenna beams as shown on the left-hand ordinate. Thus, for a path length of 200 miles (322 kilometers) the height of this common volume is 5000 feet (1524 meters). The distances shown in Figure 1 are based on an effective earth radius of 4/3 the true radius, and the heights of the common volumes assume that the antennas are close to sea level and are directed horizontally.

The expression for the refractive index of the atmosphere in N units is

$$N=\frac{AP}{T}+\left(\frac{Be}{T^2}-\frac{De}{T}\right), \quad (2)$$

where $N = (n-1)10^6$, n being the refractive index, and where the values of the constants are approximately $A = 79$, $B = 3.8 \times 10^5$, and $D = 11$.

The value of the first term of the above expression is dependent only on atmospheric pressure and temperature and is known as the "dry term," whereas the second term is dependent on water-vapor pressure and atmospheric temperature and is known as the "wet term." As the temperature increases, the "dry term" decreases for a given atmospheric pressure, but the "wet term" increases for a given relative humidity. This is because of the relation between saturation-vapor pressure and air temperature. If the atmospheric pressure and relative humidity remain constant, the refractive index increases with increasing temperature above about − 5 degrees centigrade; however, below this temperature, the refractive index increases with a decrease of temperature.

When the air temperature is low, a given change in relative humidity produces a much-

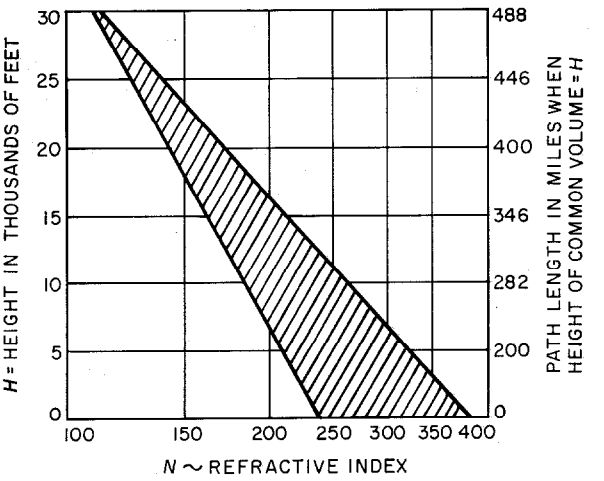

Figure 1—Variation of refractive index with height.

[3] A. C. Strickland, "Refraction in the Lower Atmosphere and Its Application to the Propagation of Radio Waves," "Meteorological Factors in Radio Wave Propagation," The Physical Society, London, England; 1946.

[4] M. Schulkin, "Average Radio-Ray Refraction in the Lower Atmosphere," *Proceedings of the IRE*, volume 40, pages 554–561; May, 1952.

smaller change in refractive index than when the temperature is high. For example, at a temperature of − 5 degrees centigrade, a change in relative humidity from 50 percent to 80 percent produces a change in the surface value of N of only 6 units or, say, about 2 percent. However, at a temperature of + 25 degrees centigrade, the same change in relative humidity results in a change in N of 40 units or, say, 13 percent.

The atmospheric pressure at the surface of the earth may vary, under extreme conditions, from 900 millibars to 1060 millibars; however, under normal conditions, the surface pressure varies from about 990 to 1030 millibars. The change in pressure experienced when going from cyclonic to anticyclonic conditions is thus about ± 20 millibars, producing a change in N of 12 units or, say, about 4 percent. It is seen, therefore, that at low temperatures, say at − 5 degrees centigrade, the normal variations in atmospheric pressure produce about twice as great a change in N as would a normal variation in relative humidity of from 50 percent to 80 percent. However, at higher temperatures, say + 25 degrees centigrade, the reverse is the case; and a change in relative humidity of from 50 percent to 80 percent results in a change in the value of N more than three times as great as would a normal change in atmospheric pressure of from 990 to 1030 millibars.

Thus, in cold climates the daily variations in the refractive index of the atmosphere are largely caused by variations in atmospheric pressure, whereas in temperate or warm climates the daily changes in temperature and relative humidity are likely to cause much greater changes in the refractive index than do the normal changes in pressure. The seasonal change at any particular location is almost entirely due to the seasonal change in temperature and relative humidity.

The refraction of rays passing through the atmosphere is due to the change in refractive index with height. The average conditions are represented by an atmosphere having a linear refractive index gradient below about 10 000 feet (9144 meters) of 11.9 N units per thousand feet; rays passing at small elevation angles through such an atmosphere have a constant curvature. It can be shown that with this standard atmosphere, the earth may be replaced by an equivalent earth with a modified radius of 4/3 the true radius, and the refracted rays may then be drawn as straight lines. In practice, however, it is found that the refractive index gradient is not, in general, linear, being greatest in the lower layers of the atmosphere; and under such nonlinear conditions, the curvature of the rays is not constant but can be determined from the refractive index distribution with altitude.[4] Considerable changes in path loss may result from variations from the normal in the vertical gradient of the refractive index; with large vertical gradients, elevated reflecting layers may be formed that, under certain conditions, greatly influence the path loss.

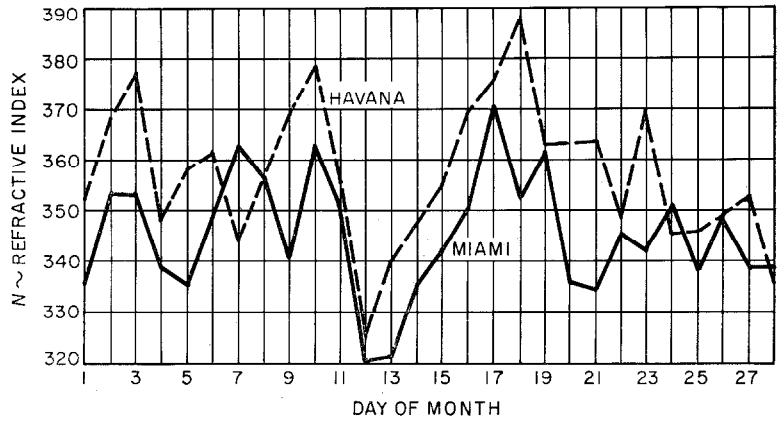

Figure 2—Surface refractivity, 19:00 Eastern Standard Time, February 1955; at Miami and Havana. The correlation coefficient is 0.60.

In considering the effect of the surface value of the refractive index of the atmosphere on radio transmission, the question arises as to what value of the refractive index should be taken when transmission paths of, say, several hundred miles length are being considered. It has been found that the surface values of N at any particular time may be quite different at points separated by such distances and that the daily variations

of N at the two ends of a beyond-the-horizon path may show little correlation. For example, Figure 2 shows the values of surface refractivity measured each day during February 1955 at points separated by about 180 miles (290 kilometers); the correlation coefficient in this case is only 0.60. However, if the values of N at the two ends of the transmission path are averaged over a week or more, it will be found that there is a much closer correlation. Figure 3 shows the surface values of N measured again at Miami and at Havana; but in this case, the average monthly values are compared showing a correlation coefficient of 0.95.

In comparing transmission loss with the surface values of the refractive index, the values of N assumed for the transmission path should, therefore, be those measured at each end of the path, and at other points on the path if possible, averaged over periods of not less than about one

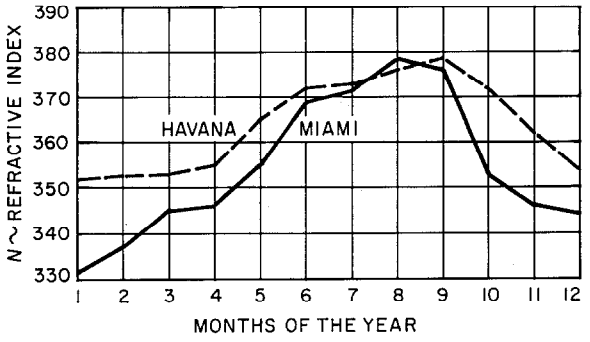

Figure 3—Surface refractivity, 1955; at Miami and Havana. Correlation coefficient is 0.95.

week and preferably over about a four-week period. Thus, the weekly or monthly median transmission loss should be compared with the median surface refractive index of the transmission path for the same period.

3. Tropospheric Propagation Characteristics

In the case of transmission far beyond the horizon at frequencies between about 400 and 2000 megacycles per second, the following general characteristics have been established:

(A) Large variations in path loss from the monthly median lasting on the average for periods of up to, say, one hour[5,6] but persisting in some cases for several days.

(B) A day-to-day variation in median path loss.

(C) A seasonal change in path loss amounting to about ± 12 decibels is usual on paths of, say, between 100 and 200 miles (161 and 322 kilometers) in length in temperate latitudes, the path loss being greater in winter than in summer.[7,8]

(D) A gaussian distribution of hourly medians on overland paths with a standard deviation of about 8 decibels.

(E) A decrease in the amplitude of the variations in path loss with increasing path length.[9–12]

In addition, there is the Rayleigh-distributed fast fading, which is not considered in this paper.

3.1 Causes of Path-Loss Variations

In considering the characteristics of radio propagation beyond the horizon, the transmission path may be thought of as consisting of two separate parts, the first being the common volume at the intersection of the two antenna beams and the second the two line-of-sight paths from the antennas to the common volume. A small fraction of the transmitted energy is

[5] H. B. Jones, "An Analysis of Within-the-Hour Fading in 100–1000 Mc Transmission," National Bureau of Standards Report *3520*, Supplement XII.

[6] K. P. Stiles, "Report on Over-the-Horizon Radio Transmission Tests Between Florida and Cuba," *IRE Convention Record*, Part 8, pages 212–216; 1956.

[7] K. Bullington, A. D. Durkee, and W. J. Inkster, "Results of Propagation Tests at 505 Mc and 4090 Mc on Beyond-Horizon Paths," *IRE Transactions on Communication Systems*, volume CS-4, pages 104–111; March, 1956.

[8] J. H. Chisholm, P. A. Portman, J. T. deBettencourt, and J. F. Roche, "Investigation of Angular Scattering and Multipath Properties of Tropospheric Propagation of Short Radio Waves Beyond the Horizon," *Proceedings of the IRE*, volume 43, pages 1317–1335; October, 1955.

[9] G. L. Mellen, W. E. Morrow, A. J. Poté, W. H. Radford, and J. B. Wiesner, "UHF Long-Range Communication Systems," *Proceedings of the IRE*, volume 43, pages 1269–1281; October, 1955.

[10] W. E. Morrow, "UHF Transmission Over Paths of 300 to 600 Miles," Unpublished.

[11] J. H. Chisholm and J. F. Roche, "Measurements of Signal Levels at UHF and SHF Propagated Through the Troposphere Over Paths 100 to 618 Miles in Length," Unpublished.

[12] L. A. Ames, E. J. Martin, and T. F. Rogers, "Long-Distance VHF-UHF Tropospheric Field Strengths and Certain of Their Implications for Radio Communications" (Abstract), *IRE Transactions on Communication Systems*, volume CS-4, pages 102–103; March, 1956.

reflected, or scattered, to the receiving antenna by inhomogeneities within the common volume; and measurements indicate that the median loss at this common volume is a function of the angle of intersection of the two antenna beams.

The transmission loss between isotropic antennas for the line-of-sight paths is given by

$$\text{decibels loss} = 37 + 20 \log F + 20 \log d, \quad (3)$$

where F is the frequency in megacycles and d the distance in statute miles. The two line-of-sight paths are subject to atmospheric refraction and, due to the small angles of elevation of the rays, are particularly sensitive to changes in the refractive-index vertical gradient in the lower atmosphere. An increase in the refraction of these rays decreases the angle of intersection of the antenna beams and is thus equivalent to a decrease in the effective length of the transmission path.

3.2 Large Short-Period Path-Loss Variations

The decrease in the refractive index of the atmosphere with height near the surface of the earth is 11.9 N units per 1000 feet (305 meters)

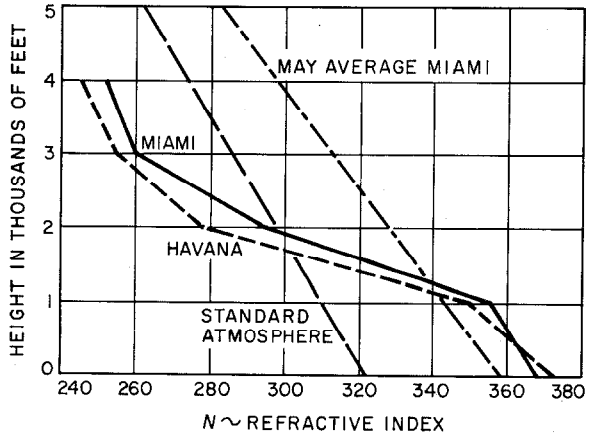

Figure 4—Gradient of the refractive index, 22:00 Eastern Standard Time, May 9, 1955; at Miami and Havana. Path loss was 17 decibels below monthly median.

for the standard atmosphere. However, under certain conditions, the N gradient with height may be above the normal value so that the line-of-sight path curvature is increased and the angular distance of the path is, therefore, decreased. Under extreme conditions, the rays may follow paths parallel to the earth's surface, or be bent downward toward the earth, giving a path loss even lower than the free-space value. On the other hand, a decrease in the N gradient

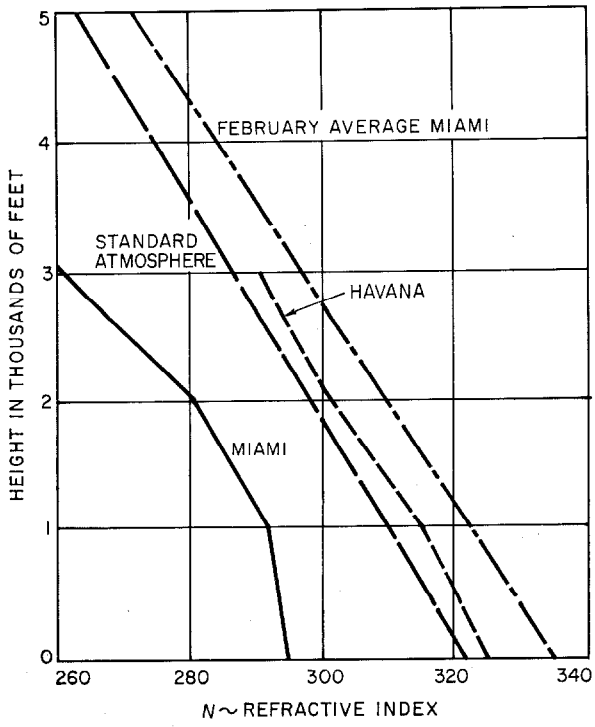

Figure 5—Gradient of the refractive index, 10:00 Eastern Standard Time, February 12, 1955; at Miami and Havana. Path loss was 25 decibels above the monthly median.

with height will result in a decrease in the refraction of the rays and an increase in the path loss. It is believed that extreme conditions of low path loss are more likely to occur on overwater than on overland paths.

Path-loss measurements made at 800 megacycles on an over-the-horizon path between Florida and Cuba showed that the exceptional conditions of path loss occurred at times when either high or low values of surface refractivity existed over the transmission path. It was also found that these exceptional values of path loss were associated with unusual variations of the refractive index with height. The average gradient of the refractive index was determined during these tests from radiosonde measure-

ments that did not, however, show the fine structure of the index gradient.

Path-loss values considerably below the monthly median were frequently recorded during the Florida–Cuba tests; for example, at about 10 PM on May 9, 1955, the measured path loss was some 17 decibels less than the monthly median value. The N gradient at this time was found to be much greater than the normal value. Figure 4 shows the decrease in N with height as measured near the two ends of the path at the time when these low values of path loss were recorded. In this figure are also shown the gradient for the standard atmosphere and the average gradient for May at Miami. It will be seen that not only was the gradient of the refractive index very high at this time, but the surface value of N was about 370 instead of the standard value of 322.

High path loss was, on the other hand, associated with low N gradients. For example, Figure 5 shows the decrease in N with height

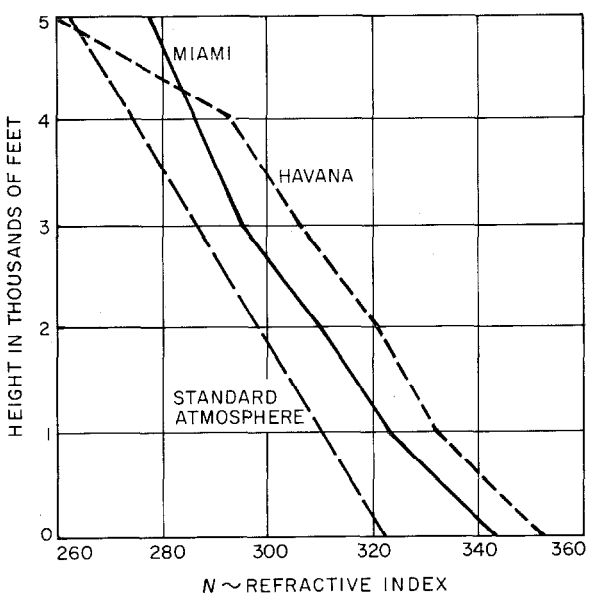

Figure 6—Gradient of the refractive index, 10:00 AM, February 23, 1955; at Miami and Havana. Path loss = monthly median.

near the two ends of the path when the recorded transmission loss was about 25 decibels above the monthly median value. For comparison, the gradients for the standard atmosphere and for the February average at Miami are also shown. It will be noted that the refractive index gradient at Miami for the first 1000 feet (305 meters) of altitude was considerably below normal at this time and that the surface value of N at Miami was only 296 instead of the standard 322.

Conditions of median path loss were, however, associated with a gradient of the refractive index close to that of the standard atmosphere. For example, Figure 6 shows the N gradients near the two ends of the path measured at about 10 AM on February 23, 1955; the normal gradient for the standard atmosphere is also shown in this figure. At the time these measurements were made, the median path loss was about 15 decibels less than would be expected from transmission loss measurements made in the northeastern United States. It will be noticed that the average N gradients were about normal at altitudes below 4000 feet (1219 meters), but the average surface value was about 347 as compared with the standard 322 value.

The path-loss extreme values measured during tests between Miami and Havana were, therefore, found to be due to a combination of unusual values of surface refractive index and to exceptional gradients of this index. Under normal conditions, however, the relatively low value of transmission loss measured on this path seemed to be chiefly due to the high average value of surface refractive index, typical of the warm humid climate of that area, and not to an unusual refractive-index gradient.

3.3 Day-to-Day Median Path-Loss Variations

Transmission loss measurements made in different parts of the world have shown daily median-path-loss variations of as much as $\pm$ 20 decibels. These variations seem to be largely dependent on the gradient and on the surface value of the atmospheric refractive index prevailing at the time along the transmission path. The daily averages of these meteorological characteristics are difficult to measure, particularly on overwater paths; and some uncertainty exists as to the relative importance of atmospheric turbulence on the daily path-loss values. However, in spite of these

difficulties, measurements show some correlation between daily values of path loss and the average surface refractive index measured at the two ends of the path.

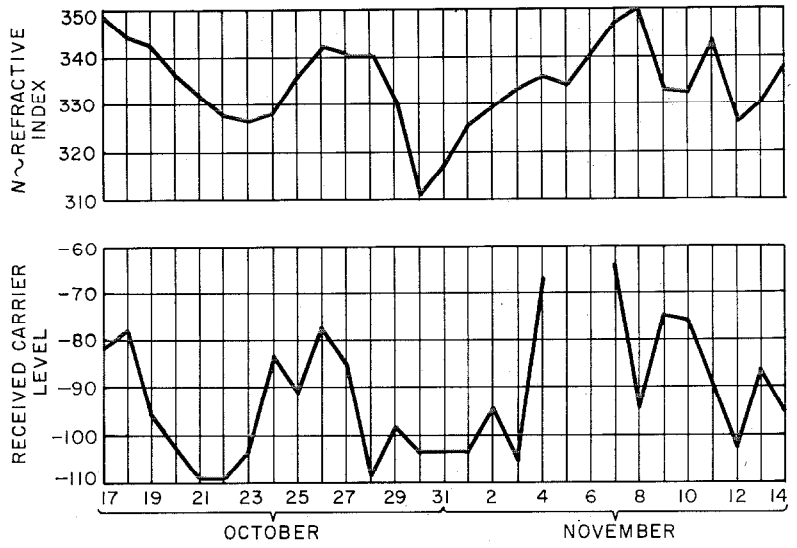

Figure 7—Path loss and refractive index, Buenos Aires to Montevideo; 1956. The correlation coefficient was 0.45.

Transmission loss tests were recently conducted on a frequency of about 900 megacycles between sites near Buenos Aires, Argentina and Montevideo, Uruguay. Figure 7 shows the daily average surface refractivity and the daily median received carrier level for one month. There is, in general, some degree of correlation between the daily refractive-index values and the daily median path loss; but as has been shown, the refractive-index gradient is also an important factor in ultra-high-frequency propagation far beyond the horizon. Daily measurements made near Buenos Aires of the refractive-index variation with height showed that at times of poor correlation between path loss and surface refractive index the gradient of the refractive index was, in general, abnormal. Since the refractive-index gradient was measured at only one end of the path, it was not possible in this case to make an estimate of the average gradient over the transmission path. More-complete information on the daily average gradient would probably have indicated the reason for the poor correlation found on certain days between the path loss and the surface value of the refractive index.

3.4 Seasonal Path-Loss Change

The refractive index near the surface of the earth varies in temperate latitudes with the seasons; the value increases as the weather becomes warmer. In most tropical and arctic areas, however, the refractive index at the earth's surface changes much less from month to month than it does in the more temperate areas of the world. This relatively small change is due to the fact that in many tropical areas the temperature and relative humidity remain more or less constant throughout the year; and in arctic areas, the low average temperature results in a fairly constant and relatively low value of the refractive index. For example, at temperatures below 0 degrees centigrade, the surface value of N varies between only about 290 and 320 for relative humidity changes of from 10 to 90 percent.

As an example of typical variations of the atmospheric refractive index, Figure 8 shows the monthly values of the surface refractive index at San Juan, Puerto Rico, at Charleston, South Carolina, and at Goose Bay, Labrador. It will be seen from this figure that the seasonal change in the refractive index is comparatively small at San Juan and at Goose Bay, being much greater at Charleston.

Measurements made at a number of locations along the Atlantic Coast, from the tropics to the arctic, show that the maximum seasonal change in the surface refractive index, of about 60 N units, occurs at a latitude of about 33 degrees north, whereas the minimum seasonal change, of about 15 N units, occurs both in the tropics and in the arctic.

It has been shown by Bean[13,14] that at a

[13] B. R. Bean, "Some Meteorological Effects on Scattered Radio Waves," National Bureau of Standards Report *3561*; December, 1955.

[14] B. R. Bean, "Survey of the National Bureau of Standards' Application of Atomospheric Refractivity Measurements to Radio Propagation Studies," National Bureau of Standards Report *5007*; August 20, 1956.

frequency of about 100 megacycles there is a close correlation between the monthly median transmission loss and the average monthly value of refractive index at the earth's surface. The

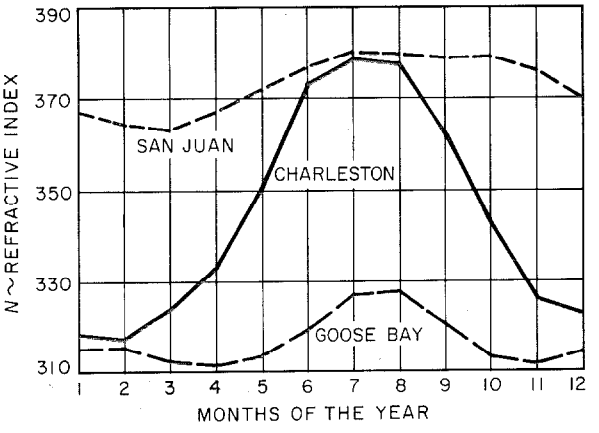

Figure 8—Average monthly values of refractive index. Latitudes of stations are San Juan = 18 degrees, 27 minutes; Charleston = 32 degrees, 30 minutes; Goose Bay = 52 degrees, 20 minutes.

surface N is, on the average, a measure of the N gradient with height; but it was shown during the Florida–Cuba tests that a gradient of N corresponding to the normal 4/3 earth radius occurred at times when the median carrier level was some 15 decibels above what would be expected from path-loss measurements made in the northeastern part of the United States. Thus, a high N value at the earth's surface, but a normal gradient, was in this case associated with low path loss.

Other path-loss measurements have also shown that there is a close correlation between the average monthly surface refractive index and the monthly median path loss.[7,8,15] For example, during 1955, transmission loss measurements were made on a frequency of 238 megacycles between the Mediterranean islands of Minorca and Sardinia. Figure 9 shows the monthly median path loss and the average monthly surface refractivity, which in this case showed a correlation of 0.76 between these monthly values.

Radio propagation measurements made on beyond-the-horizon paths thus show good correlation between the seasonal changes in median path loss and the seasonal changes in the average refractive index measured near the surface on the transmission path.

3.5 Gaussian Distribution of Hourly Medians

The distribution of the hourly median path-loss values varies with geographic location; and as has been shown, there is a close correlation between the monthly variations in path loss and the monthly variations in the surface refractive index. The distribution of the monthly median path-loss values is, thus, largely determined by the distribution of the refractive-index values; large seasonal changes in N would, thus, be expected to result in large values of standard deviation of the monthly median path-loss distribution.

However, during the Florida–Cuba tests, it was found that the extreme path-loss values, which occur, in general, for a small percentage of the time, were a function, not only of the surface N, but also of the gradient or rate of change of N with

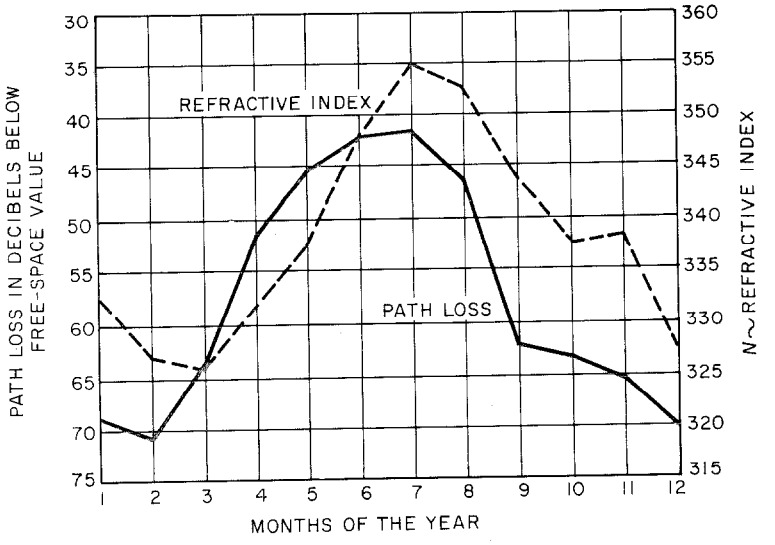

Figure 9—Path loss and refractive index for the Sardinia–Minorca circuit in 1955. Length = 240 miles = 386 kilometers; frequency = 238 megacycles. Correlation coefficient is 0.76.

[15] M. T. Decker and H. B. James, "418-Mc Propagation Measurements Over the Cedar Rapids–Quincy Path," National Bureau of Standards Report *3520*, Supplement III; July, 1955.

height. Thus, the final hourly median path-loss distribution is determined for, say, 90 percent of the time by the distribution of the surface N and the remaining 10 percent of the time by abnormal N gradients occurring at heights below the common volume.

3.6 Decrease in Loss Variations With Increasing Path Length

It has been shown that under the same climatic conditions, the long-term path-loss variations are of smaller amplitude at a distance of 300 miles (483 kilometers) than at, say, 100 miles (161 kilometers).[6–9] If the slow changes in path loss are due to refractive-index changes, not at the surface of the earth, but at some height that increases with path length, then it is clear from Figure 1 that there will be a smaller change in loss at, say, 300 miles (483 kilometers) than at 100 miles (161 kilometers). The fact that the path-loss variations have been reported to be very small at distances of about 600 miles (965 kilometers) indicates that the path-loss variations may be a function of the refractive-index variations, not at the surface of the earth, but at a height close to the intersection of the antenna beams. However this may be, the decrease in the amplitude of the long-term path-loss variations with distance suggests that the loss may be a function of the refractive-index variations, not at the earth's surface, but at a height proportional to about the square of the path length.

4. Path Loss Related to Distance and Surface Refractive Index

Path-loss measurements indicate that there is a close correlation between path-loss variations and refractive-index variations of the atmosphere at a height close to the antenna-beam intersection.

Measurements made between Florida and Cuba[6] showed that the median loss over a path length of 184 statute miles (296 kilometers) was about 53 decibels below free-space propagation. From meteorological measurements made at Miami and Havana, the average N surface value at the time of the path-loss measurements was 360; the variation in path loss was found to be 0.5 decibel per N-unit change.

Measurements on the 238-mile (383-kilometer) path between Dorado, Puerto Rico, and Ciudad Trujillo, Dominican Republic, showed a median path loss below the free-space value of about 65 decibels for an average N surface value of 364. The variation in loss in this case was about 0.4 decibel per unit change in the surface value of N.

From these results and from measurements made in the Mediterranean, in the Argentine, and elsewhere, Figure 10 has been prepared showing the median path loss as a function of distance and of the refractive-index average value at sea level for frequencies in the neighborhood of 900 megacycles. This figure summarizes the results of recent path-loss measurements and illustrates, in a general way, the relationship between median path loss, distance, and refractive-index average value at sea level. From this figure, estimates can be made of the monthly median path loss at 900 megacycles for any distance from 80 to 300 miles (129 to 483 kilometers) and for average refractive-index surface values, expressed in N units, of from 300 to 360.

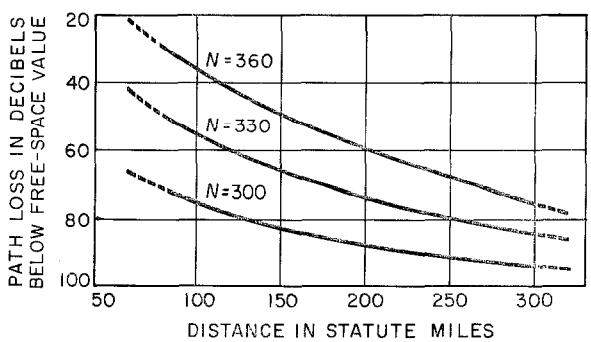

Figure 10—Tropospheric propagation far beyond the horizon at 900 megacycles. $N \sim$ refractive index at surface of earth.

5. Conclusion

Tropospheric propagation far beyond the horizon is entirely dependent on the atmosphere.

The monthly median path loss has been shown to be a function of the average monthly refractive index of the atmosphere on the transmission path. When the temperature and relative humidity are high, the path loss is low, and vice versa, thus giving rise to seasonal loss variations in temperate latitudes.

The exceptional values of path loss are chiefly due to abnormal vertical refractive-index gradients in the atmosphere of the transmission path. Extreme conditions lead to ducting or to the formation of reflecting layers resulting in low path-loss values.

Path-loss measurements show that the transmission-loss variations decrease as the path length increases, suggesting that the median path-loss variations may be a function of the variations in average refractive index at a height close to the intersection of the two antenna beams.

In tropospheric propagation far beyond the horizon, measurements indicate that the monthly median path loss is a function of average monthly surface index of refraction and of angular distance. This relation is of considerable practical interest since it may permit estimates to be made of the monthly median transmission loss over any path for which the average monthly surface index-of-refraction values are known.

Recent Telecommunication Development

Transistor Circuits

AMONG recent publications, is a new book on "Transistor Circuits" by K. W. Cattermole of Standard Telecommunication Laboratories. The subject is treated in 16 chapters, an extensive bibliography, and 6 appendixes. The scope of the book is evident from the titles of the chapters and appendixes.

Chapter 1—Introduction
Chapter 2—Semi-conductors
Chapter 3—Electrical Properties of Transistors
Chapter 4—Elements of Transistor Circuits
Chapter 5—Single-stage Amplifiers
Chapter 6—Multi-stage Amplifiers
Chapter 7—Power Amplifiers
Chapter 8—High-frequency Amplifiers
Chapter 9—Supplies and Bias Stabilization
Chapter 10—Negative Resistance
Chapter 11—Binary Circuits
Chapter 12—Waveform Generation
Chapter 13—Counting and Timing
Chapter 14—Modulation, Detection, and Frequency Changing
Chapter 15—Measurement of Transistor Properties
Chapter 16—Fields of Application

Appendix 1—Linear Network Analysis
Appendix 2—Transient Response of Transistors
Appendix 3—Band-pass Transformers
Appendix 4—Delay Networks
Appendix 5—Saturable Magnetic Materials
Appendix 6—Exponential Non-linearities

The dimensions are $6\frac{3}{4}$ by $8\frac{3}{4}$ inches (17.1 by 22.2 centimeters). The 16 chapters occupy 399 pages, the appendixes cover 26 pages, and the bibliography is of 9 pages. An 8-page index brings the total to 442. There are 288 figures and 482 numbered equations in the chapters and 17 figures and 65 numbered equations in the appendixes.

The book is published by the Macmillan Company, and is available from Heywood & Company, Limited, Carlton House, Great Queen Street, London, W.C. 2, at 70 shillings and from the Macmillan Company, 60 Fifth Avenue, New York 11, New York, at $14.00.

United States Patents Issued to International Telephone and Telegraph System; August-October 1958

BETWEEN August 1, 1958 and October 31, 1958, the United States Patent Office issued 88 patents to the International System. The names of the inventors, company affiliations, subjects, and patent numbers are listed below

R. T. Adams, ITT Laboratories, Multichannel Signal System, 2 855 462.

P. R. R. Aigrain and G. P. Intzopoulos, Laboratoire Central de Télécommunications (Paris), Electronic Switching System, 2 852 611.

M. Arditi, ITT Laboratories, Wide-Band Waveguide Circuitry, 2 854 645.

F. G. Bac, Le Matériel Téléphonique (Paris), Radio Detection and Distance Indicator, 2 855 594.

A. Beck and A. Cutting, Standard Telephones and Cables (London), Electron Velocity-Modulation Tubes, 2 857 549.

F. H. Bray and M. A. E. Butler, Standard Telephones and Cables (London), Automatic Telecommunication Exchange System, 2 851 534.

F. H. Bray, P. M. King, and J. Rice, Standard Telephones and Cables (London), Magnetic Store for Telephone Meter Impulses, 2 850 571.

A. E. Brewster, Standard Telecommunication Laboratories (London), Relaxation Oscillators and Electronic Counters, 2 856 528.

J. H. Bryant, ITT Laboratories, Electromagnetic Wave Generator, 2 848 649.

H. G. Busignies, Le Matériel Téléphonique (Paris), Position-Finding System for Gun-Fire Control, 2 855 592.

J. Culbertson, Kellogg Switchboard and Supply Company, Automatic Dial-Speed Tester, 2 857 484

F. Davidoff, Federal Telephone and Radio Company, Delay Circuit for Receiver-Indicator, 2 850 628.

G. A. Deschamps, ITT Laboratories, Microwave Transmission-Line Calculator, 2 845 711.

B. Diamond and J. B. Walker, Commercial Cable Company, Telegraph-Code Converter, 2 847 503.

S. Fong, Capehart-Farnsworth Company, Adaptor Device for Image Tubes, 2 857 589.

O. C. From, L. B. Haigh, and A. N. Gulnick, ITT Laboratories, Telephone Ringing Generator, 2 850 655.

A. W. Gent and R. T. Lawrence, Standard Telephones and Cables (London), High-Frequency Transmission-Line Systems, 2 852 753.

G. S. Giffin, D. G. Killion, and H. N. Haller, Farnsworth Electronics Company, Antenna Arrays, 2 847 672.

P. F. M. Gloess, Le Matériel Téléphonique (Paris), Electric Circuit for Use with Cathode-Ray Tubes, 2 855 593.

W. F. Glover, Standard Telephones and Cables (London), High-Frequency Electric Transformers, 2 850 709.

R. Goerlich and M. Muller, Mix & Genest (Stuttgart), Device for Storing Switching Information for Controlling Operations of Conveying Systems, 2 857 059.

F. P. Gohorel, Compagnie Générale de Constructions Téléphoniques, Le Matériel Téléphonique (Paris), Automatic Telephone Systems, 2 850 575.

F. P. Gohorel, Compagnie Générale de Constructions Téléphoniques, Le Matériel Téléphonique (Paris), Automatic Telephone System, 2 853 556.

G. C. Hartley and F. H. Bray, Standard Telephones and Cables (London), Storage of Electrical Intelligence, 2 847 657.

C. L. Heck and J. F. L. Weber, Suddeutschc Apparatefabrik (Nurnberg), Method of Producing Ferrites, 2 856 365.

R. Helmert, C. Lorenz (Stuttgart), Supervisory Control Circuit, 2 853 600.

A. Hemel, Kellogg Switchboard and Supply Company, Station-Identifying Call-Recording Telephone System, 2 848 547.

A. Heyduck, Mix & Genest (Stuttgart), Circuit Arrangement for Private-Automatic-Branch-Exchange Systems, 2 852 614.

O. Hofer, Capehart-Farnsworth Company, Rotary Coupling, 2 857 185.

J. F. Houdek, Jr., Kellogg Switchboard and Supply Company, Loud-Speaking Station for Automatic Telephone System, 2 848 552.

G. H. Hough and T. M. Jackson, Standard Telephones and Cables (London), Electric Discharge Tubes and Circuits Therefor, 2 846 611.

G. H. Hough, A. H. W. Beck, T. M. Jackson, and I. H. Fraser, Standard Telephones and Cables (London), Electric Discharge Devices, 2 856 554.

C. L. Hubbard and K. P. Russell, Capehart-Farnsworth Company, Television Cabinet Construction, 2 850 343.

F. J. Hunt, Standard Telephones and Cables (London), Method of Mounting Piezoelectric Crystals, 2 856 549.

M. G. Jaenke, C. Lorenz (Stuttgart), Selective Call Receiver, 2 853 558.

K. S. T. Janson and S. R. Nordstrom, Electric Equalizing Networks, 2 853 686.

R. Judy, Kellogg Switchboard and Supply Company, Call-Distributing Telephone System, 2 857 472.

A. G. Kandoian, ITT Laboratories, Antenna Tuning Units, 2 855 599.

A. G. Kandoian and R. E. Altoonian, ITT Laboratories, Antenna for Mobile Communications, 2 850 732.

K. Karow, Kellogg Switchboard and Supply Company, Testing Apparatus for Telephone Systems, 2 857 468.

R. Kelly and P. S. Kelly, Standard Telephones and Cables (London), Regulated Power-Supply Equipments, 2 847 584.

M. Kenmoku, Nippon Electric Company (Tokyo), Traveling-Wave Tube, 2 856 555.

W. Klein and W. Friz, C. Lorenz (Stuttgart), Traveling-Wave Tube, 2 857 547.

W. Kloepfer, C. Lorenz (Stuttgart), Circuit Arrangement for the Connection of Two-Wire Circuits to a Transmission Path in Intercommunication Systems, 2 847 563.

G. Kratt, C. Lorenz (Stuttgart), Device for the Reception and Evaluation of Telegraph Signals, 2 847 504.

G. Kratt and O. Holstein, C. Lorenz (Stuttgart), Device to Drive Circular Type-Carriers, 2 847 505.

C. C. Larson, Farnsworth Research Corporation, Television Camera-Tube Arrangement with Fading Control Utilizing an Additional Camera Tube, 2 850 565.

C. C. Larson, Capehart-Farnsworth Company, Crystal Production, 2 858 199.

E. J. Leonard, Kellogg Switchboard and Supply Company, All-Relay Frequency-Controlled Pulse Generator, 2 852 701.

A. M. Levine, ITT Laboratories, Television Receiver, 2 850 564.

A. M. Levine, ITT Laboratories, Pulse Communication System, 2 852 610.

W. Lewanda, F. Marasa, and F. F. Durst, Federal Telephone and Radio Company, Selenium Rectifiers, 2 856 364.

L. Lewin, T. H. Walker, and A. E. Pethick, Standard Telephones and Cables (London), Diversity Reception Arrangements for Radio Waves, 2 854 568.

L. Lewin and J. Setchfield, Standard Telecommunication Laboratories (London), Electric Wave Filters Employing Waveguides, 2 858 513.

C. P. Majkrzak, ITT Laboratories, Contact Pressure Indicator, 2 853 876.

N. Marchand and M. Semel, Federal Telephone and Radio Company, Phase-Comparison System, 2 850 730.

F. P. Mason and R. G. Stemp, Creed & Company (London), Automatic-Gain-Control System, 2 853 543.

B. D. McNary and L. A. Tentarelli, ITT Laboratories, Traveling-Wave Electron Discharge Devices, 2 852 416.

L. Merrill, Farnsworth Electronics Company, Voltage Comparators, 2 858 438.

H. G. Nordlin, ITT Laboratories, Electromagnetic Delay Cable and Manufacture Thereof, 2 854 639.

H. G. Nordlin, ITT Laboratories, Electromagnetic Delay Cable, 2 854 640.

B. Norris and M. McCrea, Farnsworth Electronics Company, Voltage Regulators, 2 858 498.

R. K. Orthuber and C. V. Stanley, Capehart-Farnsworth Company, Apparatus and Method for Detecting Overheated Journal Boxes, 2 856 539.

S. B. Pickles, ITT Laboratories, Television System, 2 854 506.

W. H. P. Pouliart and L. J. G. Nys, Bell Telephone Manufacturing Company (Antwerp), Pneumatic Tape Drive, 2 852 253.

H. T. Prior and E. A. Foulkes, Standard Telephones and Cables (London), Printing-Telegraph Distortion Indicator, 2 856 457.

A. J. Radcliffe, Jr., Kellogg Switchboard and Supply Company, High-Frequency Negative-Resistance Device, 2 852 680.

D. C. Rogers, Standard Telephones and Cables (London), Travelling-Wave Apparatus, 2 851 629.

M. Rogoff and C. T. Clark, ITT Laboratories, Navaglobe Receiving System, 2 852 773.

G. T. Royden, Mackay Radio and Telegraph Company, Apparatus and Method for Making Serial-Number Tape, 2 850 095.

D. R. Salmon, Standard Telephones and Cables (London), Interference-Suppressor Units, 2 855 574.

F. M. Schabauer, Mackay Radio and Telegraph Company, Automatic-Frequency Control Circuit for Frequency-Shift Radiotelegraphy, 2 855 506.

P. Schaeren, Standard Telephone et Radio (Zurich), Electrolyte for Electrolytic Capacitors, 2 851 642.

K. O. Seiler, Suddeutsche Apparatefabrik (Nurnberg), Method of Producing Semiconductor Crystals Containing P-N Junctions, 2 854 363.

K. O. Seiler and S. E. Muller, Suddeutsche Apparatefabrik (Nurnberg), Method of Purifying Semiconductor Material, 2 855 335.

D. M. Sharp, ITT Laboratories, Microwave Detector Circuit, 2 854 634.

W. Sichak, ITT Laboratories, Phase Shifter, 2 855 569.

W. Sindzinski, Mix & Genest (Stuttgart) Conveyor System, Particularly an Edgewise Conveyor System, 2 852 124.

G. Stavis, ITT Laboratories, Omnidirectional Beacon System, 2 846 677.

E. F. Tijs, Bell Telephone Manufacturing Company (Antwerp), Mounting Arrangement for Electrical Circuit Components, 2 855 580.

C. G. Treadwell, Standard Telephones and Cables (London), Electric Pulse Communication Systems, 2 852 607.

E. Uderstadt, Mix & Genest (Stuttgart), Arrangements for Selective Actuating Control Devices by Means of a Movable Magnet, 2 850 249.

S. VanMierlo, C. Weill, and M. C. E. Bataille, Laboratoire Central de Télécommunications (Paris), Circuit Arrangements for Transmitting Signals such as Ringing Signals to Subscribers to an Automatic Telephone System, 2 846 513.

C. Weill, C. Hannigsberg, and H. H. Adelaar, Bell Telephone Manufacturing Company (Antwerp), Electric Pulse Circuits, 2 853 606.

W. J. Willshire, Standard Telephones and Cables (London), Traveling-Wave Electron Discharge Device, 2 847 606.

H. O. Wolcott, Electromec, Ind., Bar-Graph Oscilloscopes, 2 848 648.

W. W. Wright, J. A. Smith, and B. D. Mills, Standard Telephones and Cables (London), Electric Discharge Devices, 2 854 601.

E. A. Zaratkiewicz, ITT Laboratories, Silicon Power Rectifier, 2 854 612.

Radio Detection and Distance Indicator

2 855 594

F. G. Bac

There is described an arrangement of two spaced transmitting stations from which pulses are transmitted at a predetermined time relationship and a receiving arrangement for receiving and displaying the pulses to determine by the difference in arrival time of the pulses the location of the receiver with respect to these transmitting stations. This covers broadly the basic principle of hyperbolic radio navigation systems such as loran.

Position-Finding System for Gun-Fire Control

2 855 592

H. G. Busignies

In this radio pulse-echo system, the echo pulses for the entire area being surveyed by the system are displayed on one oscillograph tube and a second oscillograph tube is provided for displaying on its screen only the echoes received within a small area of the total range. This patent has broad coverage on what is termed the vernier radar arrangement.

Omnidirectional-Beacon System

2 846 677

G. Stavis

This patent covers the tacan radio beacon system in which a plurality of reference signals are transmitted corresponding to the fundamental pattern of the radio beacon and a harmonic thereof. The patent also covers the direction indicator for the airborne equipment and a combination of the beacon with this airborne equipment.

Apparatus and Method for Detecting Overheated Journal Boxes

2 856 539.

R. K. Orthuber and C. V. Stanley

An arrangement for detecting overheated journal boxes is described in which a lens arrangement provides a projection of the image of the journal box onto a heat-sensitive indicator and a shutter is controlled by the operation of a railroad wheel flange to assure that the reading is made for a fixed time interval.

Method of Producing Ferrites

2 856 365

C. L. Heck and J. F. L. Weber

A method has been developed for producing manganese-zinc ferrites using manganese that has a higher degree of impurities than was previously considered possible. After the usual firing of the ferrite, the ferrite is ground and then washed in distilled water to remove these impurities. It is again pressed and heated to an annealing temperature for about an hour.

Method of Purifying Semiconductor Material

2 855 335

K. O. Seiler and S. E. Muller

This method of zone refining of a semiconductor rod employs an inductance coil to melt the rod progressively along its length. The rod is preheated to a conductive temperature by use of a toroidal washer positioned around the rod in the proximity of the coil to afford the essential heating of the semiconductor by radiation.

Bar-Graph Oscilloscopes

2 848 648

H. O. Wolcott

This patent covers the so-called bar-graph oscilloscope in which a large number of independent variables may be separately displayed as indications on the face of a single cathode-ray oscilloscope. The deflection circuit and the blanking of the beam are so controlled with respect to a gating circuit that the horizontal sweep of the oscilloscope is broken to permit individual vertical deflection for each of the desired indications to be displayed.

Contributors to This Issue

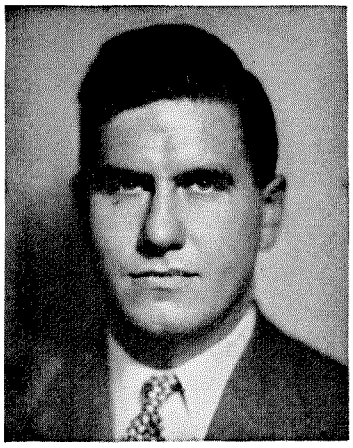

MILTON DISHAL

MILTON DISHAL was born on March 20, 1918, at Philadelphia, Pennsylvania. Temple University conferred on him the B.S. degree in 1939 and the M.A. degree in physics in 1941, both with honors. He served as a teaching fellow in physics during the post-graduate years.

In 1941, he entered the employ of ITT Laboratories, where he is now a senior scientist in charge of a group engaged in the development of radio receivers having special characteristics. Some of his work on gaussian filters is presented in this issue.

Mr. Dishal is a Fellow of the Institute of Radio Engineers. He has been active in the work of the Radio Technical Committee on Aeronautics. He is also an adjunct professor at Polytechnic Institute of Brooklyn.

• • •

A. A. DE CARVALHO FERNANDES

ANTONIO A. DE CARVALHO FERNANDES was born in Reigada, Portugal, in 1920. A graduate in electrical engineering of the Technical University of Lisbon in 1943, he remained there as an instructor in electrical engineering. In 1944, he joined the technical staff of Standard Eléctrica, Lisbon, becoming chief engineer in September, 1949; technical director in September, 1954; and managing director in May, 1957. He was appointed professor of applied electronics at the Technical University in July, 1956.

Mr. Carvalho Fernandes has published several papers on transmission lines and antennas (especially on antenna models) and a book on rhombic antenna arrays. He reports in this issue on some special rhombic antenna arrays. He is a Member of the Institute of Radio Engineers and an Associate Member of the Institution of Electrical Engineers.

• • •

W. F. GLOVER was born in St. Helens, Lancashire, England, on February 27, 1907. He received the degree of B.Eng. from Liverpool University in 1928.

On graduation, he joined Standard Telephones and Cables as a student engineer. He was transferred to the carrier and repeater section of the apparatus division in 1929 and is in charge of the development and engineering of coils for telecommunication purposes. He is coauthor of a paper in this issue on intermediate-frequency transformers.

Mr. Glover is a Member of the Institution of Electrical Engineers.

• • •

RICHARD E. GRAY was born in England in 1902. After graduating from Faraday House, electrical engineering college in London, he joined Standard Telephones and Cables in 1924.

W. F. GLOVER

From 1927 to 1939, he was with the laboratories of Le Matériel Téléphonique in Paris. In 1940, he was loaned to the Royal Aircraft Establishment at Farnborough, England, and in 1943 to the Telecommunication Research Establishment at Malvern.

He has been with ITT Laboratories since 1946. He is now working on tropospheric scatter communication and in this issue reports on the effect of the refractive index of the atmosphere on such communication. Mr. Gray is now a senior scientist of ITT Laboratories.

He is a member of the Institute of

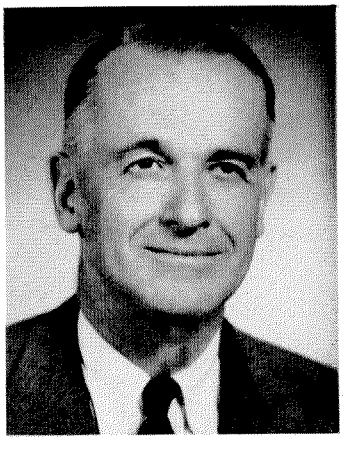

RICHARD E. GRAY

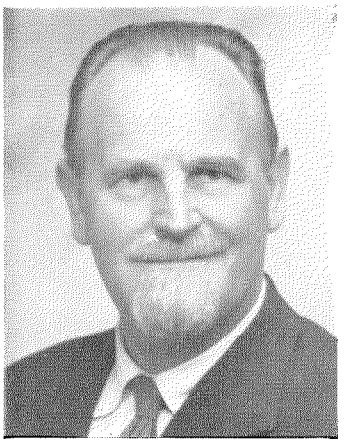

BENT BULOW JACOBSEN

Radio Engineers and of the Institution of Electrical Engineers.

• • •

BENT BULOW JACOBSEN was born in Kolding, Denmark, in 1906. He graduated in 1928 from the City and Guilds of London Engineering College. He joined the International Telephone and Telegraph Laboratories, London, in 1929 and later transferred to Standard Telephones and Cables Limited. He has worked for many years on carrier system design and more recently also on microwave radio links. He has specialized in the study of noise in long-distance transmission. Mr. Jacobsen is the author of the paper in this issue on thermal noise in radio link transmission.

He is a Member of the Institution of Electrical Engineers and of the Institution of Danish Civil Engineers.

• • •

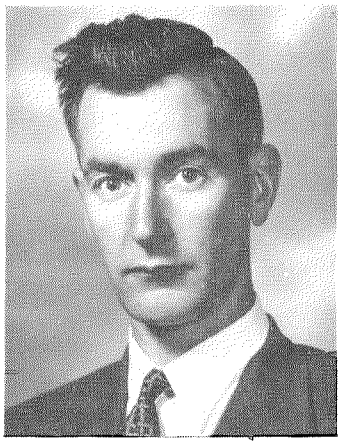

E. D. PEAKALL

E. D. PEAKALL was born in Lewisham, London, in 1923.

He joined the transmission laboratory of Standard Telephones and Cables as a student in 1945. He transferred to the coil-design group in 1949, and is at present responsible for the design and engineering of high-frequency coils for carrier transmission systems. He is coauthor of a paper in this issue on the design of an intermediate-frequency transformer.

He obtained his Higher National Certificate in Telecommunications in 1947 and is an Associate Member of the Institution of Electrical Engineers.

INTERNATIONAL TELEPHONE AND TELEGRAPH CORPORATION

Principal U. S.—Canada Divisions and Subsidiaries

DIVISIONS

Components Division, Clifton, N. J.
Kuthe Laboratories, Inc., Newark, N. J.
Industrial Products Division, San Fernando, Calif.
ITT Federal Division, Clifton, N. J., and Fort Wayne, Ind.
ITT Laboratories, Nutley, N. J., and Fort Wayne, Ind.
Kellogg Switchboard and Supply Company, Chicago, Ill.

SUBSIDIARIES

American Cable & Radio Corporation, New York, N. Y.
All America Cables and Radio, Inc., New York, N. Y.
Commercial Cable Company, The, New York, N. Y.
Mackay Radio and Telegraph Company, New York, N. Y.
Federal Electric Corporation, Paramus, N. J.
IT&T Electronics Service Company of Canada Ltd., Montreal, P.Q.
Northern Services, Inc., Anchorage, Alaska
Intelex Systems Incorporated, New York, N. Y.
Airmatic Systems Corporation, Rochelle Park, N. J.
International Electric Corporation, Paramus, N. J.
ITT Communication Systems, Inc., Paramus, N. J.
Kellogg Credit Corporation, New York, N. Y.
Royal Electric Corporation, Pawtucket, R. I.

and . . . International Standard Electric Corporation, New York, N. Y. whose principal research, manufacturing, and sales affiliates are:

ARGENTINA
Capehart Argentina S.A.I.C. (50% owned), Buenos Aires
Compañía Standard Electric Argentina, S.A.I.C., Buenos Aires

AUSTRALIA
Standard Telephones and Cables Pty. Limited, Sydney
Austral Standard Cables Pty. Limited (50% owned), Melbourne

AUSTRIA
Standard Telephon und Telegraphen Aktiengesellschaft, Czeija, Nissl & Co., Vienna

BELGIUM
Bell Telephone Manufacturing Company, Antwerp

BRAZIL
Standard Eléctrica, S.A., Rio de Janeiro

CANADA
Standard Telephones & Cables Mfg. Co. (Canada), Ltd., Montreal

CHILE
Compañía Standard Electric, S.A.C., Santiago

CUBA
Equipos Telefónicos Standard de Cuba, Havana

DENMARK
Standard Electric Aktieselskab, Copenhagen

FINLAND
Oy Suomen Standard Electric AB, Helsinki

FRANCE
Compagnie Générale de Constructions Téléphoniques, Paris
Les Téléimprimeurs, Paris
International Standard Engineering, Inc., Paris
Laboratoire Central de Télécommunications, Paris
Le Matériel Téléphonique, Paris

GERMANY
Standard Elektrik Lorenz Aktiengesellschaft, Stuttgart
Bauelemente Werk S.A.F. (division), Nuremberg
Informatikwerk (division), Stuttgart
Kabelwerk (division), Stuttgart
Lorenz Werke (division), Stuttgart
Mix & Genest Werke (division), Stuttgart
Schaub Werk (division), Pforzheim

IRAN
Standard Electric Iran A.G., Teheran

ITALY
Fabbrica Apparecchiature per Comunicazioni Elettriche Standard S.p.A., Milan

MEXICO
Industria de Telecomunicación, S.A. de C.V. (50% owned), Mexico City
Standard Eléctrica de México, S.A., Mexico City

NETHERLANDS
Nederlandsche Standard Electric Maatschappij N.V., The Hague

NEW ZEALAND
New Zealand Electric Totalisators Limited, Wellington

NORWAY
Standard Telefon og Kabelfabrik A/S, Oslo

PORTUGAL
Standard Eléctrica, S.A.R.L., Lisbon

SPAIN
Standard Eléctrica, S.A., Madrid

SWEDEN
Standard Radio & Telefon AB, Stockholm

SWITZERLAND
Standard Téléphone et Radio S.A., Zurich

TURKEY
Standard Elektrik Ve Telekomunikasyon Limited Şirketi, Ankara

UNITED KINGDOM
Creed & Company, Limited, Croydon
Standard Telephones and Cables Limited, London
Kolster-Brandes Limited, Sidcup
Standard Telecommunication Laboratories Limited, London

VENEZUELA
Standard Telecommunications C.A., Caracas

OVERSEAS TELECOMMUNICATION COMPANIES

ARGENTINA
Compañía Internacional de Radio, S.A., Buenos Aires
Sociedad Anónima Radio Argentina (subsidiary of American Cable & Radio Corporation), Buenos Aires

BOLIVIA
Compañía Internacional de Radio Boliviana, La Paz

BRAZIL
Companhia Rádio Internacional do Brasil, Rio de Janeiro
Companhia Telefônica Nacional, Curitiba and Pôrto Alegre

CHILE
Compañía de Teléfonos de Chile, Santiago
Compañía Internacional de Radio, S.A., Santiago

CUBA
Cuban American Telephone and Telegraph Company (50% owned), Havana
Cuban Telephone Company, Havana
Radio Corporation of Cuba, Havana

PERU
Compañía Peruana de Teléfonos Limitada, Lima

PUERTO RICO
Puerto Rico Telephone Company, San Juan
Radio Corporation of Puerto Rico, San Juan

SPAIN
Compañía Radio Aérea Marítima Española, S.A., Madrid

UNITED KINGDOM
International Marine Radio Company Limited, Croydon

VIRGIN ISLANDS
Virgin Islands Telephone Corporation, Charlotte Amalie

ASSOCIATE LICENSEES FOR MANUFACTURE AND SALES

FRANCE
Lignes Télégraphiques et Téléphoniques, Paris

ITALY
Società Italiana Reti Telefoniche Interurbane, Milan

JAPAN
Nippon Electric Company, Limited, Tokyo
Sumitomo Electric Industries, Limited, Osaka

SPAIN
Marconi Española, S.A., Madrid

IN THIS ISSUE

Gaussian-Response Filter Design

Transformers for Intermediate-Frequency Amplifiers

Design of Some Rhombic Antenna Arrays

Thermal Noise in Multisection Radio Links

Refractive Index of Atmosphere in Tropospheric Propagation

VOLUME 36 **1959** **NUMBER 1**

ELECTRICAL COMMUNICATION

INTERNATIONAL TELEPHONE AND TELEGRAPH CORPORATION

Printed in the
United States of America
LANCASTER PRESS, INCORPORATED
LANCASTER, PENNSYLVANIA